2016

Biomedical Applications of Thiol-Acrylate Polymers

Leah Alyce Garber
Louisiana State University and Agricultural and Mechanical College

BIOMEDICAL APPLICATIONS OF THIOL-ACRYLATE POLYMERS

A Dissertation

Submitted to the Graduate Faculty of the
Louisiana State University and
Agriculture and Mechanical College
in partial fulfillment of the
requirements for the degree of
Doctor of Philosophy

in

The Department of Chemistry

by
Leah Alyce Garber
B.S., Nicholls State University, 2011
August 2016

Acknowledgements

I would like to greatly thank my husband, John Beauchamp, for your unconditional love and support and my mother, Jennifer Garber, for her constant inspiration and shoulder to lean on. I wish to express my sincere gratitude to my advisor, Dr. John A. Pojman for his reassurance and for teaching me to look at every challenge in research as a learning experience. I also want to give a special thanks Dr. Donghui Zhang and especially to Dr. Daniel Hayes for his constant motivation and for always pushing me to work on the next best project. I also really appreciate all the assistance and training from Dr. Hollie Donze and Ying Xiao while working on the SEM and confocal microscope at the Shared Instrument Facility(SIF) at LSU. My appreciation also extends to the students working in Dr. Hayes' lab for their guidance and for teaching me about the biomedical side of research. Last but not least, high praise goes to the Pojmanite team for their encouragement, advice, and laughter especially on the stressful days.

Table of Contents

List of Abbreviations

ALP	Alkaline Phosphatate
DEA	Diethylamine
ECM	Extracellular Matrix
FBS	Fetal Bovine Serum
FTIR	Fourier Transform Infrared Spectroscopy
GA	Glutaraldehyde
hASC	human Adipose-derived Stem Cells
HBSS	Hank's Balance Salt Solution
HDMS	Hexamethyldisilazane
HA	Hydroxyapaptite
Micro-CT	Micro-Computed Technology
OCN	Osteocalcin
PBS	Phosphate Buffered Saline
PCL	Poly-ε-Caprolactone
PEG	Polyethylene Glycol
PEGDA	Polyethylene Glycol Diacrylate
PETA	Pentaerythritol Triacylate
PLGA	Poly(lactide-co-glycolide)
PLLA	Poly(L-lactide)
PMMA	Poly(methyl methacrylate)
SEM	Scanning Electron Microscopy
SNP	Silver Nanoparticles
TCP	Tissue Cultured Plastic
TCPS	Tissue Cultured Polystyrene
TEA	Triethylamine
TMPeTA	Trimethylopropane ethoxylate Triacrylate
TMPTA	Trimethylolpropane Triacrylate
TMPTMP	Trimethylolpropane Tris(3-mercaptopropionate)

Abstract

The development of biocompatible polymers using thiol-acrylate Michael addition reactions between not only acrylates and thiols but also between amines and acrylates were demonstrated. The synthesis of an *in situ* tertiary amine catalyst initiates the propagation steps of the polymerization process by subsequently reacting with trimethylolpropane tris (3-mercaptopropionate) (TMPTMP). A few notable characteristics of this reaction are tunable gel times, the capability of reaching high polymer conversion and suitable mechanical strength. With addition of hydroxyapatite to the polymeric phase and foaming, a porous bone composite was produced. Further osteogenisis and *in vivo* work using the PETA-co-TMPTMP (HA) composite material was analyzed. The PETA-co-TMPTMP-co-TMTMP with 20%HA showed an increase in osteogenic potential higher than the FDA approved PCL over the 21-day study. The rats did not exhibit any severe systemic responses from the polymer implant, and an increase in bone growth was observed for the rats containing PETA-co-TMPTMP (HA) samples compared to the rat containing no polymer. An antimicrobial study on the PETA-co-TMPTMP polymer was also performed by adding silver nanoparticles to the PETA-co-TMPTMP polymer to provide an antimicrobial component to the already well-established bone replacement polymer. By coating the polymer in a silver containing solution and adding 20%excess thiol to the polymer, it was effective at reducing common bacteria.

While the application of the PETA-co-TMPTMP polymer has proven to be effective for osteogenic bone scaffolds, the reason a material without cell adhesive moieties supported stem cell growth remained elusive. The next study used

polyethylene glycol diacrylate (PEGDA) and trimethylolpropane ethoxylated triacrylate (TMPeTA) to understand the relationship between thiol-acrylate polymers and cell adhesion. Wettability, modulus, and degradation stability were all tested, and it was observed that these properties play a role in the adhesion to these materials. As per live/dead staining, cell morphology changed to spindle shape on the lower molecular weight, 692 TMPeTA samples whereas the 912 TMPeTA's cell morphology remained the same. Cell adhesion on the TMPeTA(692) polymer versus the TMPeTA(912) is likely due to the 692 polymer yielding an overall tighter crosslinked network, and it's contact angle falling in the range for not being too hydrophilic/hydrophobic.

Chapter 1. Introduction

1.1 Thiol-Ene Chemistry

Thiol-ene chemistry, revived by Professor Charles Hoyle, takes place by the reaction between carbon-carbon double bonds and thiol functional groups(Scheme 1-1).[1,2] Two different reaction pathways occur for thiol-ene polymerizations and are noted by anti-Markovnikov radical addition and Michael addition base/nucleophile catalyzed mechanisms.[3] Thiol-ene chemistry using photo or thermal initiators (Scheme 1-2) has been studied extensively and used for many applications.[4-5] The general radical thiol-ene polymerization reaction produces thiyl radicals, which adds to an ene functional group. The hydrogen from another thiol can be abstracted in the second reaction to produce another thiol radical.

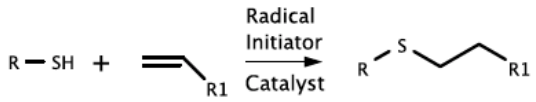

Scheme 1-1. General thiol-ene mechanism

The two radicals that were previously produced in the two propagation steps can react together to terminate the growing chains. A relatively uniform crosslinking network that usually proceeds rapidly at standard conditions without oxygen inhibition is produced. Oxygen usually inhibits radically initiated polymerization reactions, especially in thin films due to the rapid diffusion of oxygen, by forming peroxy radicals with the initiator or propagating species. The growing radical chain reacts with oxygen forming ROO• radicals that is not as reactive thus inhibiting the polymerization. On the contrary, with a thiol present, this reaction is significantly minimized by the peroxy radical reacting with the thiol by abstracting a hydrogen from it thus forming a stable species and eliminating the radical species.[6]

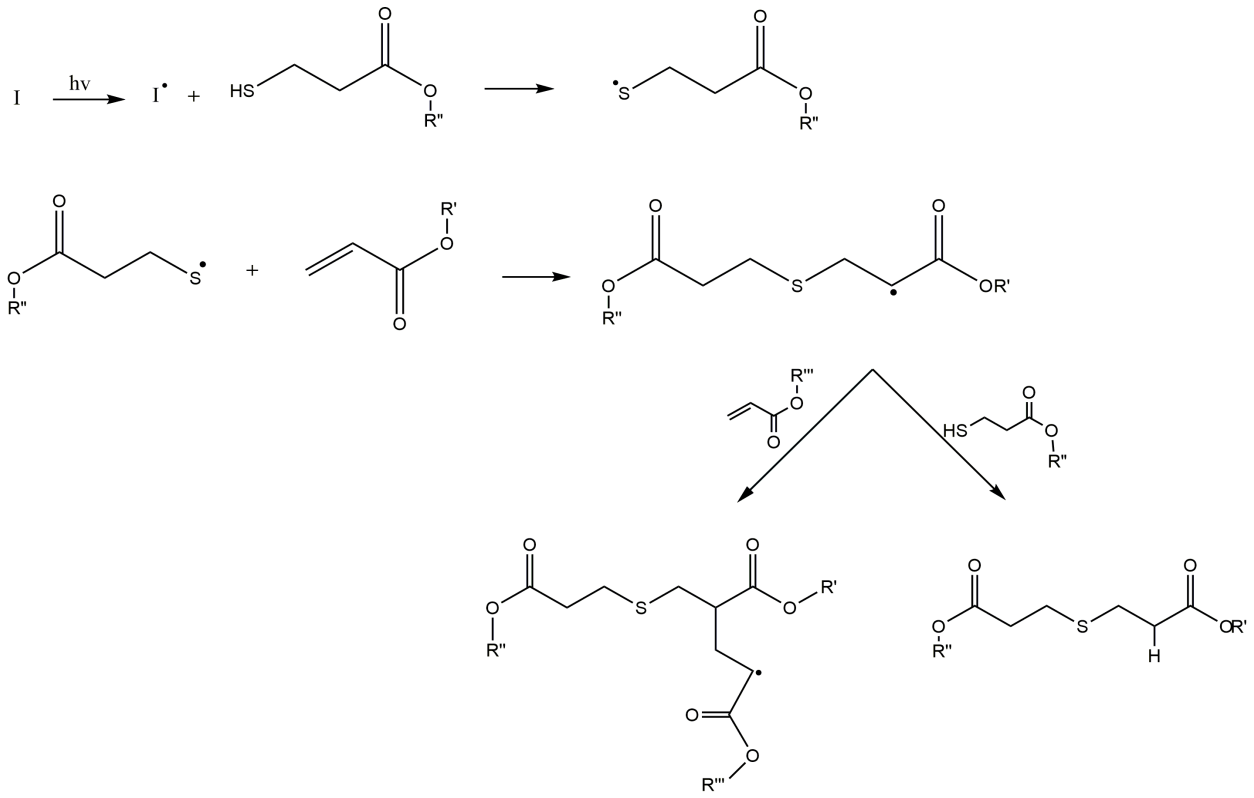

Scheme 1-2 Free-radical thiol-acrylate photopolymerization showing two pathways: acrylate homopolymerization and thiol-acrylate copolymerization.

A thiol-ene reaction using amine-catalyzed Michael addition click chemistry allows for the production of polymeric materials that have the ability to be synthesized efficiently at room temperature.[7] A Michael addition can occur between thiol containing molecules and electron–deficient molecules such as vinyl esters, acrylates, methacrylates, maleimides, and unsaturated α, β ketones.[8] Thiol-acrylate Michael addition chemistry, which will be the focus of this dissertation, is a subset of thiol-ene chemistry in which the ene species is an acrylate. Two different Michael addition thiol-acrylate anionic routes can proceed via a nucleophile-initiated mechanism or a base-catalyzed mechanism. For the nucleophile-mediated mechanism, the nucleophile attacks the β-carbon on the alkene initiating the reaction forming a strong enolate base that abstracts hydrogen from an acidic component present in the reaction as shown in

scheme 1-3. In the case for the nucleophile-mediated reaction, the acidic component is the thiol. This deprotonated thiol reacts with the electron deficient acrylate forming an enolate, which does a hydrogen transfer with another thiol thus repeating the chain propagation step. As discussed by Chan et al., if the nucleophile used for the nucleophile-initiated reaction also acts as a base such as amines, it may lead to a mix of mechanisms since the base can both deprotonate the thiol and add onto the double bond.[8]

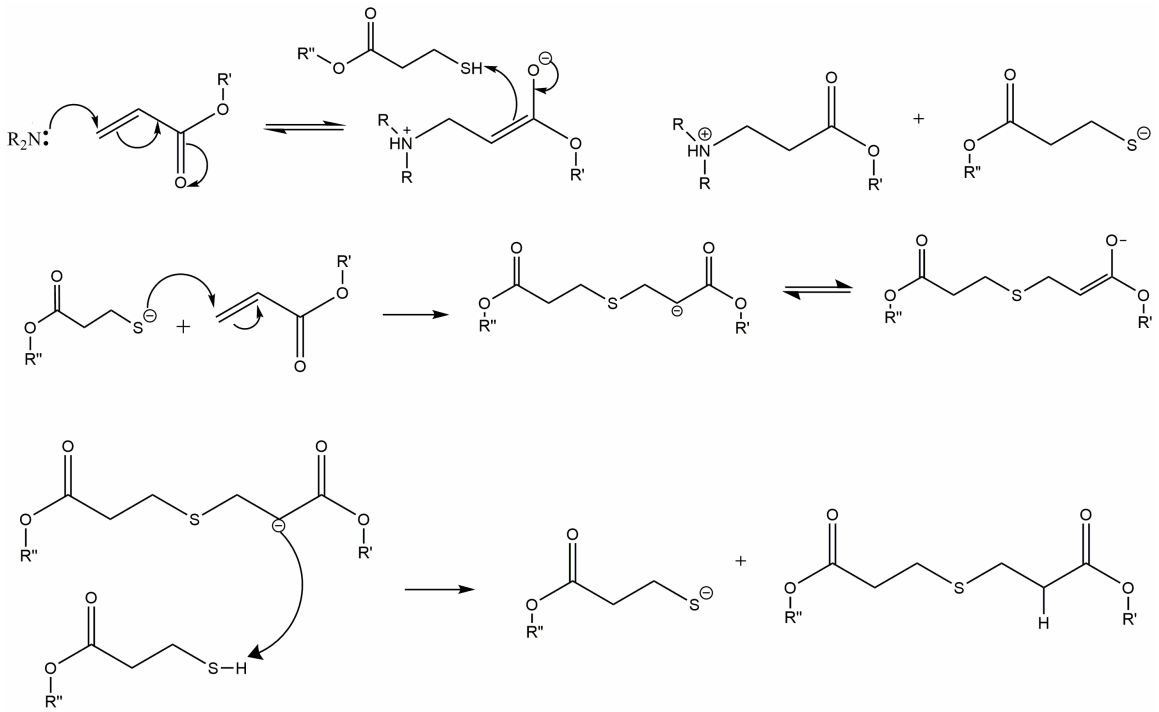

Scheme 1-3. Nucleophile-initiated thiol-acrylate mechanism using a secondary amine.

The mechanism of the base-catalyzed reaction has been thoroughly investigated and is shown in Scheme 1-4.[9] The base deprotonates a thiol forming a thiyl species, which forms an anionic species with the electron deficient enes that start a chain propagation process.[3,10] One difference between the Michael addition reaction and a free-radical thiol-ene polymerization is the absence of the self-termination step.

Termination most commonly occurs by two active radical species reacting with one another instead of the monomer or by oxygen inhibition.

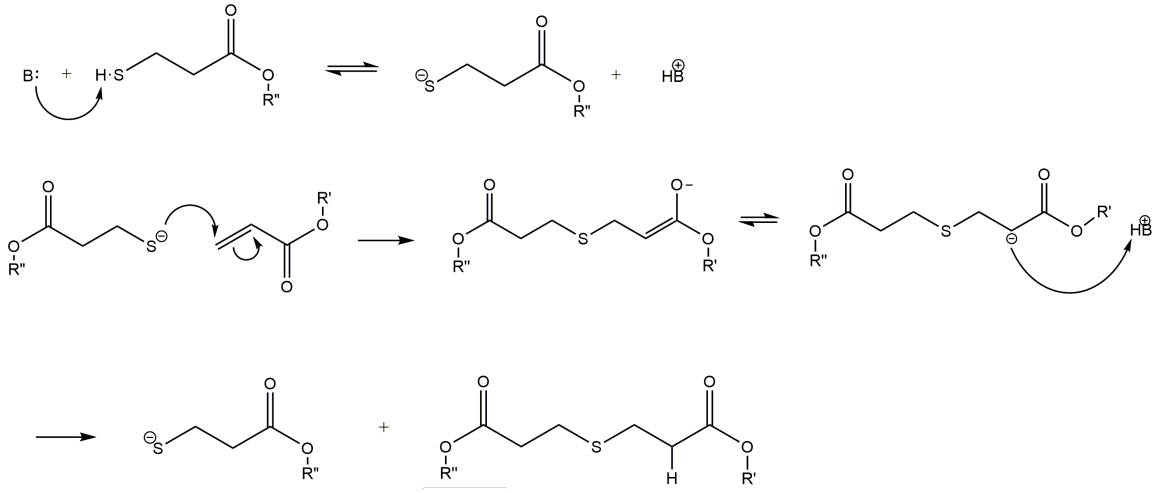

Scheme 1.4 Base-catalyzed thiol-acrylate reaction mechanism

Biomedical materials using photoinitiators such as benzoyl peroxide that generate radicals to initiate the reaction, have shown cell necrosis and aptosis.[11] Despite the harsh effects of radicals, PEG-based materials synthesized using thiol-acrylate photopolymerization chemistry have been studied extensively in many biocompatible applications such as tissue replacement due to PEG's hydrophilicity and similarities to the extracellular matrix found within the body.[12,13] As previously discussed, the thiol present in the PEG-based photopolymerization helps to minimize the radical inhibition.

A tertiary amine catalyst, synthesized by reacting a trifunctional acrylate with a secondary amine, acts as a base to deprotonate the trifunctional thiol producing a thiyl anion. This thiyl anion begins the two propagation reactions. The tertiary amine catalyst is covalently bound to the acrylate monomer, prohibiting any leaching of hazardous byproducts. Another advantage of this reaction is that no light or heating element is

needed to drive the polymerization. This reaction, therefore, is more attractive for *in situ* polymerization in a critical sized bone defect than free-radical-based methods. With the advantage of the *in situ* amine catalyst Michael addition reactions, the biomedical application of thiol-acrylate Michael addition polymerization reactions was studied thoroughly.[14,9]

1.2 Tissue Engineering

Tissue engineering uses numerous material and cell techniques to repair or replace damaged tissues such as bone, cartilage, skin, ligaments, and the heart.[15] Bone regeneration has been a well-studied area of tissue engineering often encompassing many different approaches. The current technology for bone replacement uses autografts that include the patient's bone and allografts that are harvested from a donor. Synthetic scaffolds offer an alternative to the traditional grafts, but it remains a challenge for synthetic scaffolds to meet all of the requirements needed for tissue engineering to be a successful alternative. For a scaffold to meet the requirements for bone tissue engineering, properties of a scaffold must include biocompatibility, biodegradability, mechanical integrity, and porosity.[16] The scaffold must be biocompatible and support cell adhesion. Biodegradability of a material should occur at the same rate in which the bone tissue is being regenerated while not releasing any harmful degradation products. Mechanical integrity provides enough structural support to the void space to allow for movement. Porosity allows for the transport of minerals and the elimination of wastes while providing an interconnected network of blood vessels and tissue to form.[17]

Natural polymers structures such as chitosan, collagen, and chitin have been demonstrated as scaffolds for bone replacement but tend to be inconsistent depending on the environmental sources obtained of each. Despite the drawbacks, these polymers are abundant and can easily be processed into devices by casting, extrusion, molding or coating.

Additionally several other polymer systems such as poly(ethylene glycol) (PEG),[18,19] and polyurethane (PUV),[20] have been shown to support hASC proliferation and differentiation. The clear advantage of synthetic polymers is that they are highly pure, readily reproducible and have flexible mechanical, chemical and biological properties allowing them to be tailored to suit specific functions. A significant disadvantage of using synthetic polymers is that some, such as PLGA and PLLA, degrade into products, often acids that can perturb the scaffold microenvironment leading to cell dysfunction, death and potential rejection.[21] Families of these polymers have had their structures tuned to enhance certain properties needed for bone replacement. PLLA and PLGA are structurally similar with the main difference occurring in PLLA with the pendent methyl group. The methyl group causes the molecule to have chirality opening up the possibility of different isomers depending on the application. PLGA's main disadvantage is the rapid degradation in vivo due to the extent of crystallinity contained throughout the polymer. Another polymer of interest, PCL is poorly water-soluble with a melting temperature of 58 to 63 °C.[22] Similar to PLLA and PLGA, the degradation of PCL occurs by bulk or surface hydrolysis of ester linkages resulting in a byproduct of caproic acid.[18] PCL degrades slowly in physiological conditions and can persist *in vivo* for up to 2 years.[22] At high concentrations of these

degradation products, local tissue acidity may increase, resulting in adverse responses such as inflammation or fibrous encapsulation.[22]

Common bone replacement materials are nanocomposites that contain an inorganic phase and a polymeric organic phase. The inorganic phase is usually a ceramic material that should mimic, as closely as possible, the natural bone architecture to ensure cell attachment and migration within the porous materials. Additionally, ceramics should be absorbed overtime or integrated with the surrounding tissue and eventually replaced by new or existing host tissue.[22] Bioceramics used in current hASC osteogenic studies include custom-made akermanite, β-TCP scaffolds, HA/β-TCP composites[23], and bioactive glass; commercially available scaffolds made of β-TCP (Synphare® and ChronOS®)[24], HA (Engipore®), HA/β-TCP composites (CopiOS™ Bone Void Filler)[25], Titanium (Trabecular Titanium®)[26]; and polymeric composites made of β-TCP and HA. Hydroxyapatite [$Ca_5(PO_4)_3(OH)$] is the most common ceramic used since it's commercially available and cost-efficient. It is an inorganic crystalized mineral found in teeth and bones with porosity and percent mineralization varying among bone types that enhances the osteogenic capability of polymeric materials, thus aiding in bone formation *in vivo*.[27]

One property that is important to the formation of blood vessels, vital nutrients, and mineral support of a bone scaffold is its porosity.[28,29] Fabrication methods of the scaffold affect the porosity and thus must be chosen to maintain the structure of the scaffolds. Porosity can be achieved within a polymer scaffold by thermal induced phase separation precipitation, which relies on the thermodynamic instabilities of two polymer phases. Particulate leaching only dissolves the added precipitate via evaporation of the

solvent that is added previously to the scaffold.[30] Thus, pores appear where the solvent dissolved the precipitate granules. Crosslinked thiol-acrylate polymers are often thermoset in nature, thus the use of solvents is not applicable. A fabrication method not using solvents is termed gas-foaming that involves a blowing agent (i.e. nitrous oxide) that can be applied to a nanocomposite material in a pressurized foaming apparatus. The expelled polymer/ceramic matrix has the ability to directly conform to a bone void by tuning the polymer gelation time without the need for pre-sculpting before placement into the defect.

However, the progression and expansion of synthetic composite materials used for tissue engineering caused a greater need for materials to contain an integrated antibacterial component. Many bacterial infections are associated with orthopedic surgeries that use implants, thus the prevention of acquiring such infections without having antimicrobial resistance is vital to the field of tissue engineering. Saravanan et. al demonstrated inoculation of *E. coli* and *S. aureus* by incorporating silver nanoparticles into a composite synthesized using chitosan and hydroxyapatite.[31] The mechanism to which silver ions kills bacterial cells remains elusive, but some theories note the attachment and penetration of the silver ions to the cell wall of the bacteria, which disrupts the enzyme activity.[32]

1.2.1 Cell Seeding

Cell seeding and cell encapsulation are two thoroughly researched methodologies to transport cells into the body thus decreasing the time needed for tissue regeneration. Cell seeding, the placement of cells onto the surface of a synthetic scaffold, is often used as an *in vitro* method to determine how the material will support

the growth of tissues *in vivo* on the surface. The adhesion of stem cells to a polymeric surface is a complicated process involving integrins and other ECM proteins. The mechanical strength and crosslinking density play a role by withstanding force that the cell exerts as it spreads across the polymer's surface. The wettability of a polymer determined by contact angle measurements is an important property where the contact angle should be in a moderate hydrophilicity range to support cell adhesion.

Extensive research has been performed on the functionalization or incorporation of cell adhesive moieties into synthetic scaffolds to support cell adhesion, but not many inert polymers without RGD or collagen peptides have been studied.[33] The incorporation of RGD into the polymerization process is expensive and time consuming with extensive purification needed. Rydholm et al. used unreacted thiol molecules that are usually leftover after thiol-acrylate photopolymerizations due to the homopolymerization of acrylates to attach RGD to acrylated PEG(3400).[34] Khire et. al showed how a thiol SAM gradient was used to obtain an osteoblast gradient via a Michael addition using RGDS.[35]

1.2.2 Cell Encapsulation

Cell encapsulation within a 3D matrix offers a different perspective to the 2D seeding monolayer methods by allowing cells to migrate throughout a scaffold and intramolecularly communicate with each other. The scaffold should provide structural support while still providing a means for transporting and binding the encapsulated cells together for *in vivo* purposes. With the entire 3D scaffold being comprised of cells, the size constraints of cell spreading often exhibited in cell seeding are not an issue. The

surrounding tissue *in vivo* gives off biological signals that direct tissue growth to the cells throughout the entire 3 dimensional structure.

Many different hydrogels have been used for the cell encapsulation.[36,37] Alginate is a polysaccharide of (1-4)-linked β-D-mannuronic acid (M) and α-L-gulutonic acid (G) that varies in sequence and number depending on the sources and molecular weight of the co-polymer. It forms a gel immediately by contact with a solution of $CaCl_2$. The positively charged calcium ions complexes with the negatively charged carboxylic acid component of the repeating mannuronic and gulutonic groups within alginate forming a hydrogel.

Cell-laden alginate beads have shown success in the encapsulation and viability of stem cells. Siti-Ismail et al. kept cells viable for up to 260 days in alginate-Ca beads in cell media without any external alteration.[38] While alginate beads act as a nontoxic vehicle for transplanting cells into the body, they lack the ability to adhere cells to its surface; therefore there have been a number of articles published on mixing alginate and gelatin to the alginate mixture before cells are added to it.[39] Rui et al. showed an increase in cell proliferation and adipogenic differentiation for the gelatin/alginate beads compared to the alginate beads.[40] Mixing collagen with alginate has also been successful in increasing proliferation.[41]

Other common hydrogels used for the immobilization of cells are agarose and gelatin. Agarose consists of galactose and anhydrogalactopyranose that forms a gel when cooled due to its upper critical solution temperature (UCST). The monosaccharides are water-soluble with each other and are in a random coil formation

above that temperature. Below the UCST, the structure changes to a double helix forming a gel, and the H-bonding between the water and the galactose stabilize it.[42]

Research has also been done in the Mikos research group where Wang et al. used gelatin as a leaching porogen contained within an oligo(poly(ethylene glycol)) fumarate to form a macroporous hydrogel that successfully encapsulated stem cells with viability of 16 days.[43] Hoffman et al. demonstrated how stem cells could be transplanted by encapsulating cells within a PEG based hydrogel. The degradation of the hydrogel was tuned to spatially and temporally control the migration of stem cells throughout the gel by increasing the mesh size.[44]

Kristi Anseth and colleagues have shown in numerous papers the impact of spatial and temporal control throughout the scaffold has on the regeneration process.[45] Contrary to the previous work described, polysaccharides were not used for the encapsulation process. Instead, tethering functional groups to a hydrogel was demonstrated by functionalizing PEG hydrogels with phosphates, Benoit et.al was able to tailor encapsulated stem cells to undergo osteogenisis differentiation by this method.[46]

This dissertation entails an in depth study of thiol-acrylate polymers synthesized via a base-catalyzed or nucleophile-initiated mechanism. PETA-co-TMPTMP is demonstrated in the second chapter as a highly crosslinked thiol-acrylate network that could be used a biomaterial. The PETA polymer will be mixed with hydroxyapatitie and characterized by performing mechanical and cyto-toxicity studies. PETA-co-TMPTMP was further studied in chapter three for its osteogenic capability, antimicrobial application, and *in vivo* study using a live animal spinal fusion model. The fourth chapter

characterizes different PEGDA(700) based polymers and cell behavior on them. The chapter then goes into a more detailed study focusing on two different Mn polymers with varying amine concentrations and the properties needed for the adhesion or non-adhesion of stem cells. Encapsulation of hASCs using alginate and agarose within a polymer matrix including PEGDA(700) and TMPeTA(692 & 912) polymers is also described using live/dead staining.

Chapter 2. PETA-co-TMPTMP(HA) Composites for Bone Replacement

2.1 Chapter Summary

Bone tissue engineering approaches using polymer/ceramic composites show promise as effective biocompatible, absorbable, and osteoinductive materials. A novel class of *in situ* polymerizing thiol-acrylate based copolymers synthesized via an amine-catalyzed Michael addition was studied for its potential to be used in bone defect repair. Both pentaerythritol triacrylate-co-trimethylolpropane tris(3-mercaptopropionate) (PETA-co-TMPTMP) and PETA-co-TMPTMP with hydroxyapatite (HA) composites were fabricated in solid cast and foamed forms. These materials were characterized chemically and mechanically followed by an *in vitro* evaluation of the biocompatibility and chemical stability in conjunction with human adipose-derived mesenchymal pluripotent stem cells (hASC). The solid PETA-co-TMPTMP with and without HA exhibited compressive strength in the range of 7–20 MPa, while the cytotoxicity and biocompatibility results demonstrate higher metabolic activity of hASC on PETA-co-TMPTMP than on a PCL control. Scanning electron microscope imaging of hASC show expected spindle shaped morphology when adhered to copolymer. Micro-CT analysis indicates open cell interconnected pores. Foamed PETA-co-TMPTMP HA composite shows promise as an alternative to FDA-approved biopolymers for bone tissue engineering applications.

2.2 Introduction

Bone tissue engineering shows promise as an alternative strategy to current surgical techniques to replace or restore the function of traumatized, damaged, or lost bone.[47,48] Over the past several decades, bone grafts have advanced as standard

treatment to augment or accelerate bone regeneration.[48] Autogenous and allogeneic bone grafts do not provide a clinically convenient method for conformal filling of a critical sized bone defect compared to a proposed injectable biomaterial providing mechanical support and biological cues to support bone regrowth.

To date, a clear trend towards the use of composite scaffolds as an alternative to allogeneic or autogenic bone can be observed in many of the current models.[49-52] Native bone is composed of naturally occurring hydroxyapatite (HA) crystals distributed within an organic matrix, with porosity and percent mineralization varying among bone types.[48] Synthetic HA has been widely used in bone scaffold fabrication because it possesses osteogenic properties.[53,54] While several of these studies involved the use of extracellular matrix or other naturally occurring compounds such as collagen, decellularized bone or chitosan, synthetic polymers can be highly pure, readily reproducible and have adaptable mechanical, chemical, and biological properties to suit specific clinical applications. Much of the research utilizing synthetic polymers in hASCs-combined tissue engineering has been focused on hybrid cell/scaffold constructs using degradable polyester polymers such as poly(lactide-co-glycolide) (PLGA), poly(L-lactide) (PLLA), and poly-ε-caprolactone (PCL).

Thiol-ene chemistry possesses many advantageous properties for tissue engineering applications.[48-51] Specifically; thiol-acrylate chemistry has already been used in biomedical applications, but has only been explored in photolytically polymerized systems.[34,55,56] Thiol-acrylate polymers synthesized via an amine-catalyzed Michael addition reaction have not been explored for biomedical applications. Scheme 2-1 displays how the general reaction proceeds by the formation

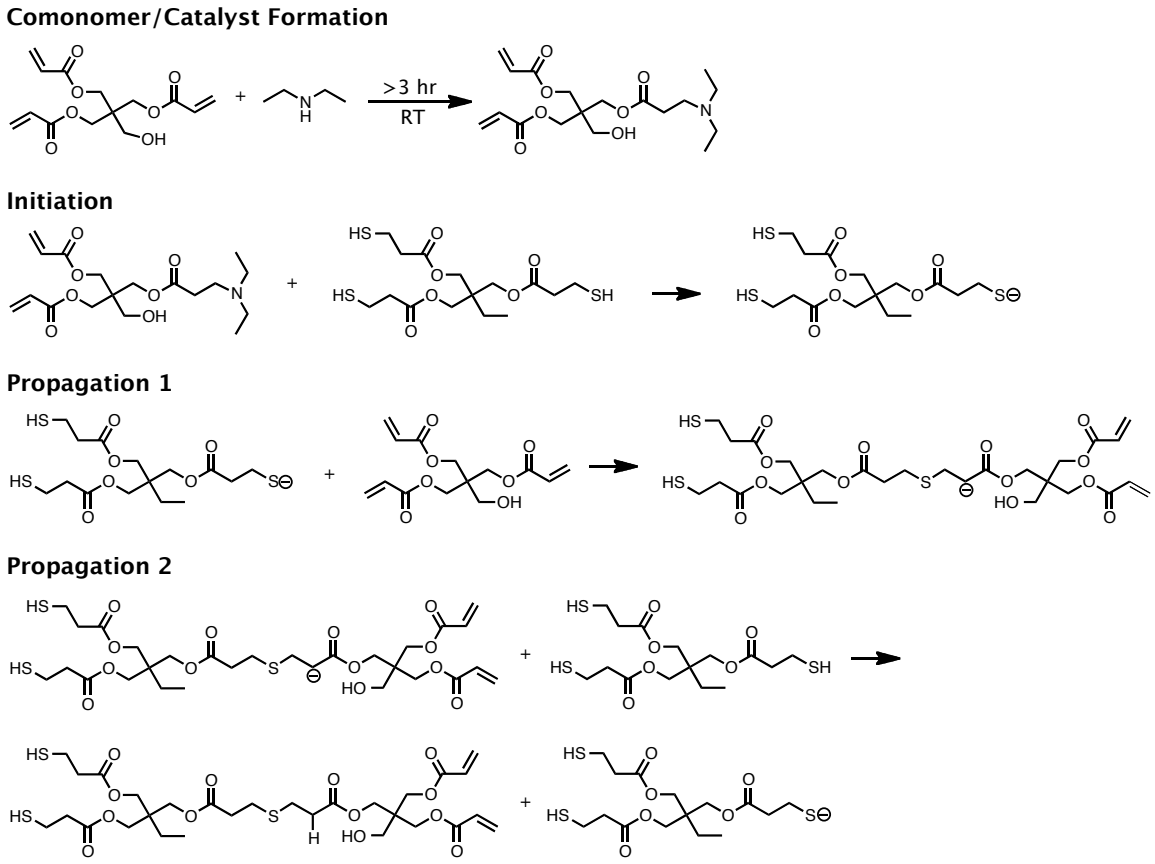

Scheme 2-1. *In situ* tertiary amine catalyzed anionic step growth polymerization mechanism.

of a catalyst/comonomer molecule through the Michael addition of the secondary amine (diethylamine) across the double bond found in acrylate monomers. These activated acrylates were then individually mixed with a thiol comonomer (trimethylolpropane tris(3-mercaptopropianate)). This *in situ* tertiary amine catalyzed Michael addition proceeds via a chain "process" due to the sequential chain transfer step after each addition. The Michael addition reaction causes the polymerization to follow the rules and attributes of a step-growth mechanism in terms of molecular weight and physical properties.

In this study, the synthesis and characterization of a novel class of thiol-acrylate copolymers has been reported.[57] The tunable gel times and mechanical properties were

determined. A series of biocompatibility tests indicate this new synthetic polymer is capable of supporting human adipose derived stromal cell culture. Furthermore, SEM and micro-CT studies illustrate the morphology of solid and foamed PETA-co-TMPTMP HA composites. These materials are a potentially transformative class of novel biomaterials with the application for *in situ* conformal polymerization at the site of trauma.

2.3 Methods and Materials

2.3.1 Chemicals

All chemicals were used as received. Trimethylolpropane triacrylate (TMPTA), poly(ethylene glycol) diacrylate (PEGDA) (Mn 700), poly(ethylene glycol) diacrylate (PEGDA) (Mn 575), poly-ε-caprolactone (PCL), trimethylolpropane ethoxylate triacrylate (TMPeTA) (Mn 912), trimethylolpropane ethoxylate triacrylate (TMPeTA) (Mn 692), trimethylolpropane tris(3-mercaptopropianate) (TMPTMP), and triethylamine (TEA) were obtained from Aldrich. Diethylamine (DEA) was obtained with 99% purity from ACROS organics, and pentaerythritol triacrylate (PETA) was obtained from Alfa Aesar.

2.3.2 Choosing Catalyst Concentration and Polymer Fabrication

Prior to choosing the base catalyst concentration for each acrylate listed in the above paragraph, further experiments were performed. Twenty stock solutions were prepared by combining PETA (9 g) with varying concentrations of DEA with respect to the acrylate functionality ranging from 2.8-35.1%. These PETA stock solutions were stirred for 3 hours prior to the addition of TMPTMP. Gel time was calculated based on two methods. The first way included pumping air through a syringe containing the PETA stock/TMPTMP solution. The time at which the air bubbles were no longer able to pass

through the solution was set as the gel time. The second method estimated gel time using the naked eye when the flow of the polymer ceased while simultaneously inverting the vial.

The 16.1% DEA stock solution was studied further since it allowed for an appropriate time range needed for mixing and application of the material or the lowest gel time. The 3-hour stir time mentioned above needed for the synthesis of the stock solution was determined by measuring the gel times as a function of stir time. An aliquot of 5 grams of the stock solution was transferred to a vial then 4.731 g of TMPTMP were added at increments of 15 minutes for the first hour then at increments of one hour until the stir time became constant.

DEA was also used to catalyze TMPeTA(692) and TMPeTA(912) at 30.2% and 14.4% DEA mol% while TEA was used to catalyze PEGDA(575) and PEGDA(700) at 0.48% and 0.68%. The amount of DEA added was determined based on the lowest gel times determined by Chris Bounds relative to acrylate functionality.[58] Since PEGDA is difunctional, a trifunctional amine was chosen to prevent losing acrylate functionality.

2.3.3 Mass Loss and Extract Cytotoxicity

With the catalyst concentrations optimized for gel time, PEGDA(575), PEGDA(700), TMPeTA(692), TMPeTA(912), PETA with and without 20% HA were subjected to mass loss and extraction testing to determine the least toxic polymer for bone replacement. All samples were weighed to obtain the initial mass before placement in stromal media (DMEM, 10% FBS, and 1% triple antibiotic solution). The samples were incubated on an orbital shaker with 5 mL stromal media at 37 ^{o}C and 200 rpm/min for 7 days. The samples were removed and weighed. The initial mass (Wi) and

the mass after the 7 day soak time (Wf) were used to calculate the relative weight%. Relative Weight (%) is calculated based on equation (2-1)

$$\text{(Eq 2-1)}\quad \text{Relative Weight}(\%) = \frac{Wi}{Wf} x100\%$$

The stromal media(extracts) from the mass loss test that the samples were soaking in for 7 days were filtered (0.2 μm pore size) and pipetted (100 μL/well) into a 96-well plate previously sub-cultured with hASC (2,500 cells/well) and incubated in a CO_2 incubator at 37 ^oC containing 5% CO_2 for 24 hours. The cellular viability on scaffold cultures was determined using the AlamarBlue® assay by adding 10 μL of AlamarBlue® reagent to each well and re-incubating at 37 ^oC in 5% CO_2 for 2 h. The fluorescence was measured at an excitation wavelength of 530 nm and an emission wavelength of 595 nm using a fluorescence plate reader. The tissue culture treated plastic 96-well plate served as a control substrate.

2.3.4 Preparation of the Foam PETA-co-TMPTMP

From the polymers fabricated in Section 2.3.2, the PETA-based polymer (PETA-co-TMPTMP) was chosen for further analysis. The preparation of the composite material was prepared by adding 16.1% PETA/DEA stock solution to TMPTMP in a 1:1 molar functionality ratio followed by 3 hours of mixing. HA (20% wt/wt) was added to the PETA-co-TMPTMP solution and cast into cylindrical molds (10 mm (diameter) x 10 mm (height)). All of the hydroxyapatite was originally added to only the stock solution at 20% w/w, but it dispersed better by splitting this amount and pre-mixing separately with the TMPTMP and stock solution. The foamed composite copolymer was fabricated by pouring the PETA-co-TMPTMP with HA into a 250 mL pressurized spray canister using 7 g-compressed nitrous oxide as a gaseous porogen. The foamed composite copolymer

was expelled from the canister into the same cylindrical molds used for solid casting. The same foamed procedure was used for the solid copolymer without HA. Another 20% HA foamed sample was prepared *in vitro* by foaming directly into a beaker containing stromal cell media instead of cylindrical molds to test the impact that the physiological solution would have on the polymerization and foam structure.

2.3.5 FTIR

The conversion of the PETA acrylate used in the thiol-acrylate reaction as a function of time involving the *in situ* amine catalyzed Michael addition was measured over a 24-hour period using a Bruker Tensor 27 FTIR. The acrylate peak at 1650 cm^{-1} was monitored and integrated at 1-minute intervals. Equation 2-2 shows the percentage conversion calculation in real time, where T is conversion at a particular time interval, A is the peak area, and To is time the in initial time at 0 minutes.

$$\text{(Eq 2-2).} \quad \%\text{Conversion}(T) = \frac{A(To) - A(T)}{A(To)} \times 100\%$$

2.3.6 Mechanical Testing

Compression testing was performed on four specimens of each PETA scaffold type (foamed PETA-co-TMPTMP with HA (20%), *in vitro* foamed PETA-co-TMPTMP with HA (20%), foamed PETA-co-TMPTMP without HA, and solid PETA-co-TMPTMP) at room temperature using a hydraulic universal testing machine (Instron Model 5969, Canton, MA, USA) at an extension rate of 0.5 mm/min to a maximum compression strain of 90%. The solid PETA scaffolds were prepped in a PDMS cylinder mold that measured 10 mm (diameter) × 10 mm (height) and the foamed samples were prepared in a weigh boat and cut using a 10 mm (diameter) x 10 mm (height) biopsy punch.

2.3.7 PETA-co-TMPTMP Mass Loss and Extract Cytotoxicity

Each PETA composite copolymer-HA (foam and solid) as a function of composition was analyzed for mass loss and extract cytotoxicity. PCL foam, prepared through thermally-induced phase separation,[59] served as a positive control, and a solid cast PETA composite provided an internal comparison for previous experiments. The same mass loss and extraction procedure used for the selection of polymers above was used for the PETA samples (Section 2.3.3).

2.3.8 hASC Isolation and Culture

Liposuction aspirates from subcutaneous adipose tissue were obtained from three donors. All tissues were obtained with informed consent under a clinical protocol reviewed and approved by the Institutional Review Board at the Pennington Biomedical Research Center. Isolation of hASC was performed as described elsewhere.[60] The initial passage of the primary cell culture was referred to as “Passage 0” (p0). The cells were passaged after trypsinization and plated at a density of 5,000 cells/cm^2 (‘‘Passage 1’’) for expansion on T125 flasks in order to attain 80%. Passage 2 of each individual was used for cell viability test after acute exposure to the scaffold medium extractives and on scaffolds after loading using a spinner flask.

2.3.9 hASC Loading on Scaffolds and Culture

5 μL (1.0×10^4 cells/μL) of Passage 2 of each donor (n = 3) were pooled and directly seeded on the top of each sample. After 30 min of incubation at 37 °C and 5% CO_2, the opposite side of each sample was loaded with the same number of cells by the same approach. Experimental groups included: PETA-co-TMPTMP solid, PETA-co-TMPTMP foam, PETA-co-TMPTMP+HA solid, PETA-co-TMPTMP+HA foam, PCL solid

and PCL foam. Scaffolds seeded with hASCs were immediately transferred to new 48-well plates and cultured in stromal media (DMEM, 10% FBS, and 1% triple antibiotic solution) for 7 days followed by sample collection to assess cell viability with AlamarBlue® stain.

2.3.10 *In Vitro* hASC Viability on Scaffolds with AlamarBlue®

The viability of cells within the scaffolds in stromal media was determined after 7 days using an AlamarBlue® metabolic activity assay. The scaffolds were removed from culture, washed three times in PBS, and incubated with 10% AlamarBlue® in Hank's balanced salt solution (HBSS) without phenol red (pH 7) for 90 min. Aliquots (100 µL) of AlamarBlue®/HBSS were placed in a 96-well plate in triplicate, and the fluorescence was measured at an excitation wavelength of 530 nm and an emission wavelength of 595 nm using a fluorescence plate reader.

2.3.11 *In Vitro* hASC Viability on Scaffolds with PicoGreen®

Scaffolds were sectioned using forceps and then incubated with 0.5 mL proteinase K (0.5 mg/mL) at 56 ºC overnight. The mixture was centrifuged for 5 minutes at 108 G, and 50 µl aliquots of the mixture were mixed with 50 µl PicoGreen® dye solution (0.1 g/mL, Invitrogen®) in 96-well plates. Samples were excited at 480 nm and total DNA concentration was compared to the live control. Scaffold without cells were used to subtract the background fluorescence emission from all readings.

2.3.12 SEM Analysis

The solid precast PETA-co-TMPTMP polymer was gelled in a 12-well plate to form a thin layer (1 mm thickness). The polymers seeded with stem cells were fixed first for 30 mins by 2% glutaraldehyde (GA) (made with 2parts Cocadylate, 1 part 8% GA

and 1 part distilled H_2O). The samples were subjected to a dehydration procedure by using 30-100% ethanol solution increasing by 10% increments every 30 minutes. 100% HDMS (hexamethyldisilazane) was added to the samples to replace the dried air and ethanol overnight. A conductive platinum coating was applied using EMS550X sputter coater for 2 minutes followed by standard SEM analysis. *In situ* and *in vitro* foamed samples were also subjected to standard SEM analysis.

2.3.13 Micro-CT Analysis

Three PETA-co-TMPTMP foams were fabricated with pressurized extrusion foaming as described with the first two foams having 0 and 20% HA content. The third sample also had a 20% HA content, but was foamed into the beaker containing stromal media (*in vitro*). Samples were sliced into 1-2 mm approximate cuboids of 10-15 mm height. Samples were imaged with 11 keV monochromatic x-rays with 2.5 μm/px resolution at the tomography beamline at the Center for Advanced Microstructures and Devices (Louisiana State University, Baton Rouge, LA). Projections numbered 720 corresponding to Dq = 0.25; projection exposure time varied between 2 and 4 seconds, but reconstruction algorithms ensure normalized data. The two different datasets are directly comparable, both as an aggregate dataset and as slices. Reconstruction data are 16-bit signed integer with mean air intensity scaled to zero. Pore size was measured using ImageJ 64.

Volume renderings were produced from the 3 foamed samples 3D data using Avizo 7.0.1 (Visualization Services Group). Two overlapping sub-volumes are rendered simultaneously, one with a red-orange-white colormap corresponding to trithiol-triacrylate foam, and the other with a blue-green colormap corresponding to HA

inclusions. Orthogonal slices, made using ImageJ, have equal scale, brightness, contrast, and grey map settings.

All results were expressed as mean ± SEM. Normality of the data was confirmed using the Shapiro-Wilk test ($P < 0.001$). Data were analyzed with one or two-way analysis of variance (ANOVA), followed by Tukey's minimum significant difference *post hoc* test for pairwise comparisons of main effects. For all comparisons, a P-value < 0.05 was considered significant.

2.4 PETA Characterization Results/Discussion

Thiol-acrylate chemistry incorporates nearly all the materials used in the synthesis process into one complete network greatly reducing the risks of leaching toxic monomers and short chain oligomers, as is observed with other techniques.[61,62] Additionally, bioactive compounds such as peptides can be copolymerized as has been demonstrated with photoinitiated thiol-acrylate chemistries.[63] Third, and perhaps most importantly, these materials can rapidly polymerize in situ and in an *in vitro* environment through an attached tertiary amine, self-catalyzed ‘‘chain’’ process.

These materials have broadly tunable mechanical and chemical properties in that many compositions of polymer chain repeating units with thiol and acrylate moieties can be created using the same approach and biocompatible reaction scheme. By varying the number of functional moieties, straight chain, branched, and crosslinked compositions can be synthesized. However, for *in situ* polymerization to be practical, gel times must be tunable across a range from minutes to hours, which is easily achievable using this thiol-acrylate system. The strength of these materials can also be manipulated by varying the initial DEA concentration, as the functionality and crosslink

density are both a function of the DEA concentration. This is caused by the first Michael addition with the secondary amine, which results in the loss of an acrylate functionality to the trifunctional acrylate.

2.4.1 Determining Gel Times

The method in which the gel times were estimated by using the naked-eye to determine when the polymer no longer flows produced shorter gel times compared to the method using the air-flow apparatus. To prevent underestimating the gel times, the air apparatus gel time method was used.

As shown in Figure 2-1, the PETA-co-TMPTMP gel time point decreased as the DEA catalyst concentration increased as seen in the left hand side of the graph, which was the expected trend due to the increased reaction rate.[14] However, the gel time started to increase between the samples containing 16.1 and 17.8 mol% DEA and continued with increasing DEA mol%. The unexpected increase in the gel time could be explained via FTIR analysis. Using critical % conversion equation ρ_c from Carother's theory and Flory and Stockmayer theory,

(Eq. 2-3): Flory and Stockmayer: $\rho_c = 1/(1 + f - 2)^{1/2}$

(Eq. 2-4) Carother's: $\rho_c = 2/f_{avg}$

it was found that increasing the DEA mol% past 17.8% caused a higher percent conversion to be necessary for gelation. The increase in amine catalyst decreased the acrylate functionality, which is indirectly related to ρ_c. Due to the loss of monomer functionality, ρ_c rapidly increased thus prohibiting gelation from taking place within the expected time.

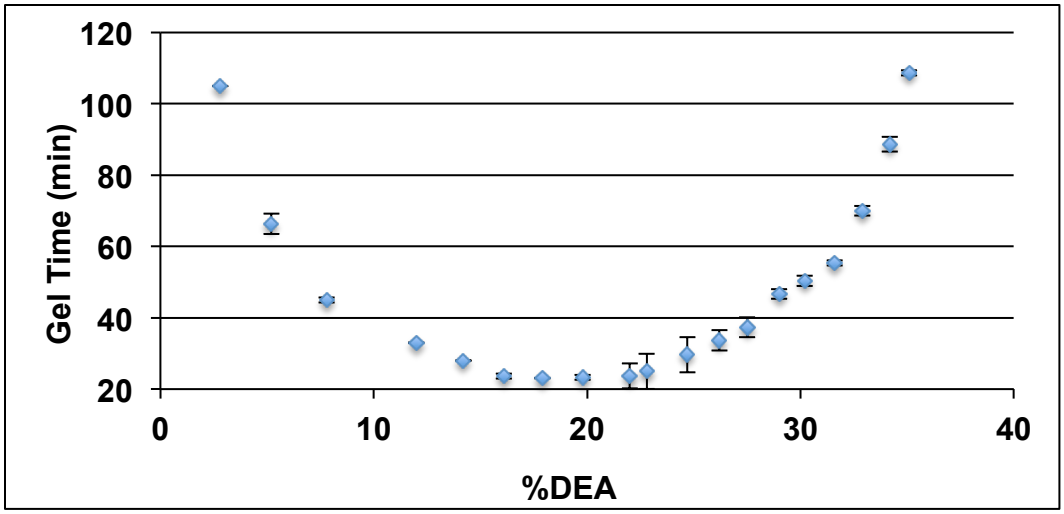

Figure 2-1. Gel times as a function of amine catalyst relative to acrylate functionality.

The 16.1% DEA was chosen for PETA because it produced the lowest gel time of ~23.5 minutes. The gel times as a function of stir time increased for the first 2 hours as shown in Figure 2-2 then became constant. A 50 mL stock of PETA and DEA was stirred, and 5 mL of the stock was extracted at time intervals of 5, 15, 30, 45, 60, 120 ,180, 240, 300, 360, and 420 minutes. TMPTMP was added to each 5 ml stock aliquot and the gel time was calculated until it equilibrated. It was concluded that 3 hours would be sufficient for the amine to complete a Michael addition with the acrylate.

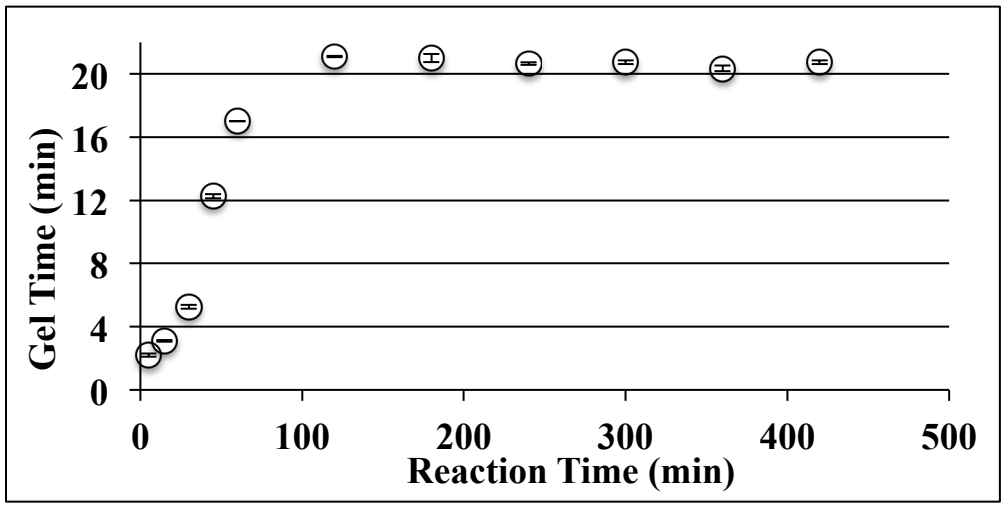

Figure 2-2. The gel times of 16.1%DEA/PETA stock as a function of reaction time.

The amounts of catalyst chosen for the TMPeTA(692) and TMPeTA(912) were based on calculated gel times from Chris Bounds,[58] but the gel times obtained did not match the trend that was noted in the PETA polymer. The gel times did not decrease then increase. This observation will be discussed in a later chapter. TEA was used to catalyze the PEGDA(575) and PEGDA(700) reaction to prevent a % loss of the acrylate functionality, since a trifunctional amine cannot add via Michael addition to an acrylate. Only a small amount is needed for a base catalyst reaction to polymerize, therefore less than 1% TEA was used for each.

2.4.2 FTIR

It was concluded from studying the reaction kinetics using FTIR that by varying the DEA concentration that the gel time and kinetics were somewhat related. Even though the gel time analysis trend appears that the reaction rate decreases after the catalyst concentration increases past 17 mol%, the FTIR disputes that observation showing an increase in the rate at high DEA concentrations. The acrylate peaks were integrated, and conversion was calculated to give at least 95% acrylate conversion in less than a 24-hour period of time shown in Figure 2-3. The 2.8% DEA polymer reached 95% conversion in 24 hours but a continued study showed that it reached a full 100% conversion in 32 hours. 16.1% DEA and 35.1% DEA reached full conversion in the 24 hour time period.

2.4.3 Choosing Acrylate Monomer Based on Mass Loss/Extract Cytotoxicity

The PETA-co-TMPTMP polymer was chosen for further analysis as a potential bone repair composite because the gel time could be optimized to ~20 min gel time. PETA was the most attractive acrylate in terms of biocompatibility and mass loss data.

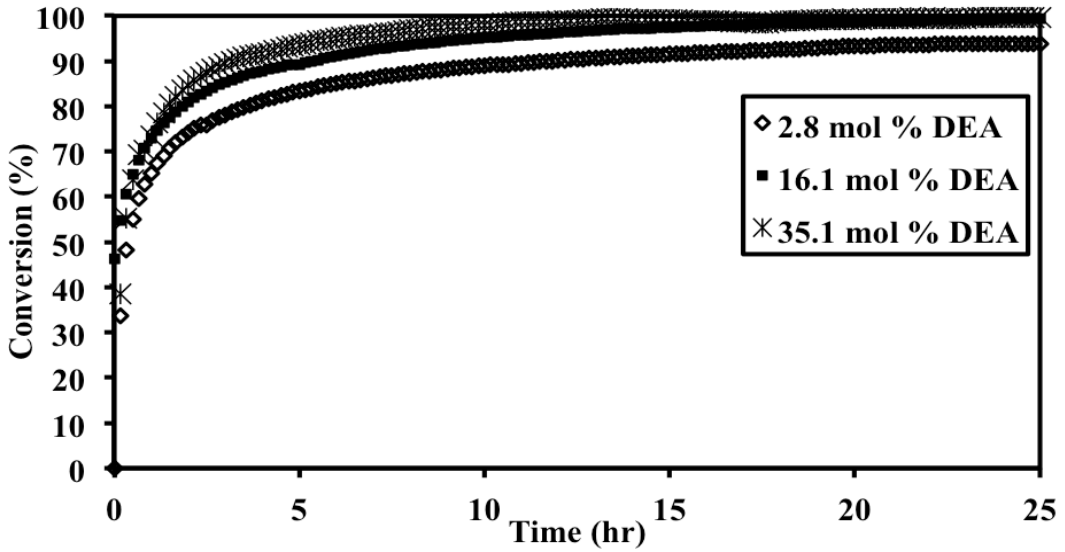

Figure 2-3. The %acrylate conversion over 24 hours for the 2.8%, 16.1%, and 35.1% DEA PETA-co-TMPTMP polymers.

In Figure 2-4, the conversion of AlamarBlue® by PETA and PETA-HA polymers is statistically the same as the tissue culture treated plastic and PCL control samples.

The mass loss over a week of exposure to physiological solution is represented in Figure 2-5. Both PETA and PETA-HA demonstrated greater stability than other

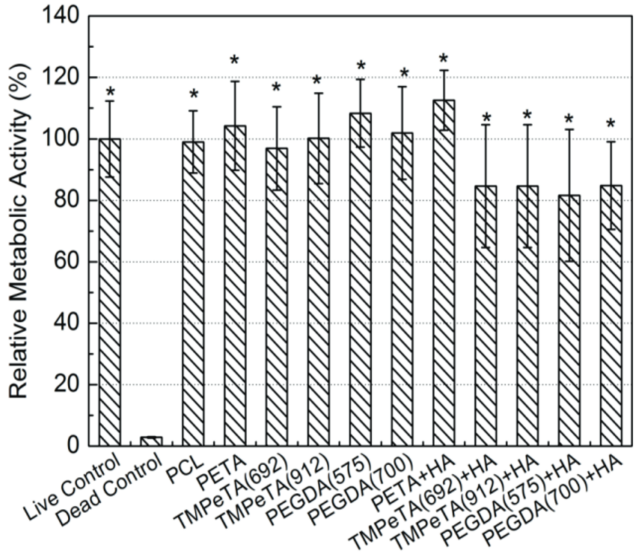

Figure 2-4. Relative metabolic activity of hASC in thiol-acrylate extractives as measured by Alamar blue fluorescent conversion. Relative fluorescent units have been normalized to live control. The asterisk indicates the sample is significantly different from the dead control.

experimental materials tested with similar losses to PCL. Greater physiological stability is considered an asset in the proposed application as bone regeneration time is often on the order of weeks to months.[47] The TMPeTA polymers and composites degraded much more rapidly than PETA, and the mass loss correlates with a possible hydrolysis reaction that would occur at more basic conditions.

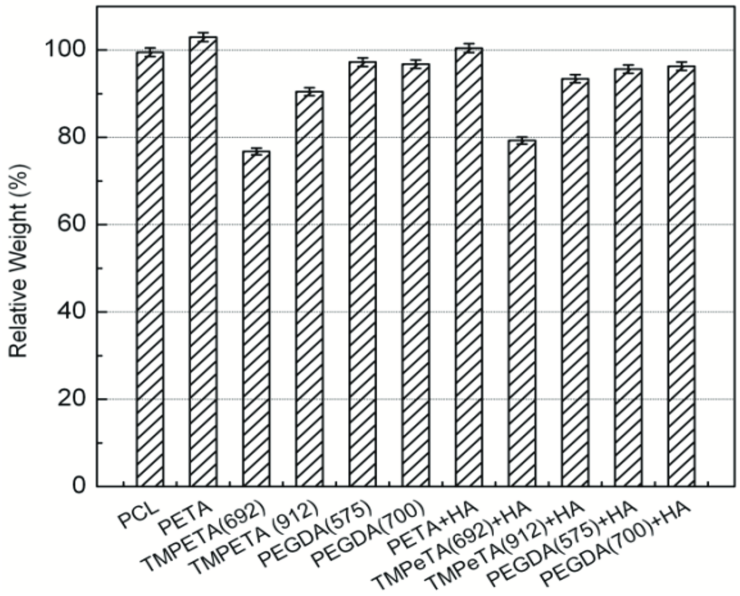

Figure 2-5. Mass loss after 7 days of incubation in stromal media. Samples are normalized to the starting mass for each sample.

2.4.4 Mechanical Testing

Biomimicry of the complex mechanical properties of native tissues proves elusive; native tissue presents unique mechanical properties of nonlinear viscoelasticity and strain-dependent moduli.[64] The compressive strength of human cortical and cancellous bone are 130–180 MPa and 4–12 MPa, respectively.[65] The mechanical testing of solid/foam PETA-co-TMPTMP materials is shown in Figure 2-6. Additionally, it was found that the maximal compressive strength of this PETA-co-TMPTMP (HA) solid at 90% strain is 19.23 $\pm$ 1.39 MPa, while the pure PETA-co-TMPTMP solid is 7.71 $\pm$

0.09 MPa. This result indicated that the introduction of ceramics improves the mechanical strength of the PETA copolymer similar to previously published results.[66,67] The compressive strength of PETA-co-TMPTMP (HA) foam is 0.72 ± 0.07 MPa while the pure PETA-co-TMPTMP foam is 0.14 ± 0.02 MPa. The foamed polymer has decreased mechanical strength compared with the solid polymer due to the large porosity. The mechanical properties of the copolymer polymerized *in vitro*, 0.84 ± 0.05 MPa, and *in situ*, 0.85 ± 0.06 MPa, in physiological media were very similar, indicating the presence of aqueous physiological media during the polymerization and foam structure formation has little impact on morphology and mechanical properties.

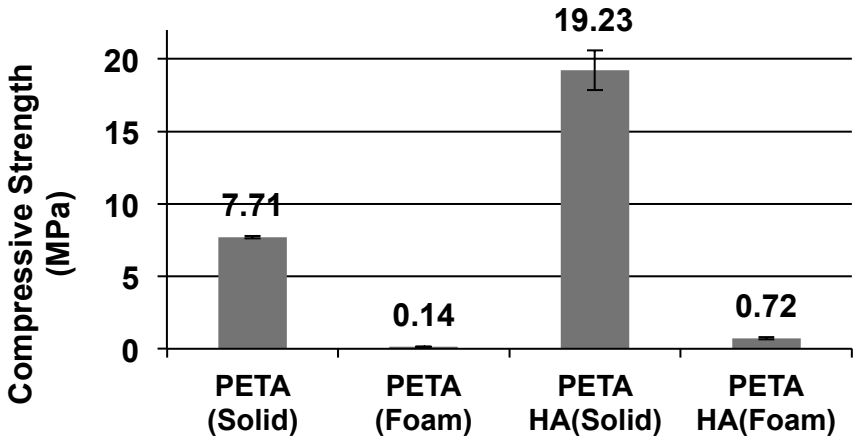

Figure 2-6. Compressive strength of PETA foamed/solid polymers with 0% and 20% HA. The introduction of ceramics improves the mechanical strength of the PETA-co-TMPTMP copolymer.

2.4.5 Mass Balance of PETA-co-TMPTMP

The polymer samples were extracted for 7 days in the stromal medium to determine the extent of mass loss. These extracts were later used in cytotoxicity testing. The copolymer-HA composite foam and solid cast copolymer were found to have significantly greater mass loss than the PCL control foam. The mass loss is believed to occur as a result of hydrolytic chain scission in a manner similar to the degradation of

PCL in physiological solutions.[68] The PCL sample increased in mass likely as a result of mineralization or nonspecific protein deposition (Figure 2-7). Similarly to PLLA and PLGA, the degradation of PCL occurs by bulk or surface hydrolysis of ester linkages resulting in a byproduct of caproic acid.[69] At high concentrations of these degradation products, local tissue acidity may increase, resulting in adverse responses such as inflammation or fibrous encapsulation.[47]

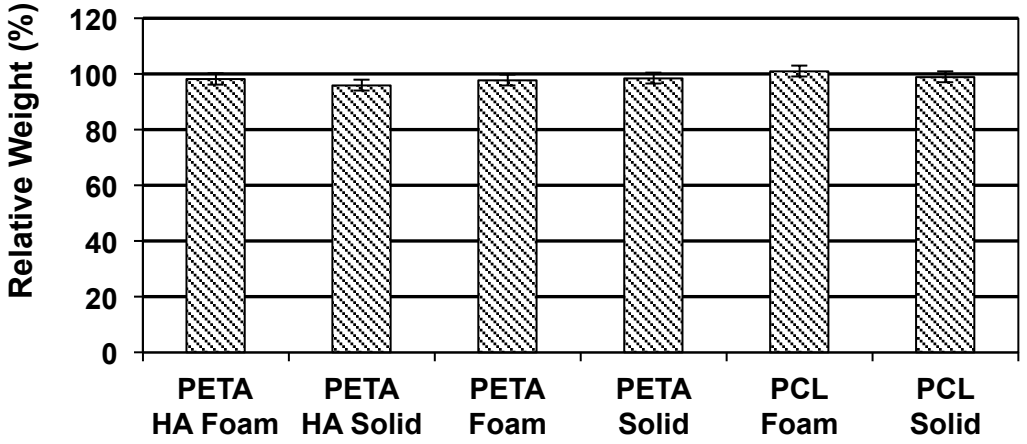

Figure 2-7. Mass loss of foamed samples after 7 days of incubation in stromal media. Samples are normalized to the starting mass for each sample.

2.4.6 Cytotoxicity of PETA Extracts

PCL foam was fabricated by thermally-induced phase separation from 1,4-dioxane followed by lyophilization.[59] Tissue culture treated polystyrene served as a positive control, while ethanol treated hASC served as a negative control. Cells exposed to both the copolymer and copolymer/HA composite (solid and foam) extracts had significantly higher metabolic activity than the dead control or cells exposed to the PCL extract (Figure 2-8, A). The reduction of hASC metabolic activity cultured on PCL does not correlate with a significant mass loss (Figure 2-7), indicating that this reduction in activity is likely not related to the generation of acidic PCL degradation products. The

technique for synthesizing the foamed version of PCL uses a harsh solvent that may not have been removed by freeze-drying.

2.4.7 Biocompatibility Test of hASC Cells on PETA-co-TMPTMP

The ability of the PETA-co-TMPTMP polymer to support hASC cell adhesion and short-term culture was evaluated using AlamarBlue® metabolic activity assays and SEM to examine cell morphology. Cells were cultured on solid cast PETA and PETA-HA (20% wt/wt) composite samples for 4 days in stromal media and assayed for fluorescent AlamarBlue® conversion; styrene treated tissue culture plates (TCP) served as a positive control. Compared with the positive control, hASC cultured on both the copolymer and the copolymer-HA composite had significantly lower metabolic activity (Figure 2-8, B).

Additionally, it appears that cells cultured on the copolymer-HA composite have significantly lower metabolic activity than cells on the non-composite. This may be a result of reduced metabolic activity associated with the differentiation of stem cells exposed to HA, a known osteogenic compound and may not be indicative of reduced biocompatibility.[55] Based on Figure 2-8, C**,** composite and PCL foam, but significantly lower metabolic activity than cells on tissue cultured treated polystyrene. Although the foam PETA copolymer has a much larger surface area than solid PETA copolymer, the results indicated that both forms of PETA copolymer supports hASC growth around the same level compared with the positive control.

2.4.8 DNA Quantification on Scaffolds (PicoGreen® Assay)

DNA content of hASC cultured on pure PETA, PETA composite, and PCL scaffolds was compared as a relative measure of cell viability and proliferation. After 4

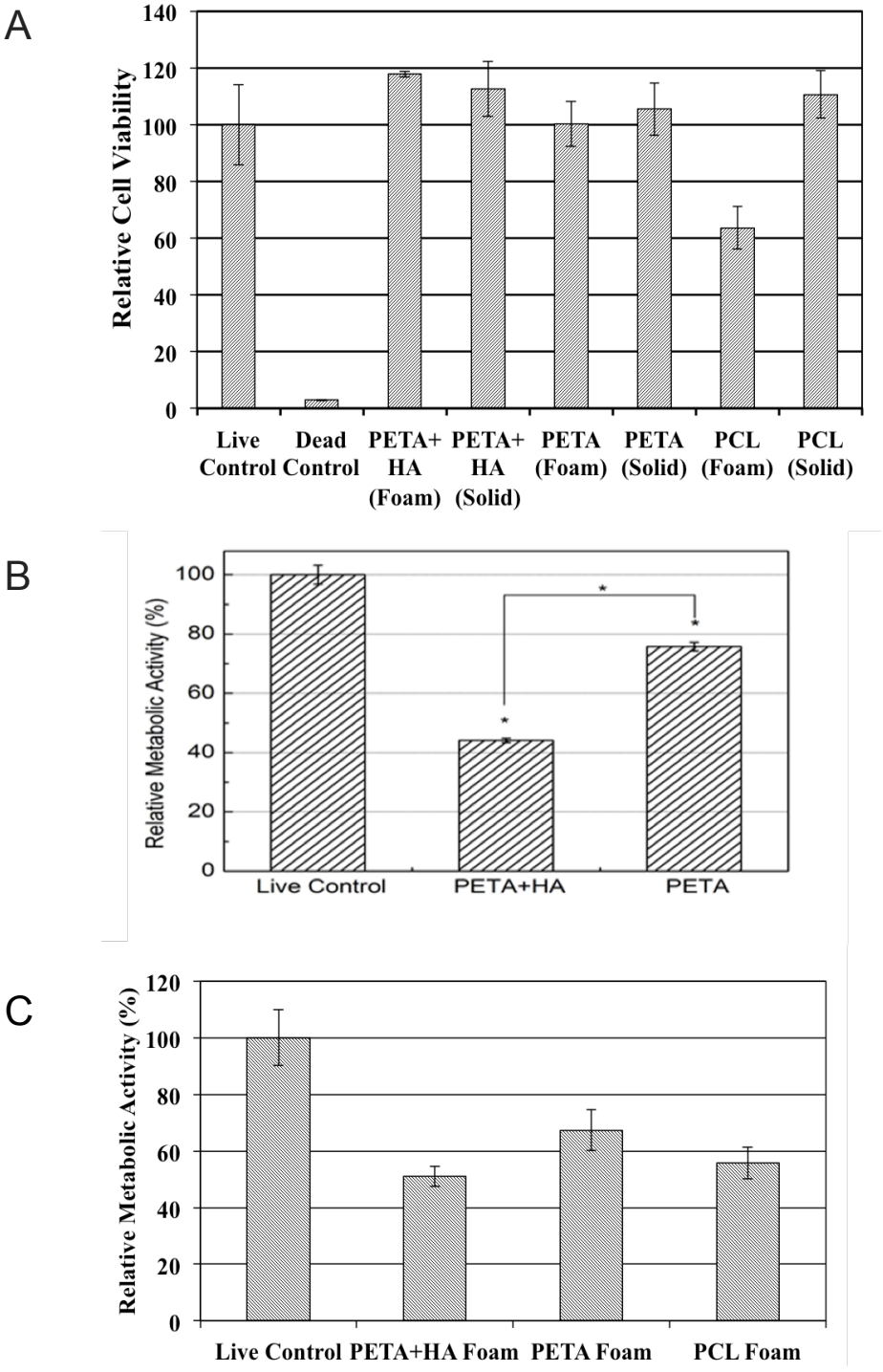

Figure 2-8. Relative metabolic activity of hASC determined AlamarBlue® conversion. Asterisk indicates the sample is significantly different from the live control. A. Exposure to 7 day stromal media extracts from PETA-co-TMPTMP, PETA-co-TMPTMP(HA), and PCL foams and solids. B. Cultured on solid cast PETA-co-TMPTMP and PETA-co-TMPTMP(HA) composites. C. hASCs cultured on foamed PETA-co-TMPTMP and PETA-co-TMPTMP(HA) composites.

days, the highest DNA content was observed in the PETA (20% HA) scaffold, 66.7% of the TCP control. The relative DNA content of the pure PETA-co-TMPTMP and PCL scaffolds are 56% and 65% of the live control, respectively (Figure 2-9). The DNA content from cells cultured on all experimental samples is similar indicating that the total number of cells does not vary significantly with composition. This result is in contrast to the metabolic activity results (Figure 2-8, A), which indicate a significantly reduced metabolic activity for cells grown on composite PETA-co-TMPTMP (HA) samples. This further supports the hypothesis that the cells on PETA-co-TMPTMP (HA) are likely in a reduced metabolic state as a result of early stage osteogenic differentiation.[70]

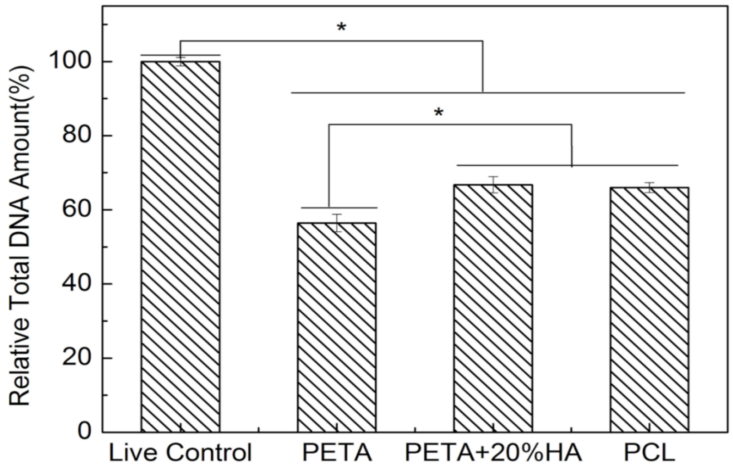

Figure 2-9. Relative total DNA amount as determined by Picogreen® assay for hASC cultured on foamed PETA-co-TMPTMP and PETA-co-TMPTMP(HA) composites. The results are normalized to the live control. Astericks indicate significant difference among the samples.

2.4.9 SEM Analysis

The PETA-co-TMPTMP foam materials were found to have a largely closed celled structure with a pore size ranging from 200 to 300 μm (Figure. 2-10 right). A comparative image of the cast solid copolymer of the same composition can be seen in the left panel of Figure 2-10. The bubbles in the solid sample (Figure 2-10 left) are likely

a result of air introduced during the mixing procedure. The size of the pores found in the foamed sample fall within the range of pores found in native cancellous bone.[71] SEM analysis also indicates that there is no substantial difference between the *in vitro* and *in situ* (20% HA) foamed samples in terms of porosity and morphology (Figure. 2-10, A–D).

Morphological analysis was performed after culturing the hASC for 7 days on the solid cast PETA-co-TMPTMP films. The cells were fixed and imaged by SEM in an effort to evaluate the cell morphology on the thiol-acrylate copolymer. From these images, it appears that hASCs adhere well and take on the expected spindle-shaped during culture on the thiol-acrylate copolymer films (Figure 2-11). It is likely the thiol groups impart a negative charge to the PETA co-polymer, potentially increasing the adhesion, spreading, and proliferation of hASC cells on these surfaces compared with neutral surfaces.[72,73]

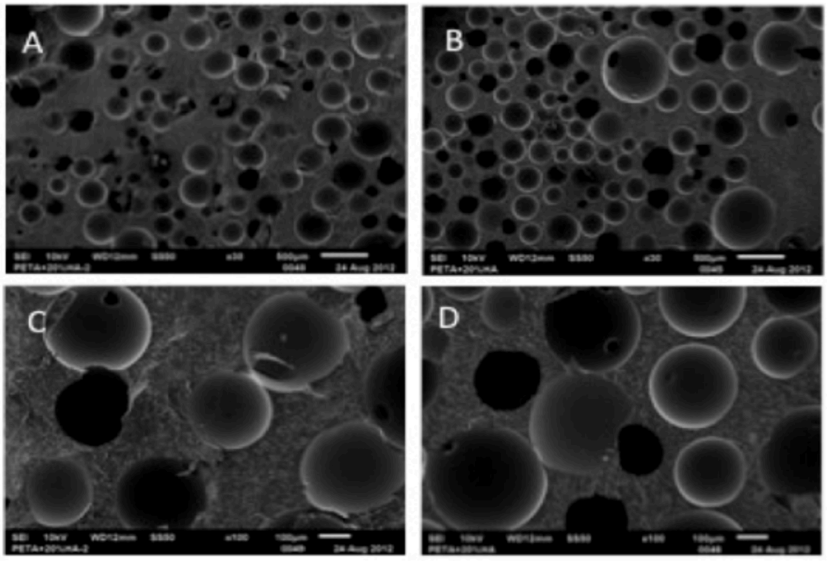

Figure 2-10. SEM images of in vitro PETA-co-TMPTMP + HA foam (A&C) and in situ PETA-co-TMPTMP+HA foam (B&D). Magnification is x100 (A&B) AND x1000(C&D), scale bars are 100 and 10μm, respectively.

At lower magnification (100x) (Figure 2-11, C), a confluent cell population is seen spreading more or less uniformly across the surface, while at higher magnification (1000x) the aligned spindle shaped morphology of individual cells can be clearly seen (Figure 2-11, D). Cell free controls (Figure 2-11, A-B) are included in this image for comparison.

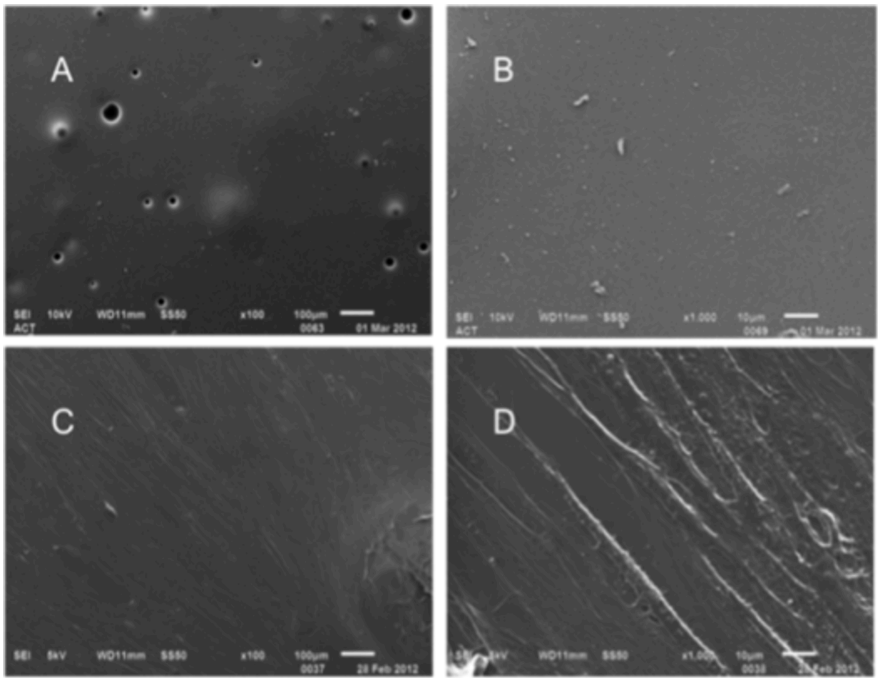

Figure 2-11. SEM images of PETA solid cast polymer films (A & B) and hASC after culture for 7 days on PETA films. Magnification is x100 (A & C) and x1000 (B&D), scale bars are 100 and 10 μm, respectively.

2.4.10 Micro-CT Analysis

Micro-CT image data (Figure 2-12, A–C) show good contrast between HA and polymer, confirming suitability of micro-CT as an appropriate study of the HA distribution and pore morphology. Volume renderings **(**Figure 2-13, A**)** were generated from PETA-co-TMPTMP foam 3D data using Avizo 7.0.1 (Visualization Services Group). Figure 2-13, B (*in situ*) and 2-13, C (*in vitro*) were generated from PETA-co-TMPTMP with 20% HA foam 3D data. Two overlapping subvolumes are rendered simultaneously, one with

a red–orange–white colormap corresponding to thiol-acrylate foam, and the other with a blue–green colormap corresponding to HA inclusions. Volume renderings indicate open-

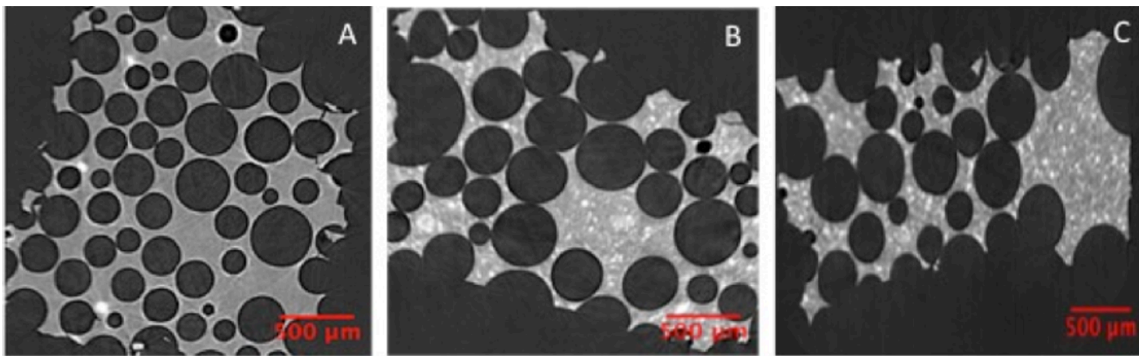

Figure 2-12. 2D slices of micro-ct images using Image J. (A) 0%HA foamed (B) In situ foamed 20%HA (C) In vitro foamed 20%HA.

cell foam and interconnectivity. An interconnected pore structure can provide support for cell migration, differentiation, nutrient transport,[74,75] and in some cases, the formation of blood vessels[76-78] can be established in the pore network. HA inclusions with the size of 10–50 µm were aggregated showing that a higher torque and speed of the stirrer are needed to achieve better homogeneity. Measurements using NIH ImageJ from these datasets indicate pores ranging from 100 to 500 µm for control (0% HA) and 20% HA.

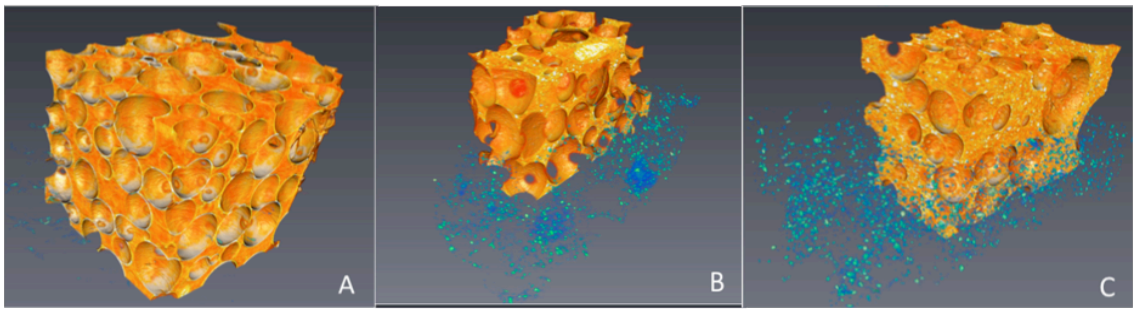

Figure 2-13. Micro-CT obtained 3D data with two overlapping subvolumes rendered simultaneously. Red-orange-white colormap corresponds to the PETA-co-TMPTMP foam, and the blue-green corresponds to HA inclusions. A. 0%HA foamed. B. In situ foamed 20%HA. C. In vitro foamed 20%HA

2.4.11 Bone Adhesive Supplementary Data

PETA-co-TMPTMP was tested for its ability as an adhesive for bone by placing 20% HA PETA-co-TMPTMP excess acrylate and excess thiol formulations in between two deer bones obtained by the LSU FACES lab. It was subjected to shear and tensile testing. Initially, the bond between the polymer and bone was failing quicker than the polymer itself; therefore a hole was drilled in the bone. The two pieces of bone were bonded together by adding 20% excess thiol PETA-co-TMPTMP to one bone and 20% excess acrylate to the other bone. PMMA (poly-methyl methacrylate) is a FDA approved material used for bone adhesive; therefore it was used for comparison. The results (Figure 2-14) show PMMA has higher tensile strength, but the PETA-co-TMPTMP had comparable shear strength, which demonstrates that the PETA-co-TMPTMP is comparable to an already used surgical adhesive material.

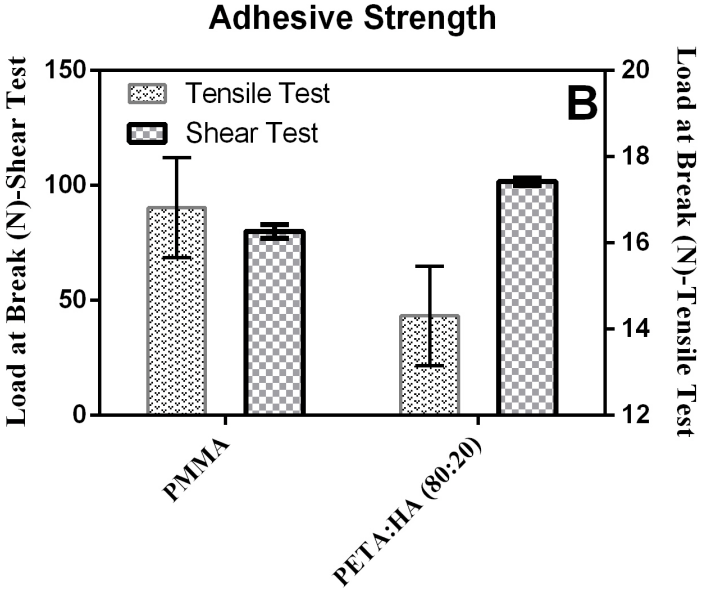

Figure 2-14. Shear and tensile strength of PMMA and 20%HA PETA-co-TMPTMP

2.5 Conclusion

The step-growth nature of the amine-catalyzed Michael addition reaction reduces the potential for unreacted monomer or radicals from leaching into the body, as would typically occur using a chain-growth mechanism involving a free-radical process. *In situ* polymerization opens the opportunity for the development of absorbable foams for the conformal repair of critical sized tissue defects, which can be easily delivered in the clinical surgical setting. This represents a substantial improvement over current synthetic polymers such as PCL or PLGA, which are foamed externally prior to surgical insertion, and methyl methacrylate bone cements, which are largely inert, nonporous, and permanent. The SEM analysis, mechanical testing, and micro CT data support that there is no distinct difference between the PETA-co-TMPTMP foam made *in situ* and *in vitro*. Although this material has many potential advantages, future work includes the development of a homogenous HA containing polymer network, osteogenic studies and improved mechanical strength of the foamed PETA-co-TMPTMP with varying HA concentrations. It is clear that scaffold technology plays a critical role in the success of the current stem cell based bone tissue engineering paradigms. Although a variety of different materials, both ceramics and polymers, have been tested in combination with hASC, Lendeckel et al.[79] note that composite scaffolds may offer a better clinical outcome as a result of improved mechanical and biological properties. Calcium phosphate nanoscale ceramic particles of HA and β-TCP will be used as the inorganic osteogenic phase and thixotropic agent in future studies.

Chapter 3. Osteogenic, *In Vivo*, and Antimicrobial Study

3.1 Chapter Summary

A thiol-acrylate-based copolymer synthesized via an amine-catalyzed Michael addition was studied *in vitro* and *in vivo* to assess its potential as an *in situ* polymerizing graft or augment in bone defect repair. The blends of hydroxyapatite (HA) with pentaerythritol triacrylate-co-trimethylolpropane tris(3-mercapto(PETA), cast as solids or gas foamed as porous scaffolds, were evaluated in an effort to create a biodegradable osteogenic material for use as a bone-void-filling augment. Osteogenesis experiments were conducted with human adipose-derived mesenchymal stromal cells (hASCs) to determine the ability of the material to serve as an osteoinductive substrate. Poly(ε-caprolactone) (PCL) composites PCL:HA (80:20) (wt/wt%) served as the control scaffold, while the experimental scaffolds included PETA:HA (100:0), (85:15), (80:20), and (75:25) composites (wt/wt%). The results indicate that PETA:HA (80:20) foam composites had higher mechanical strength than the corresponding porous PCL:HA (80:20) scaffolds made by thermo-precipitation method, and in the case of foamed composites, increasing HA content directly correlated with increased yield strength. For cytotoxicity and osteogenesis experiments, hASCs cultured for 21 days on PETA:HA scaffolds in stromal medium displayed the greatest number of live cells compared with PCL:HA composites. Moreover, hASCs cultured on foamed PETA:HA (80:20) scaffolds resulted in the greatest mineralization, increased alkaline phosphatase (*ALP*) expression, and the highest osteocalcin (*OCN*) expression after 21 days. Overall, the PETA:HA (80:20) and PETA:HA (85:15) scaffolds had higher mechanical strength and cytocompatibility compared with the PCL:HA control. An antimicrobial component was

added to the PETA:HA polymer using silver nanoparticles that brought the PETA scaffold to the next level to prevent against common infections associated with orthopedic surgeries. The results of the 6-week *in vivo* biocompatibility study using a posterior lumbar spinal fusion model demonstrate that PETA:HA can be foamed *in vivo* without serious adverse effects at the surgical site. Additionally, it was demonstrated that cells migrate into the interconnected pore volume and are found within centers of ossification.

3.2 Introduction

For the past several decades, the standard treatment to augment or accelerate bone regeneration has been the implantation of bone grafts.[80] Allogeneic bone grafts that are from a donor are costly, require time-consuming bone banking procedures, and have the potential for disease transmission. Autogenous bone grafts, coming from the patient's own body, have long been used as bone replacements but require additional surgeries, which increases the risk of site morbidity and the burden on health care providers.[81] Moreover, these techniques do not address the need for a clinically convenient and biodegradable method for conformally filling a critical-sized bone defect while providing mechanical support and biological cues necessary to promote bone regrowth.

The mechanical strength of scaffolds plays an important role in the tissue regeneration process by providing structural support while healing takes place. Synthesizing a material that has comparable mechanical properties to bone while still maintaining other important properties needed for bone replacement remains a challenge. *In situ* gelling biomaterials comprised of polyethylene glycol diacrylate

(PEGDA), synthesized using Michael addition reactions with thiol,[82] show promise as injectable tissue replacements due to their lack of toxic degradation products.[83] However, PEGDA based materials usually lack the sufficient mechanical strength for them to be used in a bone application. A recent study presented a solution to overcome lower mechanical strength by combining both weak and strong crosslinking networks.[84] This results in a stronger hybrid copolymer due to the lower density crosslinking network acting as an energy absorber for the highly cross-linked portion.

Artificial composite scaffolds, whether bioderived, synthetic, or hybrids, while studied extensively as alternatives for bone grafting and augmentation, have yet to see wide clinical adoption.[85] Composite structures with calcium phosphates and magnesium silicates encompassing the bioactive ceramic portion have been studied thoroughly to improve both the mechanical and osteogenic properties of scaffolds but an *in situ* polymerizing, biodegradable bone augment or graft with biomimetic morphology and mechanical properties remains elusive.[85-87]

The introduction of artificial bone scaffolds into the body does, however, trigger complications to arise from orthopedic surgeries causing significant infection at the injury site. Bacterial infections caused from orthopedic surgeries are often associated with aliphatic ester based bone grafts such as poly-L-lactic acid (PLLA) and poly-L-glycolic acid (PLGA) that exhibit *in vivo* degradation causing the release of acidic by-products. By preventing the formation of bacterial colonies with improved antimicrobial therapy, the number of amputation procedures after bone augmentation surgeries has decreased significantly.

An initial study conducted by our group demonstrated the formation of a porous interconnected scaffold derived from the product of an amine-catalyzed Michael addition polymerization reaction.[9] This thiol-acrylate reaction proceeds through a nonradical, step-growth process catalyzed by an amine/acrylate comonomer that is consumed in the reaction and incorporated into the growing polymer. Porous composite scaffolds made with this system were found to support human mesenchymal stromal/stem cell growth and to possess similar mechanical properties to cortical bone.[88]

In order to integrate an antimicrobial portion into a highly crosslinked scaffold, silver nanoparticles (SNPs) were chosen as an antimicrobial agent, because they offer a safe and effective broad-spectrum defense against bacterial colonies and can be easily incorporated into the thiol-acrylate polymer.[89] SNPs also possess higher reactivity compared to other antimicrobial agents and greater surface-to-volume ratio.[90] The sulfur found in the thiol group and silver form a bond,[91,92] therefore monomers with thiol functionality are promising for the adsorption of silver nanoparticles.

The fabrication method of a scaffold can have a substantial impact on mechanical properties and biofunctionality by controlling porosity and interconnectivity. These factors influence cell attachment, proliferation, extracellular matrix production, and the transport of nutrients and wastes.[59,93-96] Solid freeform fabrication, thermal precipitation, gas foaming, and solvent casting followed by particulate leaching are the common approaches for making porous scaffolds for bone repair.[95,96] Except for gas foaming, these methods are not readily applicable to thermoset polymers due to their crosslinking densities and viscoelastic properties. Gas porogens and foaming apparatuses have the potential to be readily adapted to filling conformal defects in a

clinical environment, similar to other surgical devices in use, such as fibrin sealant [97,98] and bone putty.[99]

In this chapter, the *in vitro* characterizations of the mechanical and osteoinductive properties are demonstrated for the gas-foamed nanocomposite scaffold consisting of a thiol-acrylate copolymer with nanoscale hydroxyapatite (HA) inclusions. Scaffolds were prepared using a gas-phase propellant and foaming agent to investigate the relationship of scaffold composition to morphology, mechanical properties, cytocompatibility, and osteogenic properties. The impact of varying HA concentration in the pentaerythritol triacrylate-co-trimethylolpropane (PETA) polymer on morphology is illustrated using scanning electron microscopy (SEM) and micro-computed tomography (micro-CT) imaging. Mechanical testing was conducted to determine the compressive yield strength and modulus of the PETA based material. PETA/PEGDA hybrid materials are also synthesized and mechanically characterized to offer an alternative material that is more hydrophilic. To evaluate cytocompatibility and osteogenic activity, human adipose-derived mesenchymal stromal cells (hASCs) were used as a model cell type. Metabolic activity, DNA content, calcium deposition, and the expression of the osteogenic markers alkaline phosphatase (*ALP*) and osteocalcin (*OCN*) were quantified with respect to scaffold composition.

An antimicrobial study using silver nanoparticles in the polymerization method of the thiol-acrylate copolymer was studied using two different approaches, coating and incorporating. A 6-week *in vivo* study was also conducted to assess the basic biocompatibility of the foamed composite and the feasibility of *in situ* foaming for a boney fusion model.

3.3 Materials and Methods

3.3.1 Preparation of PETA-co-TMPTMP Materials

All chemicals were used as received: Trimethylolpropane tris(3-mercaptopropianate) (TMPTMP), PEGDA(polyethylene glycol diacrylate) (PEGDA)(575), and PEGDA(700) were obtained from Aldrich, diethylamine (99% purity) (DEA) was obtained from ACROS organics, and pentaerythritol triacrylate (PETA) was obtained from Alfa Aesar.

The preparation of the foamed/solid composite scaffolds were prepared by formulating PETA with 16.1% DEA, mixing with a stir rod for 3 hours, and adding TMPTMP in a 1:1 molar functionality as described in the previous chapter.[9] Several concentrations of copolymer PETA-co-TMPTMP (PETA) with HA were studied; the first number in the abbreviation denotes the polymer content while the second number provides the amount of HA found in the composite as a wt/wt percentage (100:0, 85:15, 80:20, 75:25). For this chapter, the PETA-co-TMPTMP polymer will be abbreviated as PETA when discussing the copolymer's concentration with the HA. The highest HA concentration successfully obtained was 25% HA. The 30% HA sample was too viscous to expel through the canister. The mixtures were cast into cylindrical molds (10 mm (diameter) × 10 mm (height)) forming a solid scaffold. The foamed composite copolymer was prepared by pouring the (PETA:HA) (150 g in total) into a 250 mL pressurized spray canister using 7 g-compressed nitrous oxide as a gas foaming agent. The foamed composite copolymer was expelled from the canister into the same cylindrical molds used for solid casting.

3.3.2 Fabrication of PEGDA Hybrids

Prior to synthesizing the PETA/PEGDA hybrids, three different PEGDA Mn ((PEGDA(250), PEGDA(575), and PEGDA(700)) were synthesized. DEA (3%) was added to the three different PEGDA Mn. Each PEGDA monomer with DEA was added to TMPTMP at a 1:1 ratio (acrylate:thiol). The PEGDA(700) was chosen for further analysis. Different % DEA (1.5, 1,8, 2, and 3%) were added to the PEGDA(700) monomer and added to TMPTMP in a 1:1 ratio(acrylate:thiol).

Four different hybrids were synthesized. The first tested all Mn's to analyze if the results will agree with the PEGDA polymers without the addition of PETA. The first was formulated by mixing a 16.1% PETA/DEA stock with either PEGDA(250), PEGDA(575), or PEGDA(700) monomer. 20 and 50% excess thiol with respect to the PETA acrylate functionality was then added. This excess amount of thiol was added in order to react with the PEGDA monomer to ensure that all thiol and acrylate groups were reacted in a 1:1 ratio.

The second and third hybrid formulation added PEGDA(700), % triethylamine (TEA), PETA stock containing 16.1% DEA, and TMPTMP needed for a 1:1 reaction with both PEGDA(700) and PETA (all acrylates). The second added all components at once. The third separately mixed PEGDA(700)/16.1%TEA/TMPTMP and PETA/DEA (16.1%) stock/TMPTMP, stirred 6 minutes, then added the PEGDA(700)/TEA/TMPTMP mixture to the PETA Stock/TMPTMP.

The fourth hybrid formulation used DEA, instead of TEA, with PEGDA(700). The TMPTMP added was calculated the same as in the previous two formulations. Different ratios of PEGDA(700) and PETA noted by PEGDA:PETA(4:1), PEGDA:PETA(2:1),

PEGDA:PETA (1:1), PEGDA:PETA(1:2), and PEGDA:PETA(1:4) were synthesized based on the ratio acrylate moles of each.

3.3.3 Mechanical Analysis PETA-co-TMPTMP and PEGDA Hybrids

Solid and foamed PETA-CO-TMPTMP scaffolds, molded to a 6 mm (diameter) x 12 mm (height) cylinder, were tested to determine maximal compressive strength and modulus. All scaffolds were subjected to compression, and the ultimate compressive strength was reported at 30% strain. A universal testing machine was used at an extension rate of 0.5 mm/min.

Prior to choosing the Mn of PEGDA(700), three different Mn (250, 575, 700) of PEGDA catalyzed with 3% DEA were tested. Once PEGDA(700) was chosen, different %DEA was used to determine if mechanical strength is affected by amine content. PEGDA(700) 1.5, 1,8, 2, and 3% DEA were subjected to compressive testing. All four of the main categories of hybrids described in Section 3.3.2 were subjected to mechanical testing. The modulus was calculated by taking the slope of the most linear portion of the stress versus strain graph before failure.

3.3.4 Micro-CT Analysis

Four PETA:HA (100:0), (85:15), (80:20), (75:25) foams were fabricated by pressurized extrusion foaming and prepared as described previously.[9] The imaging was conducted at the Center for Advanced Microstructures and Devices (Louisiana State University, Baton Rouge, LA) using a tomography beamline with 13 keV monochromatic x-rays with a 2.5 μm/px resolution. Projection exposure time varied from 2-4 seconds with Dq = 0.25 corresponding to the number of image slices (520). Reconstruction data are 16-bit signed integer with mean air intensity scaled to zero.

Avizo 7.0.1 (Visualization Services Group) generated the volume renderings from the 3D data of the four foamed samples with two overlapping sub-volumes displayed simultaneously. The blue-green colormap represents the hydroxyapatite inclusions, and the red-orange colormap represents the copolymer foam. NIH Image J generated 2-D orthogonal slices using the same data with a scale equivalent to that of the 3-D rendering possessing grey map settings. An approximate pore size was also measured using Image J. The orthogonal and micro-CT datasets are directly comparable, both as an aggregate dataset and as slices.

3.3.5 hASC Loading on Scaffolds and Culture

hASCs were isolated based on Section 2.3.5. Passage 2 of each donor (n = 3) were pooled and directly loaded on a single face of each scaffold type at a density of 5.0×10^4 cells/ 5 µL. After 30 min of incubation in a saturated humidity atmosphere incubator at 37 ^{o}C and 5% CO_2, the same hASC dose was directly applied on the opposite side of each scaffold. Control groups included PCL:HA (100:0) and PCL:HA (80:20) scaffolds. Experimental groups included PETA:HA (100:0), (85:15), (80:20), (75:25) scaffolds. Scaffolds loaded with hASCs were instantly transferred to 48-well plates and cultured in stromal or osteogenic media for 21 days with weekly sample collection.

3.3.6 *In Vitro* hASC Metabolic Activity on Scaffolds

The metabolic activity of cells within the scaffolds at 7, 14 and 21 days in stromal and osteogenic media was measured by AlamarBlue® metabolic activity assay (Invitrogen). The scaffolds were removed from culture, washed three times in Phosphate Buffered Saline (PBS), and incubated with 10% AlamarBlue® in Hank's

balanced salt solution (HBSS) without phenol red (pH 7) for 90 min. Aliquots (100 μL) of AlamarBlue®/HBSS were placed in a 96-well plate in triplicates, and the fluorescence was measured at an excitation wavelength of 530 nm and an emission wavelength of 595 nm using a fluorescence plate reader. DNA content, calcium deposition, and the expression of the osteogenic markers alkaline phosphatase (*ALP*) and osteocalcin (*OCN*) were quantified with respect to scaffold composition by colleagues in the Louisiana State University bioengineering department.

3.4 Materials and Methods for Antimicrobial Study

3.4.1 Antimicrobial Scaffold Fabrication

Silver nanoparticles (SNPs) were added to the polymer/HA composite using two different methods (incorporation and coating) with preparation of the composite described previously in Section 3.3.1. The incorporation method involved dispersing HPC-SNPs with a size distribution of 25-75 nm in 9.3% (w/v) butanol (100, 1000, 1500 ppm) by ultrasonication. The solvent containing SNPs were combined with the PETA/DEA/HA mixture before foaming with the TMPTMP. After adding the PETA/DEA/HA/solvent-SNP mixture to the TMPTMP, it was placed into a 250 ml pressurized spray canister. For the incorporation method, three solvents including ethanol, butanol, and isopropanol were studied initially to determine if solvent selection affected the gel time or foaming process of the polymerization.

The coating method entailed soaking the pre-formed sample in ethanol, isopropanol, or butanol containing 1000 ppm SNPs. Adding 20% excess TMPTMP during the polymer fabrication step and soaking for 24 hours in the SNP solvent dispersion were steps used to prepare the PETA-co-TMPTMP antimicrobial foam. The

foamed samples were washed with PBS to remove excess SNPs and subsequently freeze-dried to remove any residual solvent.

3.4.2 Mechanical Testing and Silver Morphological Analysis

Compressive strength was measured for the antimicrobial and control (PETA-CO-TMPTMP) foam or solid using a universal testing machine. The incorporating and coating constructs were subjected to compression testing at a rate of 0.5 mm/min until 90% extension was reached.

The SEM silver morphological analysis included, all of the scaffolds (incorporating and coating). The samples were placed on the EMS550X sputter coater, which applied a conductive platinum coating for 2 minutes followed by standard SEM imaging.

3.4.3 Silver Release Study and Antibacterial Testing

The amount of silver released from each sample was determined using inductively coupled plasma optical emission spectrometry (ICP-OES). The *in vitro* contact times required for the elimination of two model organisms, *Staphylococcus aureus* and *Escherichia coli* were investigated for the scaffolds fabricated by the two methods.

3.5 *In Vivo* Study

3.5.1 Scaffold Preparation and Surgical Implantation

5 male Fischer rats (Harlan Sprague-Dawley) were randomly assigned to three different treatment cohorts: (1) one rat was implanted with pre-sculpted (20% HA); (2) three rats were implanted with PETA-CO-TMPTMP + 20% HA foamed *in situ*; (3) one rat was implanted with PETA-CO-TMPTMP + 0% HA foamed *in situ*. The autoclaved

stock/HA and TMPTMP/HA pre-polymer mixture were placed into a 250 mL pressurized spray canister using 7 g of compressed nitrous oxide as a gas foaming agent. The spray canister components were gas sterilized before surgery. The foamed composite copolymer was expelled from the canister into a sterilized pan. The composite was cut into a rectangular prism with dimensions (15 × 10 × 1 mm) for rat 1. For rats 2, 3, & 4, the pre-polymer mixture was foamed as described previously, but foamed into a 5 ml syringe for surgical application. The same foaming process was implemented in rat 5, but it contained 0% HA in its formulation.

The rat posterolateral lumbar spinal fusion surgery was performed according to previous studies.[100] Prior to general anesthesia, rats were treated with a subcutaneous injection of 0.5 mg/kg butorphanol (Torbugesic; Fort Dodge Animal Health) and 0.02 mg/kg glycopyrrolate (Robinul; Fort Dodge Animal Health, Fort Dodge, IA). In order to induce anesthesia, rats were administered isoflurane 20 mins later in an induction chamber. The isoflurane was maintained at 1.5% via nose cone on a Bain circuit for the remainder of the procedure. The lumbar region was clipped and aseptically prepared with 70% isopropanol betadine. A posterior midline skin incision was made over the lumbar spine. Two fascial incisions were made 3 mm lateral and parallel to the spinus processes. The L4 and L5 transverse processes were exposed using a combination of sharp and blunt dissection that was limited to the specific area of interest. A scalpel was used to decorticate each transverse process next to the spine. The surgical sites were thoroughly lavaged with physiologic saline. In rat 1, solid scaffolds were placed were placed adjacent to both sides of the spine such that they spanned between the midpoint of each transverse process. For the remaining rats, 3 ml of the foam scaffold was

applied so that the scaffold spanned between the center of each transverse process next to the spine. Fascial and subcutaneous incisions were closed separately with 3-0 polyglactin 910 (Vicryl; Ethicon) in a simple continuous pattern. To prevent migration, closure of the fascia around the implants effectively obliterated any potential space. A subcutaneous, subcuticular suture pattern was used for skin closure (Vetbond, 3M).

Five animals were humanely euthanized by CO_2 asphyxiation at 3 weeks (rat 3) or 6 weeks (rats 1, 2, 4, 6) after surgery.[101] At three weeks, no significant results were shown in radiographs, micro-CT, or histology. Therefore, no results from rat 3 were reported in the Results and Discussion sections.

3.6 Results/Discussion (PETA-co-TMPTMP Osteogenic Characterization)

3.6.1 Mechanical Testing

Figure 3-1 shows the compressive yield strength of the foamed HA:PETA (100:0), (85:15), (80:20), (75:25) and solid PETA. The compressive strength of the foamed PETA steadily increased with increasing HA content; however, the solid samples had a slightly different trend. The addition of 15% HA resulted in a significant increase in mechanical strength, but there is no increasing trend in yield strength with additional HA. As such, HA:PETA (85:15), (80:20), (75:25) solid scaffolds exhibited approximately the same compressive strength. The increase in yield strength seen in solid samples is predictable and similar to that seen with other nanoscale polymer fillers.[67,102] As porosity played no role in the solid samples, the increase in viscosity with increasing HA content beyond 15% did not affect the solid's mechanical strength.

Therefore, it is believed that the porosity of the foamed scaffolds is responsible for the different trends between solid and foamed scaffolds. As mentioned above for the

SEM analysis increasing HA content resulted in reduced pore size and interconnectivity. This decrease in pore size resulted in a more solid and stronger structure. Other studies have shown a similar trend of decreasing porosity with increasing HA content.[103] The pore size decreased with increasing HA signifying the direct relationship between the foam characteristics and mechanical strength. The solid samples' compressive strength did not change as a result of increasing HA content which shows that the porosity plays a major role in compressive strength not addition of filler.

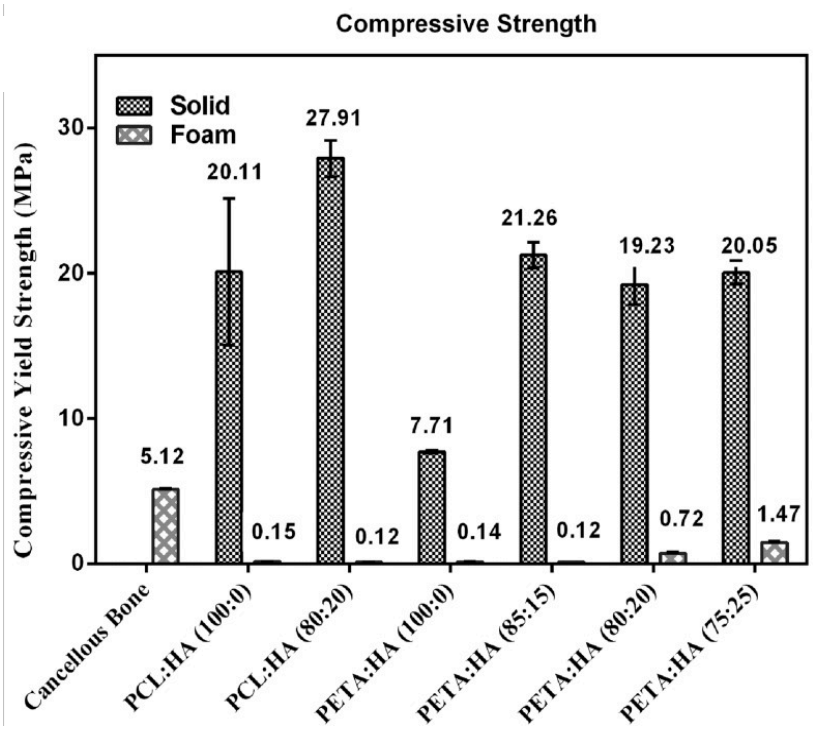

Figure 3-1. The compressive strength of PETA:HA (100:0), PETA:HA (85:15), PETA:HA (80:20), PETA:HA (75:25), PCL (80:20), PCL (100:0), and cancellous bone.

3.6.2 Mechanical Analysis of the PEGDA Hybrids

The PEGDA hybrids were synthesized and analyzed to find an alternative to PETA-co-TMPTMP that not only had higher mechanical strength, but also an increase in hydrophilicity. Mechanical analysis was conducted to determine the ultimate modulus

and compressive strength of the PEGDA hybrids and how different PEGDA(Mn), DEA (%), excess TMPTMP, and PEGDA to PETA ratios affected mechanical strength.

Prior to formulating the hybrids, the Mn of PEGDA was chosen based on mechanical strength. As shown in Figure 3-2, the PEGDA(700) and PEGDA(250) exhibited relatively the same strength and modulus while the PEGDA(575) was lower in strength. Due to having the longest backbone out of the three Mn's, the PEGDA(700) may have a higher chance of entangling, which may be contributing to the higher

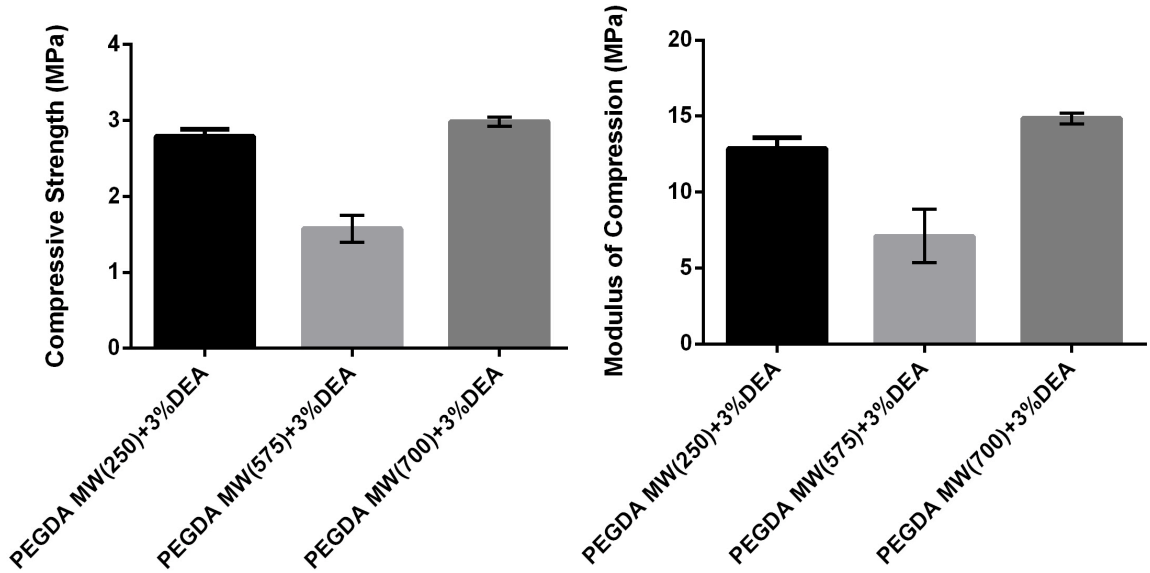

Figure 3-2. The compressive strength and modulus of PEGDA(250)-co-TMPTMP, PEGDA(575)-co-TMPTMP, and PEGDA(700)-co-TMPTMP.

strength.[104] The PEGDA(250) took ~3 hours to gel while PEGDA(575) and PEGDA(700) only took 5-10 minutes which may also increase its strength since the functional groups had more time to diffuse through and form bonds. More investigation is needed to understand the sharp decrease in gel time such as rheology to determine more accurate gel times. The PEGDA(700) Mn was chosen for further mechanical testing due to its gel time and higher overall mechanical strength. Changing the DEA (%) did not

change mechanical strength significantly as shown in Figure 3-3, therefore the basis of

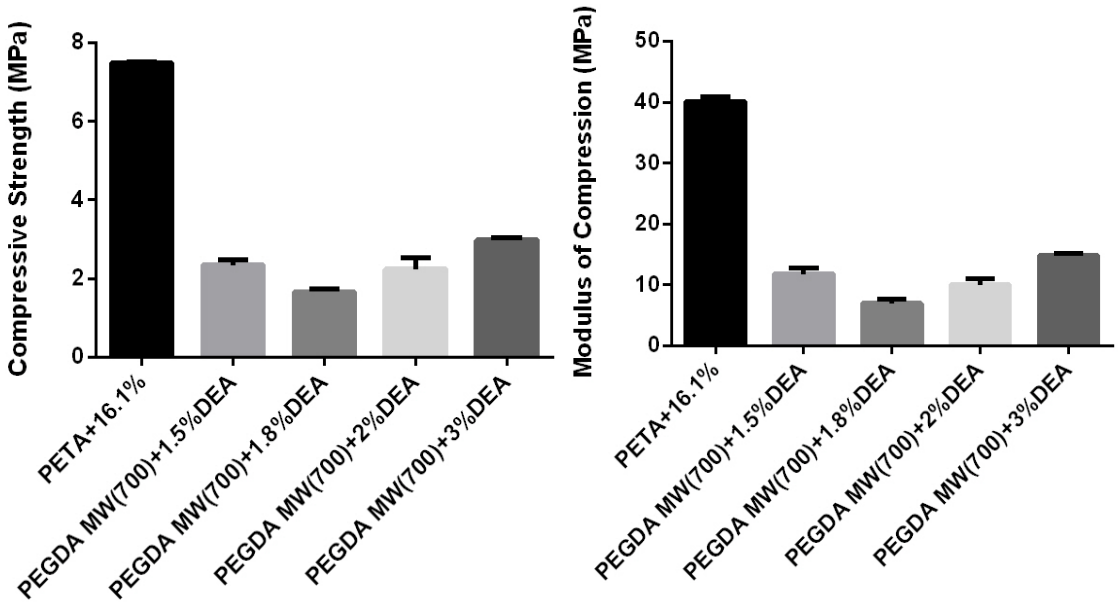

Figure 3-3. The compressive strength and modulus of PEGDA(700)-co-TMPTMP with varying DEA(%).

choosing DEA was on gel time and not mechanical strength. In the next chapter, the PEGDA(700)-co-TMPTMP polymer will be described in more detail.

For the first set of hybrids, the PEGDA monomer was added to the tertiary amine catalyst (PETA/DEA stock solution) with 20 and 50% excess TMPTMP amounts (Figure 3-3). The (575) Mn yielded the lowest strength for both the 20% and 50% excess thiol hybrid polymers compared to the (700) and (250) Mn (Figure 3-4). These trends agree with the results shown in Figure 3-2 with both PEGDA(575) polymers showing a drop in mechanical strength compared to the other two Mn This confirmed that the PEGDA(700) will be used for the three remaining hybrids. All three formulations gelled in less than 1 minute, therefore no further testing was performed on this hybrid set.

PEGDA(700)/16.1% TEA/TMPTMP and PETA/DEA (16.1%) stock/TMPTMP were mixed separately to allow each to react for 6 minutes before mixing all together. By substituting TEA for DEA for PEGDA(700), the mechanism proceeded via two

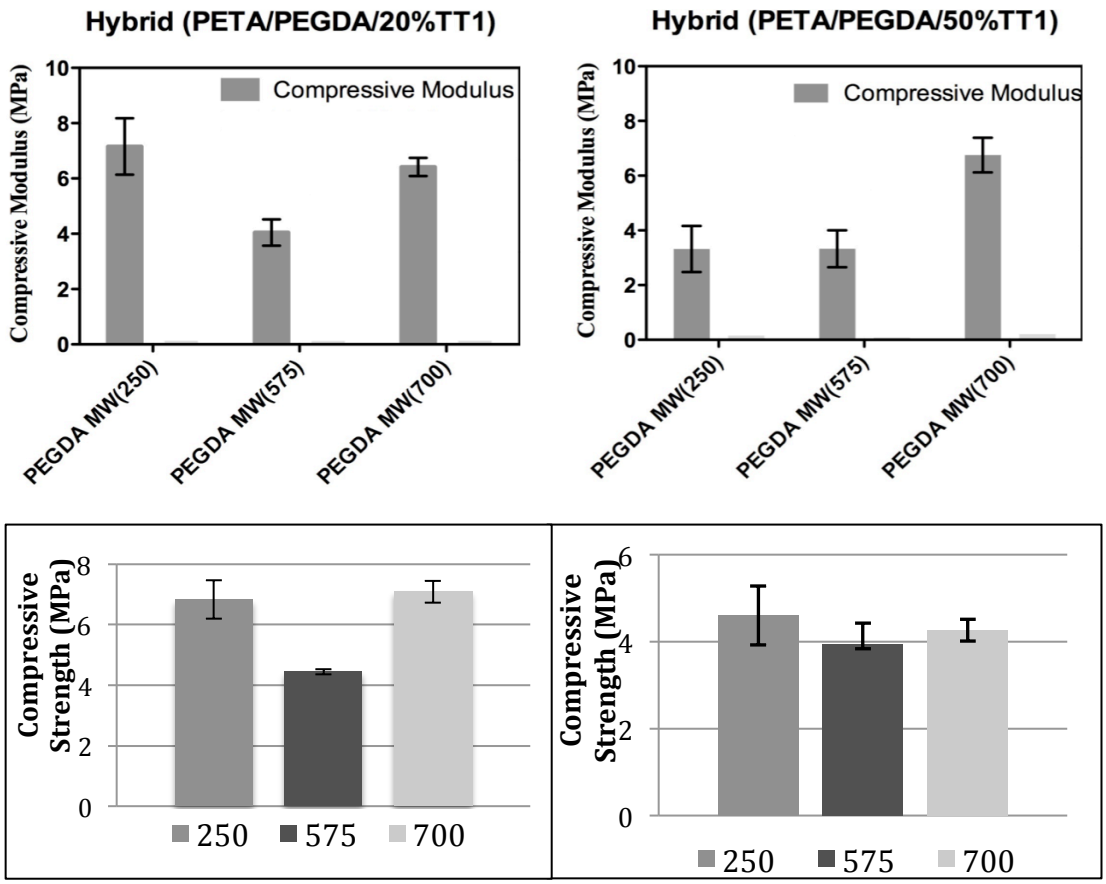

Figure 3-4. The compressive strength and modulus of PEGDA(250,575,700)/ PETA hybrids synthesized with 20% and 50% excess thiol

competing base-catalyzed mechanisms, which demonstrated modulus comparable to PETA-co-TMPTMP (Figure 3-5).

Figure 3-6 shows the compressive strength and modulus for the hybrids of different ratios of PETA to PEGDA(700). The PEGDA(700)/PETA hybrids containing the higher ratio of PETA yielded a higher compressive strength, which is attributed to the PETA-co-TMPTMP being a stronger polymer by itself than the PEGDA(700) polymer. On the contrary, the third hybrid formulation, specifically the 1:2 ratio of PEGDA:PETA that used TEA to catalyze the reaction yielded a modulus comparable to PETA-co-TMPTMP(Figure 3-5). Three out of the four hybrids proved to be weaker overall than the PETA-co-TMPTMP polymer. These hybrid materials could still offer an alternative if

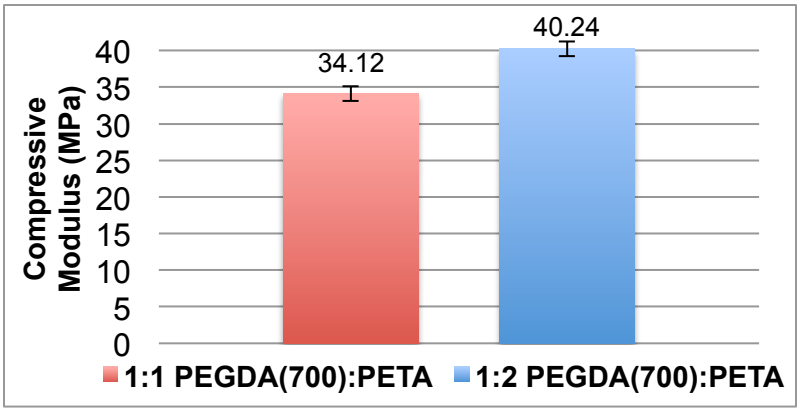

Figure 3-5. Compressive Modulus of Hybrid ratios of (PETA stock):(PEGDA(700)TEA)

a more hydrophilic polymer is needed for a particular application. For example, in the *in vivo* section of this chapter, one of the disadvantages of PETA-co-TMPTMP that will be discussed is that it did not stick to bone well, and a more hydrophilic polymer, like a PEGDA-PETA hybrid may help address this shortcoming. The hybrids were not studied further because they did not provide an increase in mechanical strength, therefore the remainder of this chapter focuses on the PETA-co-TMPTMP(HA) composites.

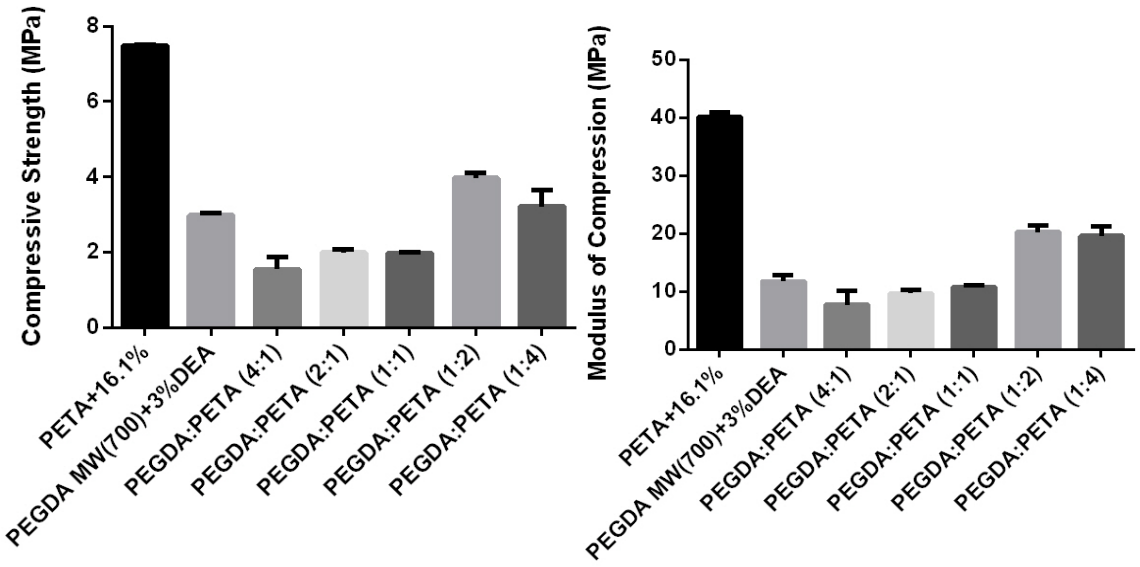

Figure 3-6. Compressive strength and modulus of PETA 16.1% DEA, 3% DEA PEGDA(700), and different PEGDA(700):PETA ratios

3.6.3 Morphological (SEM)

The effect of the foaming method was examined further by expelling the foam into a beaker filled with stromal media. The SEM imaging (Figure 3-7) of the *in vitro* foamed sample had the same porous structure as the polymeric foam being expelled into a dry mold. Nucleation of the gas porogen, nitrous oxide, cannot occur at high viscosity. The effect the HA content had on the porosity of the foamed samples was also studied, and it was concluded that the porosity decreased as the concentration of the HA increased. This trend is the result of the diffusion and expansion rate of the nitrous oxide bubbles that are released by the foaming apparatus. The gaseous bubbles evaporate out of the polymer/HA composite very rapidly when the viscosity of the samples is low. However, the viscosity begins to increase with each 5% increase of HA, therefore the expansion and diffusion of the gaseous bubbles are prohibited at high HA

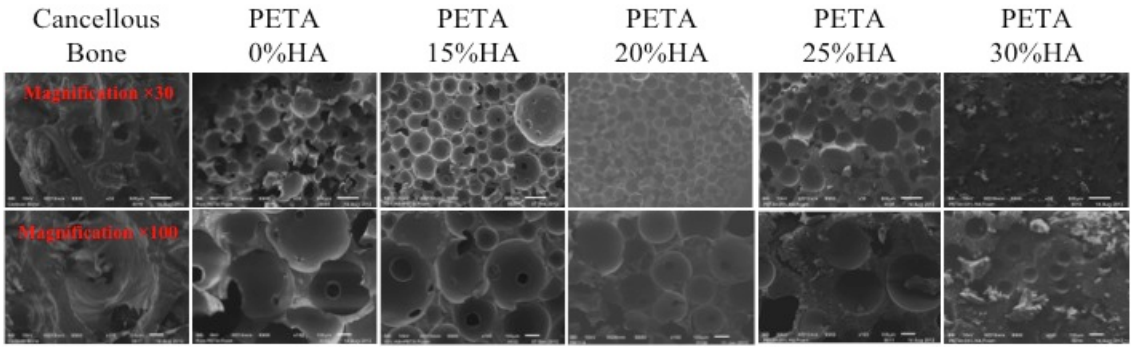

Figure 3-7. Scanning electron microscopy analysis of pentaerythritol triacrylate-co-trimethylolpropane (PETA): hydroxyapatite (HA) (100:0), (80:15), (80:20), and (75:25) scaffolds.

concentrations (25 and 30%). The pore size decreased with increasing HA signifying the direct relationship between the foam characteristics and mechanical strength. The solid samples' compressive strength did not change as a result of increasing HA content which shows that the porosity plays a major role in compressive strength not addition of

filler. The highest HA concentration successfully obtained was 25% HA. The 30% HA sample was too viscous to expel through the canister.

3.6.4 Micro-CT

There is a limitation associated with the amount of material that SEM can qualitatively analyze, reducing the generalizability of the data. To address this limitation, the interconnectivity, pore volume, and ceramic phase distribution of HA-PETA copolymer composites and PCL (control) were further analyzed by micro-CT. Micro-CT image analysis is a more sensitive method for estimating porosity of materials when compared to SEM, flow porosimetry, and gas adsorption.[105] Volume renderings (Figure 3-8) were generated from PETA-co-TMPTMP and PCL composite foam 3D data using

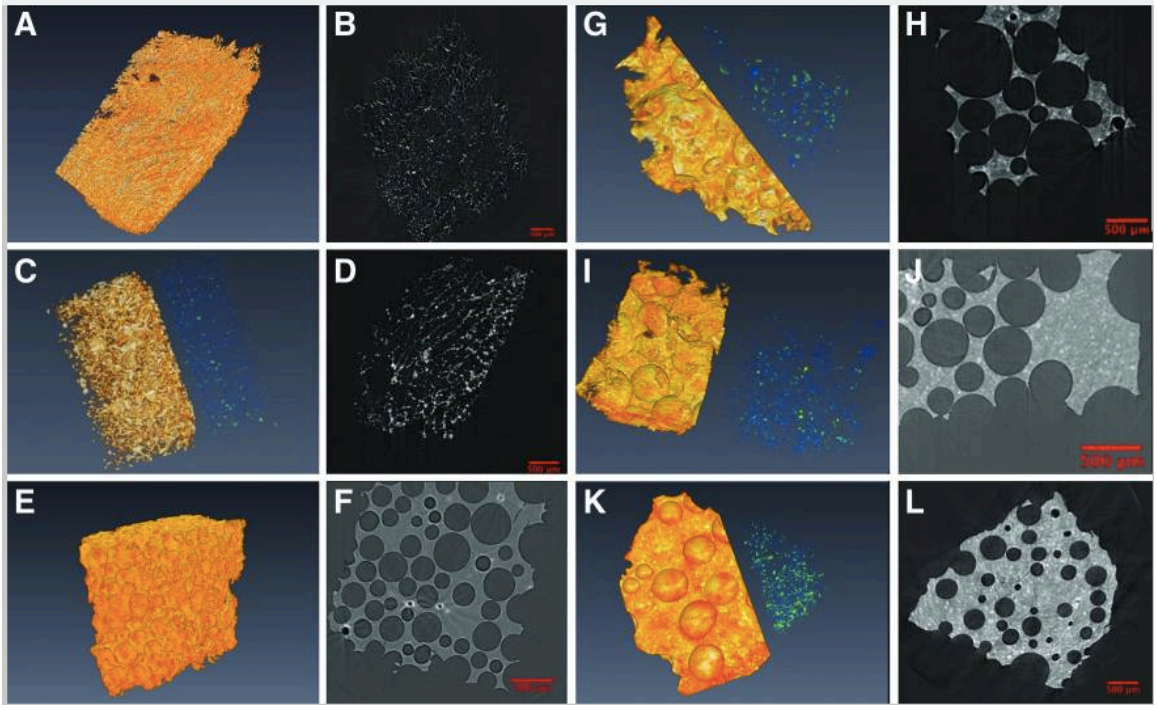

Figure 3-8. Micro-CT of Avizo rendering pictures (3D & 2D). The blue-green colormap represents the HA inclusions, and the red-orange colormap represents the copolymer foam. (A, B) PCL:HA (100:0), (C, D) PCL:HA (80:20), (E, F) PETA:HA (100:0), (G, H) PETA:HA (85:15), (I, J) PETA:HA (80:20), (K, L) and PETA:HA (75:25) scaffolds. Each scale bar in the 2D pictures indicates 500 μm.

Avizo 7.0.1 (Visualization Services Group). Two overlapping subvolumes were rendered simultaneously, one with a red-orange-white colormap corresponding to thiol-acrylate foam, and another with a blue-green colormap corresponding to ceramic HA additives.

3.6.5 hASC Metabolic Activity and Proliferation on Scaffolds Cultured

AlamarBlue® conversion to its fluorescent form is a convenient measure of metabolic activity and is frequently used as an indicator of cell viability. All scaffold samples were seeded with hASC and cultured in stromal or osteogenic media for 21 days. The AlamarBlue® conversion was measured at 7, 14 and 21 days. Among all the scaffolds, PETA:HA (100:0) showed highest metabolic activity, followed by PCL:HA (100:0) in osteogenic media. In stromal media, PETA:HA (100:0) scaffolds exhibited highest metabolic activity at 7 and 14 days while PCL:HA (100:0) presented with highest metabolic activity at 21 days (Figure 3-9). With the addition of HA to PETA-co-TMPTMP and PCL containing scaffolds, decreased metabolic activity was observed in stromal and osteogenic media. Significant differences in metabolic activity between stromal and osteogenic media were observed at all-time points for PCL:HA (100:0) and PCL:HA (80:20) scaffolds. This data is in agreement with previous studies that indicate that the metabolic activity of hASCs is expected to decrease as cells commit to an osteogenic lineage.[59,106]

As for PETA:HA (100:0) control, significant differences were only observed for 7 and 14 days. Almost no metabolic activity was measured in PETA:HA (75:25) scaffolds likely as a result of the reduced pore size and interconnectivity reducing the number of viable cells in the scaffold. PETA:HA samples, regardless of HA content, showed no differences in metabolic activity between stromal and osteogenic conditions. This

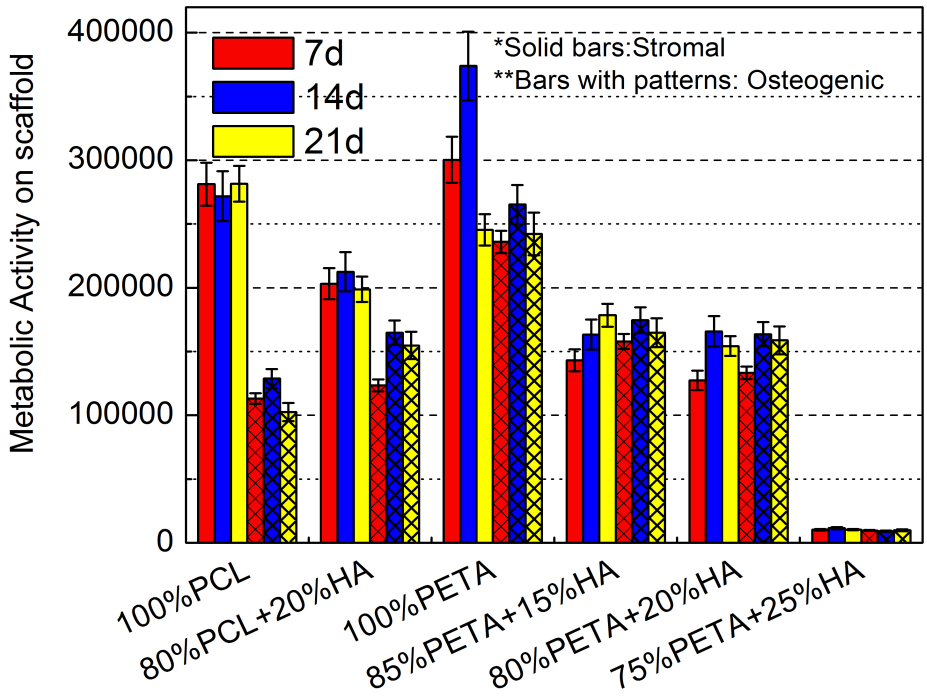

Figure 3-9. Relative metabolic activity of hASCs on PETA:HA(100:0), (85:15), (80:20), (75:25) scaffolds in stromal and osteogenic media.

reduction in metabolic activity is common during the osteogenic differentiation of mesenchymal stromal cells. hASC cultured on HA containing scaffolds would be expected to begin differentiation into an osteogenic linage regardless of the media condition, potentially accounting for the differences in metabolic activity between HA-containing and control samples cultured in stromal media.

3.7 Antimicrobial Results/Discussion

Synthetic scaffolds containing antimicrobial components have been shown to reduce the bacteria associated with hospital-acquired infections.[107] Silver nanoparticles (SNPs) were added to the polymer/HA composite by dispersing in different solvents in order to develop an antimicrobial component within the biomaterial. Foaming of the polymer with different solvents including ethanol, butanol, isopropanol, and propanol had different effects on the polymerization process.

Propanol decreased the polymer gel time from 20 to 5 minutes; therefore, no further testing was performed using propanol as the SNP dispersion solvent. The ethanol solvent caused partial aggregation of HA, but required no post-treatment. Isopropanol also did not require post-treatment, but the nitrous oxide pores formed collapsed quickly. The results for the solvents were likely due to solubility with nitrous oxide and different polar interactions between the polymerization and the alcohols. The butanol distributed HA well throughout the polymer, but it did require post treatment of freeze-drying for complete removal. Butanol was chosen for further experimentation for it was the only solvent that did not effect the gelation time and foaming process. Different concentrations of butanol relative to the total amount of polymer plus the HA amount were tested to examine the effect the different concentrations had on the dispersion of SNPs and the mechanical compressive strength. Concentrations below 9.3% did not disperse SNPs well; therefore, the minimum concentration of 9.3% butanol was needed for the dispersion of the SNPs. The compressive strength was not significantly different for concentrations above 9.3% (Figure 3-10); therefore, the 9.3% was chosen to ensure the lowest amount of solvent needed was used for the synthesis.

The incorporation method of the nanoparticle solvent solution into the pre-polymer network before gelation had a significant effect on the ultimate compressive strength by causing it to decrease compared to the control. Since the coating method was synthesized with 20% excess thiol, the mechanical strength also dropped due to the presence of unreacted monomers as shown in Figure 3-11. The control contained zero solvent SNP solution and was synthesized using a 1:1 ratio of acrylate to thiol.

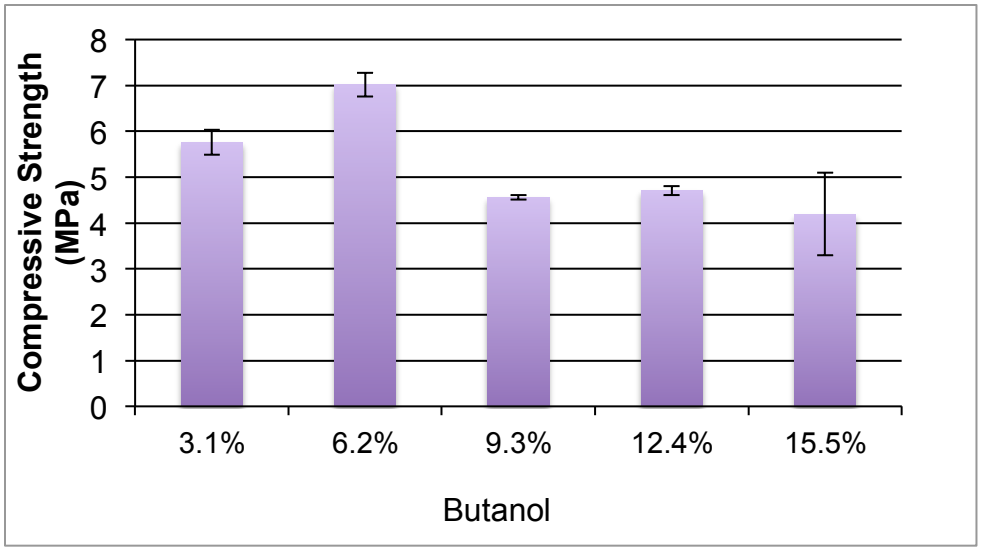

Figure 3-10. Compressive strength of the polymer as a function of %butanol relative to total HA + polymer

SEM imaging comparing the surfaces of the coating method prepared scaffolds versus the incorporated scaffolds was performed. The silver particles are visibly shown on the surface (Figure 3-12, A), while the incorporating appears to have no silver particles on its surface (Figure 3-12, B).

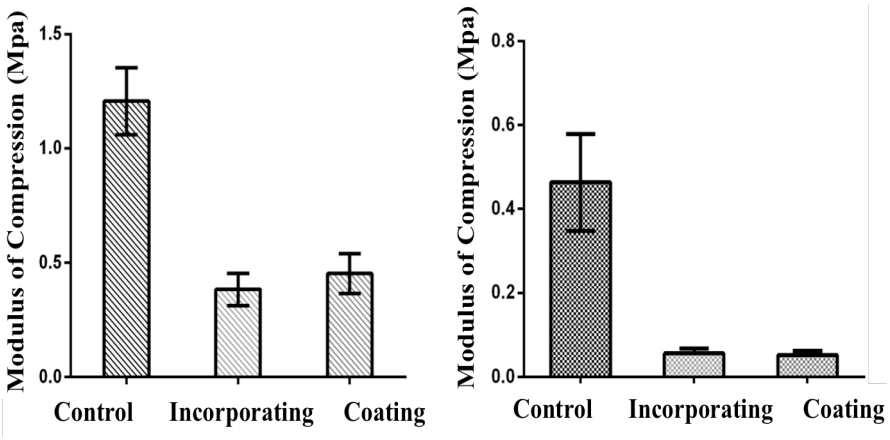

Figure 3-11. Mechanical Analysis of foamed scaffolds prepared by the incorporating and the coating method.

Both the incorporating and coating method samples were placed in PBS for 3 days after the silver nanoparticles were added in each way. 100 ul of PBS was removed

every 24 hours for analyzing released SNPs from the scaffold as shown in Figure 3-13. For studying the residual SNPs on the scaffold, the polymer was dissolved in a piranha solution then analyzed using ICP-OES. During the 72-hour ICP-OES analysis, the

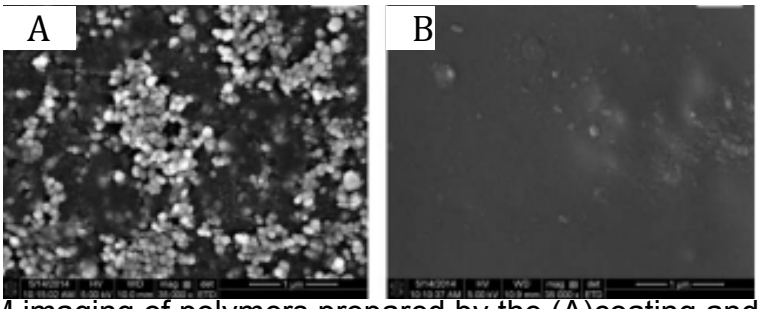

Figure 3-12. SEM imaging of polymers prepared by the (A)coating and (B)incorporating methods.

scaffolds fabricated by the incorporating method released no detectable amount of silver as shown in Figure 3-13, B. However, the amount of silver found within the polymer + HA matrix steadily increased with increasing SNP concentration. The monomers, PETA and TMPTMP, used have a small molecular weight yielding a tighter crosslinking density, which trapped the silver within the matrix.

For the coating method, the highest silver concentration released was after 72 hours. (Figure 3-13, A) The amount of SNPs being released increased with each 24-hour time point showing that the diffusion of PBS through the scaffold was relatively slow. These trends are ideal for the defense against infection associated with orthopedic implants. There was no statistical difference in the amount of silver released from the different solvents (ethanol, butanol, isopropanol). The amount of silver found within the polymer was the highest during the first 24 hours and slightly decreased over the 72-hr study. The coating method contained a lower crosslinked network attributing to the increased release of SNPs and the surface coated with SNPs,

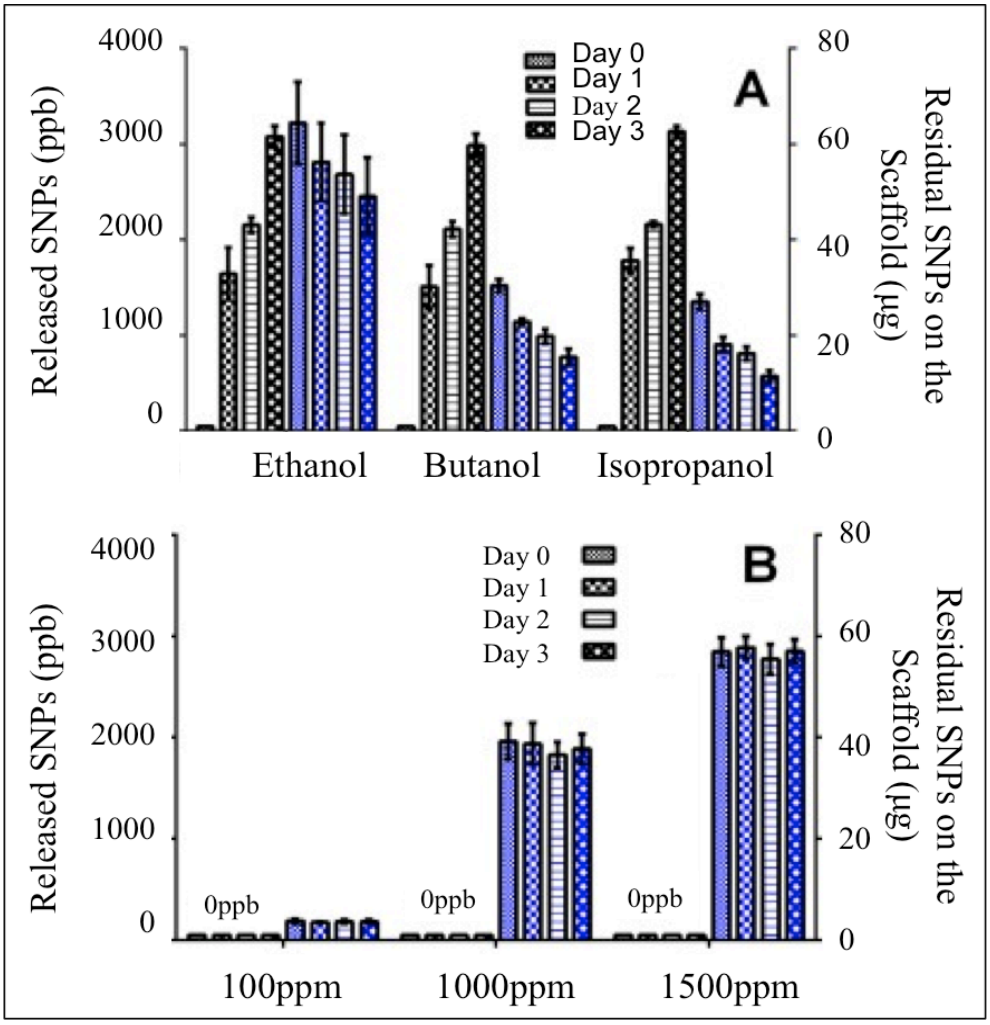

Figure 3-13. ICP-OES analysis of the released silver content and the residual SNPs within the scaffolds prepared by the A. Coating method B. Incorporating method

Colleagues performed antimicrobial studies on each scaffolds against *Escherichia coli* and *staphylococcus aureus,* and it was concluded that the coating method reduced *S. aureus* and *E. coli*, while the incorporating method did not. (Figure 3-14) This is likely due to the low silver release from the incorporating scaffolds shown in ICP-OES. The PETA-HA-SNP can be implemented in nanocomposite bioscaffolds to create engineered, active, and antimicrobial tissue scaffolds.

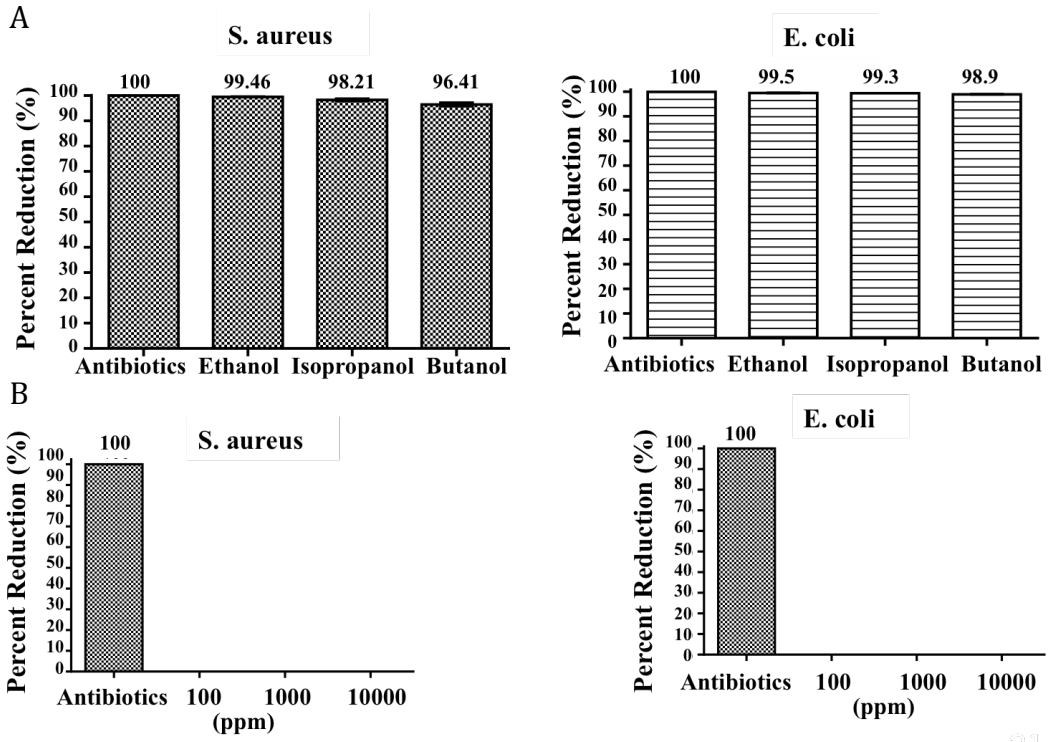

Figure 3-14. (A) % Reduction of the coating method(A) using various solvents against S. aureus and E. coli. (B)% Reduction against *S. aures* and *E.coli* using different SNP concentrations for the incorporating method.

3.8 *In Vivo* Results

Normal weight gain (90.7 ± 5.9 g) and behavior were observed for all rats. The rats survived the spinal fusion surgery and up to 6 weeks post-op, which was the duration of the experiment. Slight calcification was observed at 3 weeks after implantation, and became more evident after 6 weeks. Compared to the rats containing the directly injected foamed PETA-co-TMPTMP scaffolds, the rat implanted with the pre-fabricated sample increased slower in intensity at 6 weeks after implantation. The rat implanted with 0% HA pre-sculpted PETA-co-TMPTMP scaffolds showed little to no calcification, which is in agreement with the *in vitro* osteogenesis study. This study demonstrated that 0% HA scaffolds do not significantly induce the osteogenic markers expression with respect to the control.

To analyze bone formation, micro-CT was performed on the extracted spinal defect section from each rat shown in Figure 3-15. At 6 weeks post-op, rats injected with foamed *in vivo* scaffolds showed non-continuous ossified regions among the entire defect area. During the closure of the surgical site, the foamed *in vivo* structure may have separated from the spinal defect resulting in non-continuous bone formation exhibiting poor interconnectivity and porosity.

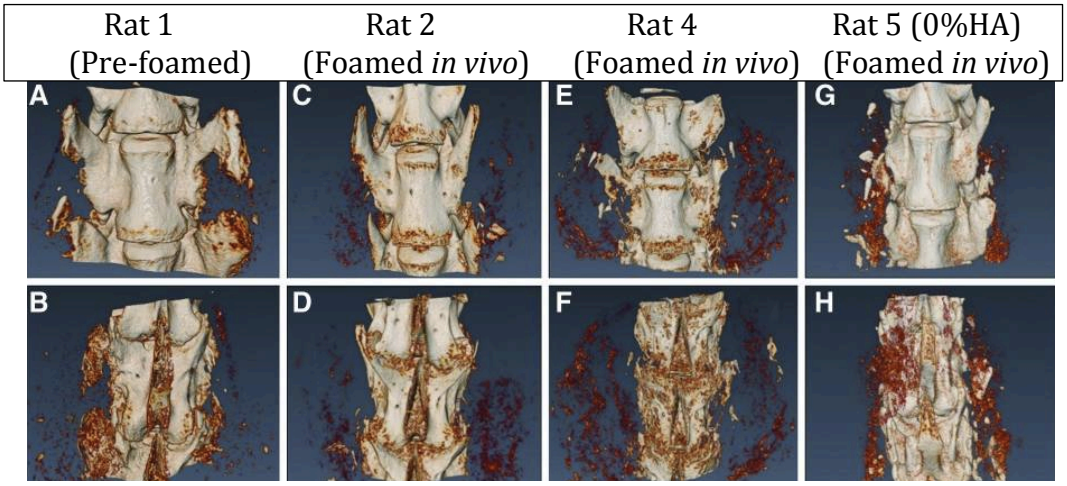

Figure 3-15. Micro-CT data of the L4 (top) and L5 (bottom) vertebral bodies from the *in vivo* study. The light-colored regions indicate densification in scaffolds.

3.9 Discussion/Conclusion: overall

Bone tissue engineering involving polymer/ceramic composites presents an attractive alternative approach to the repair and regeneration of damaged or traumatized bone tissue.[47,80] Several studies have previously explored the potential use of thiol-acrylate chemistry for biomedical devices, but radical-based photoinitiators are usually used to drive the polymerization process.[34,56,59] A nonradical-based polymerization method is potentially less cytotoxic and therefore more amenable to *in situ* polymerization. The amine-catalyzed Michael addition for thiol-acrylate polymerization described in this study has potential advantages compared to

photoinitiated reactions because the chain propagation does not require a free radical initiator during the polymerization reaction. The mechanism of this amine-catalyzed reaction has been previously investigated.[9,14] The general reaction occurs via the formation of a catalyst/comonomer molecule by the Michael addition of a secondary amine across the alkene end group found in acrylate monomers. The *in situ* catalyst produced reacts with a trifunctional thiol and trifunctional acrylates forming a high-density crosslinked copolymer. The step growth nature and the incorporation of the tertiary amine catalyst reduce concerns about potential leaching of free-radical initiators and unreacted monomer. This reaction, therefore, is potentially more attractive for *in situ* polymerization for bone formation than comparative free-radical-based methods.

The PCL-based scaffold was synthesized via a thermal precipitation method resulting in pore size, volume, and interconnectivity that are largely independent of solution viscosity.[108] Results showed that such characteristics were directly influenced by the viscosity of the stock solution in the polymerization of PETA-co-TMPTMP composites.[109] It is well documented that an interconnected pore structure can help support cell migration, cell differentiation, nutrient transport,[75,74] and, in some cases, formation of blood vessels.[76-78] Because HA was found to decrease interconnectivity, it was expected that the highest HA concentration sample PETA:HA (75:25) would not provide a suitable environment for cell in-growth and nutrient/waste transport. Electron microscopy images and micro-CT analysis indicate that PETA:HA (75:25) scaffolds lack interconnectivity of the void volume providing for cell penetration and nutrient/waste transport required for cell growth and differentiation. The analysis of cell viability and expression of osteogenic markers further supported this hypothesis.

The decreased metabolic activity of PETA:HA composites compared with the PETA-co-TMPTMP control is likely related to differences in cell function, not cell number, attributed to osteogenic differentiation of hASCs. The decreased cell proliferation and metabolic activity also had an inverse relationship with the increased calcium deposition and expression of osteogenic markers. This data further supports the hypothesis that HA induces osteogenesis, resulting in decreased metabolic activity and proliferation.[110,111]

Further experimentation by colleagues showed that calcium deposition correlated with the expression of *ALP* and *OCN* in hASCs cultured on PETA:HA (85:15) and PETA:HA (80:20) scaffolds, which were significantly greater than PCL:HA (80:20), pure PCL, and PETA control scaffolds in both media conditions, providing a further indication that scaffolds composed of PETA may be an appropriate material for the repair of bone defects. Increased alizarin stain uptake in PETA:HA (80:20) and PETA:HA (85:15), compared with PCL:HA (80:20), does not correlate with increased cell density or metabolic activity but does correlates with increased *ALP* and *OCN* expression. PETA-co-TMPTMP is better able to induce the expression of osteogenic markers than PCL, but further comparisons at differing concentrations and with other degradable resins are required to test this hypothesis. Cross-sectional images of PETA:HA (75:25) scaffolds demonstrate poor alizarin red penetration, providing further support that the void volume is not substantially interconnected.

Although increasing HA content resulted in reduced pore size and interconnectivity, it provided a more solid and stronger structure for the scaffold. Other studies have shown a similar trend of decreasing porosity with increasing HA

content.[103] The increase in compressive strength seen in solid samples is predictable and similar to that seen with other nanoscale polymer fillers.[102,67] As porosity played no role in the solid samples, the increase in viscosity with increasing HA content beyond 15% did not significantly affect the mechanical strength.

By soaking the PETA based polymer in solvent containing SNPs, the coating method was proven to be an effective way to not only transport an antimicrobial element within the thiol-acrylate copolymer, but also to release and fight the microbes most commonly associated with orthopedic infections. The incorporating method did not release any silver according to the ICP-OES results leading to no defense against the *E.coli* and *Staph. aureaus*. During the *in vivo* study, the structure of the *in-situ*-polymerized foam sample may have been disrupted when the surgical site was closed during the surgery. Poor porosity and interconnectivity could be the reason why the densified regions of the radiographs were noncontinuous.[112] Overall results suggest that PETA:HA scaffolds could be a suitable substrate for bone regeneration.

Chapter 4. Cell Adhesion to Thiol-Acrylate Materials

4.1 Chapter Summary

Thiol-acrylate materials have been demonstrated to have therapeutic potential as biocompatible scaffolds for bone tissue regeneration due to their osteoconductivity, biodegradability, and well-suited mechanical properties. This chapter connects the mechanical properties and stability of thiol-acrylate polymer networks with cell adhesion and proliferation of human adipose derived stromal cells. The other polymers presented in this chapter, polyethylene glycol diacrylate (PEGDA(700))-co-trimethylolpropane ethoxylate triacrylate-co-trimethylolpropane tris(3-mercaptopropionate)(TMPTMP) and TMPeTA-co-TMPTMP, was synthesized by a simple amine-catalyzed Michael addition reaction without any complicated functionalization using cell adhesive proteins. Physical, mechanical, and chemical characterizations were performed on the polymeric substrates, followed by preliminary *in vitro* cytocompatibility tests. Live/dead stain assays showed significant differences in cell survival for TMPeTA of differing molecular weight (692 and 912 g/mol). Collectively, these results highlight the potential for these thiol-acrylate based polymers to be a versatile, biocompatible scaffold for tissue engineering applications.

4.2 Introduction

The process of cell adhesion is important as it directs cell-cell communication, migration of cells, and cell survival. The ability of stem cells to adhere to a given surface sets the foundation for cells to organize and form highly structured tissues. Integrating a polymer based scaffold that supports cell attachment *in vitro* can subsequently allow for

in vivo tissue formation, readily addressing supply and costs associated with bone grafts as well as providing other benefits.[113]

Successful cell adhesion to a substrate requires the adsorption of three protein classes: extracellular matrix (ECM), transmembrane, and cell adhesion receptor proteins. Surfaces that lack the ability to interact with these proteins, such as (polyethylene glycol) (PEG), exhibit weak interactions between the substrate and the cells preventing cell adhesion from occurring.[114,115] Alternatively, PEG based materials have been shown, as successful carriers for cell encapsulation, which is a substitute for cell seeding for the transport of cells *in vivo* that does not require cell adhesion.[62,116] To address the challenges of attaching cells to polymeric surfaces, adhesive moieties such as RGD or collagen have been used to improve cell adhesion.[33,113,117,118] However, the incorporation of RGD into synthetic scaffolds is an expensive process that includes lengthy synthetic techniques usually followed by post-purification steps.[119,120]

Several polymer characteristics affecting cell adhesion *in vitro* and subsequently tissue formation *in vivo* are wettability, mechanical integrity, and surface charge.[121,122] A hydrophilic polymer can greatly enhance cell function by aiding in the adsorption of extracellular proteins.[123] While, the surface charge of the polymer contributes to the material's hydrophilicity, it also affects cell adhesion by promoting interactions with charged species in the extracellular matrix.[121,124] The mechanical properties of the polymer surface play a role in cell adhesion since cells usually attach to relatively stiff materials by transmembrane receptors (integrins), which connect the cytoskeleton of the cells to the substrate.[125,126] This phenomenon is illustrated by a change in cell morphology when attachment to an appropriate substrate occurs.[127,128]

Prior research has explored scaffolds fabricated using pentaerythritol triacrylate-co-trimethylolpropane tris(3-mercaptopropionate) (PETA-co-TMPTMP), another thiol-acrylate polymer, as potential bone augments and grafts. These materials promote cell adhesion/proliferation without the need for cell adhesive proteins or amino acid chains, such as RGD.[9,112,129] The high conversion and lack of radical production, characteristic of these base-catalyzed, thiol-acrylate step-growth polymerizations, contribute to the cytocompatibility of PETA and support its application as an *in situ* polymerizing biomaterial, but the chemical moieties and properties of these materials that promote cell adhesion remain to be elucidated.

The purpose of this study was to demonstrate the effect amine content, monomer molecular weight, reaction synthetic route, and average functionality have on cell adhesion. Several polymer compositions, in which the monomer or base catalyst content was altered, were synthesized similar to PETA by a base-catalyzed Michael addition reaction that proceeds by a step-growth polymerization. Along with the TMPeTA (692 & 912) polymers, polyethylene glycol diacrylate (PEGDA) (700) polymers will also be synthesized via nucleophile-initiated and base-catalyzed reaction routes with different material properties analyzed. Initial characterization studies of TMPeTA(692) and TMPeTA(912) polymers were performed to examine the mechanical properties, hydrolytic stability, and hydrophilicity of the polymers. Live/dead staining and PicoGreen® quantification of DNA were used to quantify the attachment and proliferation of human adipose-derived adult stem cells (hASCs) onto the thiol-acrylate material. A proof of concept encapsulation technique will also be presented to demonstrate an alternative method for transporting cells *in vivo*.

4.3 Materials/Methods

4.3.1 Preparation of PEGDA(700) Nucleophile-Initiated Polymers

As discussed in a previous chapter, the PEGDA(700) monomer was chosen for further analysis due to its higher modulus and compression strength compared to the 250 and 575 PEGDA molecular weights. DEA (0.5%, 1.0%, and 2%) was added to PEGDA(700) and shaken by hand for 1 minute. TMPTMP was added in a 1:1 molar ratio to the PEGDA monomer. Besides the 1:1 formulations of acrylate to thiol, excess thiol concentrations were also prepared using 10%, 20%, 30%, and 40% thiol and added to the PEGDA(700)/DEA solution.

4.3.2 Gel Time

The gel times were calculated for the 0.5%, 1%, and 2 % DEA PEGDA(700) samples in a 20 ml glass vial by starting the timer as soon as TMPTMP is added and stopping the time when the PEGDA(700)/TMPTMP/DEA solution ceased to flow when the vial was inverted.

4.3.3 FTIR Conversion Analysis

FTIR was performed on the PEGDA(700) polymers with varying amine concentrations (0.5%,1.0%, and 2.0% DEA). The polymer precursor mixture was placed between two KBr plates and spectra were taken every 2 minutes for 12 hours. Using OPUS^{TM} software (Bruker Optics, Germany), each acrylate functional peak (1618-1635 cm^{-1}) was integrated and the area was used to determine % conversion. % Conversion was calculated based on the following formula:

$$\text{(Eq. 4-1)} \quad \%\text{Conversion}(T) = \frac{A(T_o) - A(T)}{A(T_o)} \times 100$$

PEGDA(700)/0.5% DEA/20% excess thiol samples were also tested to measure the conversion and to quantify any unreacted monomers still present.

4.3.4 Swelling

The swelling ratio was calculated by soaking triplicates of 0.5% DEA PEGDA(700) polymer samples in 5 ml of PBS. The samples were cured for 48 hours, and were punched out using a 10 mm biopsy punch. The dry weight (Wd) was found prior to submerging the samples in PBS, and the “wet” polymer weights (Ws) were measured every hour until the sample reached an equilibrium weight, which took 10 hours.

$$\text{(Eq. 4-2)} \quad \%\text{Swelling} = \frac{Ws - Wd}{Wd}$$

4.3.5 hASC Isolation and Culture

Subcutaneous adipose tissue liposuction extracts were acquired from three donors under an approved IRB protocol (LSU#E9239). The procedure involving the hASC isolation is described elsewhere.[60] “Passage 0” refers to the primary cell cultures initial passage and is denoted as p0. The hASCs were trypsinized, split, and plated at a density of 5000 cells/cm^2 (“Passage 1”) for expansion on T125 flasks to attain 80% confluency. For all cell-based tests, passage 2 was used.

4.3.6 Cell Seeding on Solid Constructs

Prior to polymerization, the monomers were sterilized by filtering through a 0.45 μm nylon syringe filter (Celltreat). After sample preparation according to Section 4.3.1, the 8 sample groups were immersed in stromal media (Dulbecco’s modified Eagle’s medium (DMEM/F12), 10% FBS (Fetal Bovine Serum), 1% triple antibiotic solution) for 24 hours. hASCs were added to each sample with the concentration of 50,000 cells/well

in a 48 well plate then incubated at 37 °C for a set amount of days depending on the specific experiment.

4.3.7 Cell Morphology Analysis Using Scanning Electron Microscopy

HASCs were seeded according to Section 4.3.6 on the 0.5% DEA polymer for 24 hours. After the allotted incubation time, the stromal media was removed and the preparation for SEM began. The following protocol was used for cell fixation to image cell morphology on the 0.5% DEA PEGDA(700) 1:1 polymer:

1. Add 2% Glutaraldehyde(GA) (2 parts cocadylate (buffering agent), 1 part 8% GA, 1 part DI water) to scaffolds; wait overnight
2. Add 30% ethanol, 50% ethanol, 70% ethanol, 80% ethanol, 90% ethanol, 100% ethanol; wait 30 minutes in between each ethanol addition
3. Add 1:2 HDMS:ethanol; wait 30 minutes
4. Add 1:1 HDMS:ethanol; wait 30 minutes
5. Add 100% HDMS; wait 30 minutes

The above protocol was repeated for a second trial. FAA (formalin, ethanol, and acetic acid) fixative was used for the third trial in place of GA. FAA fixation was repeated. For the next trial, CO_2 drying was used in place of adding HDMS in steps 3-5.

4.3.8 AlamarBlue® of PEGDA(700)

AlamarBlue® was used to test the relative metabolic activity of cells seeded on PEGDA(700) 0.5% DEA 1:1(acrylate:thiol) polymers, (polycaprolactone)PCL solid, and a positive control after 3 days of incubation at 37 °C. The positive control consisted of hASCs seeded onto the tissue-cultured well plate and the PCL was obtained from SIGMA Aldrich, melted flat onto the well plate. For the 7 day study, 10, 20, 30, and 40%

excess thiol concentrations were tested along with 0.5% DEA PEGDA(700)1:1 polymers.

4.4 Materials and Methods (PEGDA(700) Base-Catalyzed)

4.4.1 Polymer Preparation

DEA % (1.0, 2.0, 3.5, 5.0, 7.5, and 9.0) were added to PEGDA(700). 7.5% and 10% PBS (relative to PEGDA(700) weight) was added to the PEGDA(700)/DEA stock solution and stirred for 24 hours. TMPTMP was added in a 1:1(acrylate:thiol) molar ratio including the percentage amine that reacted with the acrylate into the calculation.

4.4.2 Gel Time and Swelling

The gel time was measured based on the method described in Section 4.3.2 for each polymer synthesized in Section 4.4.1. The swelling ratio at one hour was calculated for each polymer synthesized in Section 4.4.1 based on the initial mass (Wd) and the mass after the polymers were soaking in PBS for one hour (Ws). The equation used for the %swelling calculation is found in Section 4.3.4.

4.4.3 Mechanical Strength

PEGDA(700) polymers catalyzed by 1%, 2%, 3.5%, 5.0%, 7.5%, and 9% DEA were gelled in a cylindrical mold and subjected to compressive mechanical testing after 48 hours of cure time. Cylindrical solids with dimensions of 45 mm (diameter) × 25 mm (height) were tested to determine maximal compressive strength and bulk modulus. Scaffolds were subjected to compression testing at 90% strain. A universal testing machine (Instron Model 5696, Canton, MA, USA) was used at an extension rate of 0.5 mm/min.

4.4.4 AlamarBlue® on Extracts of PEGDA(700) Base-Catalyzed Polymer

The stem cells were isolated and seeded according to Section 4.3.4 directly on a 48 well plate. Prior to polymerization, the monomers were sterilized by filtering through a 0.45 μm nylon syringe filter (Celltreat). After sample preparation according to Section 4.4.1, 6 PEGDA sample groups (1, 2, 3.5% DEA with 7.5% PBS and 10% PBS) were immersed in 5ml stromal media (Dulbecco's modified Eagle's medium (DMEM/F12), 10% FBS (Fetal Bovine Serum), 1% triple antibiotic solution) for 7 days. hASCs were added to each well plate's surface with the concentration of 50,000 cells/well in a 48 well plate then incubated at 37 °C for 24 hours. 300 μl of the media that the polymer samples were soaking in were extracted and placed in the well plates with previously seeded cells. These extracts were tested for cell viability 24 hours later using AlamarBlue®.

4.4.5 Live/Dead Staining

To assess the viability of hASCs on the polymer scaffolds, live/dead staining (Cell viability®, Invitrogen- using a Leica TCS SP2 spectral Confocal) was performed 24 hours after cell seeding. The following polymers were tested: PEGDA (2, 5, 9% DEA), PETA (2.8 and 16.1% DEA), and TMPTA (2.8% and 16.1% DEA) with each having 10% PBS added initially to synthesize the stock solution containing the acrylate plus DEA with the exception of PETA. 300 μl of PBS containing 4 μM EthD-1 and 2 μM Calcein-AM (Invitrogen) was added to each sample followed by incubation at room temperature for 45 min. The samples were then imaged using a fluorescent microscope (Zeiss SteREO Lumar.V12 fluorescence stereomicroscope) to detect live (green) and dead (red) cells on the samples.

4.5 Materials and Methods (TMPeTA(692&912))

4.5.1 Preparation of Thiol-acrylate Materials (TMPeTA(692&912))

All chemicals were used as received. Trimethylolpropane ethoxylated triacrylate (TMPeTA) (692 & 912) and trimethylolpropane tris(3-mercaptopropianate) (TMPTMP) were obtained from Sigma Aldrich. Diethylamine (DEA) was obtained with 99% purity from ACROS Organics. The DEA was added to TMPeTA/PBS (wt% relative to acrylate amount) with increasing mol% relative to acrylate functionality forming a stock solution. The polymer was prepared by adding TMPTMP to this TMPeTA/DEA stock solution in a 1:1 molar functionality of acrylate to thiol. Eight different sample groups were fabricated for the following characterizations with 692 and 912 TMPeTA with 2.8, 5.0, 10, 16.1% DEA.

4.5.2 Mechanical Testing

The procedure described in Section 4.4.3 was repeated for all 8 samples of TMPeTA(692) and TMPeTA(912) polymers. Cylindrical solids of the polymers with dimensions of 45 mm (diameter) × 25 mm (height) were tested to determine maximal compressive strength and bulk modulus at 90% strain at an extension rate of 0.5 mm/min.

4.5.3 Contact Angle Measurement

Contact angles were determined using VCA Surface Analysis System with Optima XE software for the 692 and 912 TMPeTA fabricated with 2.8, 5.0, 10, 16.1% DEA relative to acrylate functionality. Nanopure water (5 µl) was dispensed automatically and allowed to equilibrate for 30 seconds on three separate locations of each polymer sample.

4.5.4 Mass Loss

The 692 and 912 TMPeTA with 2.8%, 5.0%, 10%, 16.1% DEA polymer samples were fabricated as noted above and punched into cylinder shaped (10 mm (diameter) x 10 mm (height)) constructs. The samples were freeze-dried for 24 hours, then submerged in 5 ml DMEM/F12 media for 7 days at 37 °C. The samples were washed and freeze-dried after the 7-day incubation to remove any absorbed moisture.

4.5.5 Live/Dead Staining

Live/dead staining (Cell viability®, Invitrogen – using a Leica TCS SP2 spectral Confocal) was performed to assess the viability of hASCs on the solid constructs 1, 4 and 7 days after seeding. The solid constructs were prepared as in Section 4.5.1, which included TMPeTA(692) and TMPeTA(912) catalyzed by 2.8%, 5%, 10%, 16.1% DEA. The live dead staining was prepared and imaged according to Section 4.4.5.

4.5.6 Quantification of DNA on Polymeric Samples

Total DNA content was used to determine the proliferation of cells on each sample. All the samples were lysed using 0.5 mg/ml of Poteinase K overnight at 56 °C. DNA quantification was done by mixing 50 µl of the Proteinase K solution and 50 µl of PicoGreen® dye solution (Invitrogen™Quant-iT™ PicoGreen® dsDNA Assay Kit) in 96 well plates.[9] 100 µl of dye was used as a background and was subtracted from the data. Samples were excited at 480 nm with an emission wavelength of 520 nm, and the total DNA concentration was compared to a standard curve generated from serial dilutions of hASC in order to calculate the number of the cells in each well.

4.6 Results/Discussion

PEG-based scaffolds have shown promise in the field of bone tissue engineering due to their similarity to the extracellular matrix and their biocompatibility.[117] Most thiol-ene synthesized PEG hydrogels are converted to solid 3D hydrogels by way of photopolymerization.[61,130,131] However, the swollen 3D structures lack the mechanical strength needed for bone replacement applications. Despite the low mechanical properties, PEG monomers still remain attractive for biomaterial synthesis by aiding in the attachment of the scaffold material to osteogenic tissue. The hydrophilicity of the PEG network can be manipulated by changing the monomer molecular weight, which changes the hydrophilic backbone length.

The synthesis of neat PEGDA stocks was experimented with similar to the PETA polymer by attempting a Michael addition of DEA to the PEGDA monomer followed by stirring for 3 hours. No gelation occurred after TMPTMP addition. The gel times did not yield the bell curve plot that was shown for gel times of the PETA polymer graph (Figure 2-2) that illustrated a decrease in gel time then a switch to increasing gel time. This unusual observation of the system not gelling was analyzed further. Despite decreasing and increasing the stir times of the PEGDA/DEA solution, gelation only occurred after adding the DEA to the PEGDA immediately prior to adding the TMPTMP. It was likely that the amine was not adding on to the acrylate as in the PETA system described in chapter 2, thus free DEA molecules were evaporating due to its high vapor pressure; therefore, the addition of the thiol did not cause it to gel. Also, the Michael addition reaction of the amine to the acrylate may be slower than the evaporation of the amine. Since the formation of a tertiary amine catalyst (stock solution) proved not as simple as

for the PETA system, a nucleophile-initiated system was synthesized and characterized. The gel times, % acrylate conversion[132], and swelling ratios were measured. Additionally, SEM imaging was used in conjunction with cell fixation techniques to study cell morphology.

4.6.1 Gel Time and FTIR (Results)

The gel time ranged from 1-7minutes for the samples (Figure 4-1) showing a decrease in gel time with increasing amine catalyst. FTIR was used to determine conversion of acrylate groups as a function of time for the polymer formulations using 0.5%, 1.0%, and 2% DEA. The % acrylate conversion was determined via the equation described in Section 4.3.3. The acrylate conversion (Figure 4-2, A) for the 1.0 and 2.0% DEA PEGDA(700) polymer reached an average of 90%. The 0.5% DEA yielded an average conversion of 97%.

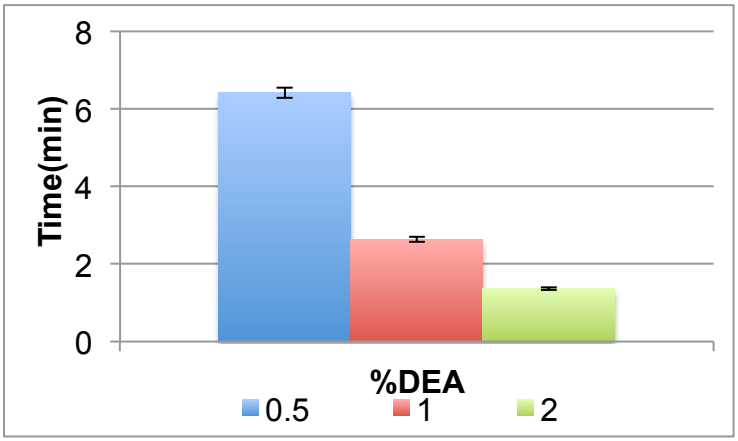

Figure 4-1. Gel time as a function of DEA concentration for the PEGDA(700) nucleophile-initiated polymers.

The 1 and 2% DEA concentrations reached gelation in ~1-2 minutes which may affect diffusion of the reactive groups likely causing the lower conversion while the 0.5% gelled in 6 minutes allowing more time for the functional groups to react before gelation significantly causes a decrease in diffusion of the molecules. Since the 0.5% DEA

PEGDA(700) polymer reached the highest acrylate conversion, it was the only concentration studied for the swelling and cell studies. The 20% excess thiol concentration and the 1:1(acrylate:thiol) over ~12 hours were both subjected to FTIR testing to compare the rate of acrylate conversion between the two formulations (Figure 4-2, B). The excess thiol polymer behaved as expected with the acrylate groups being

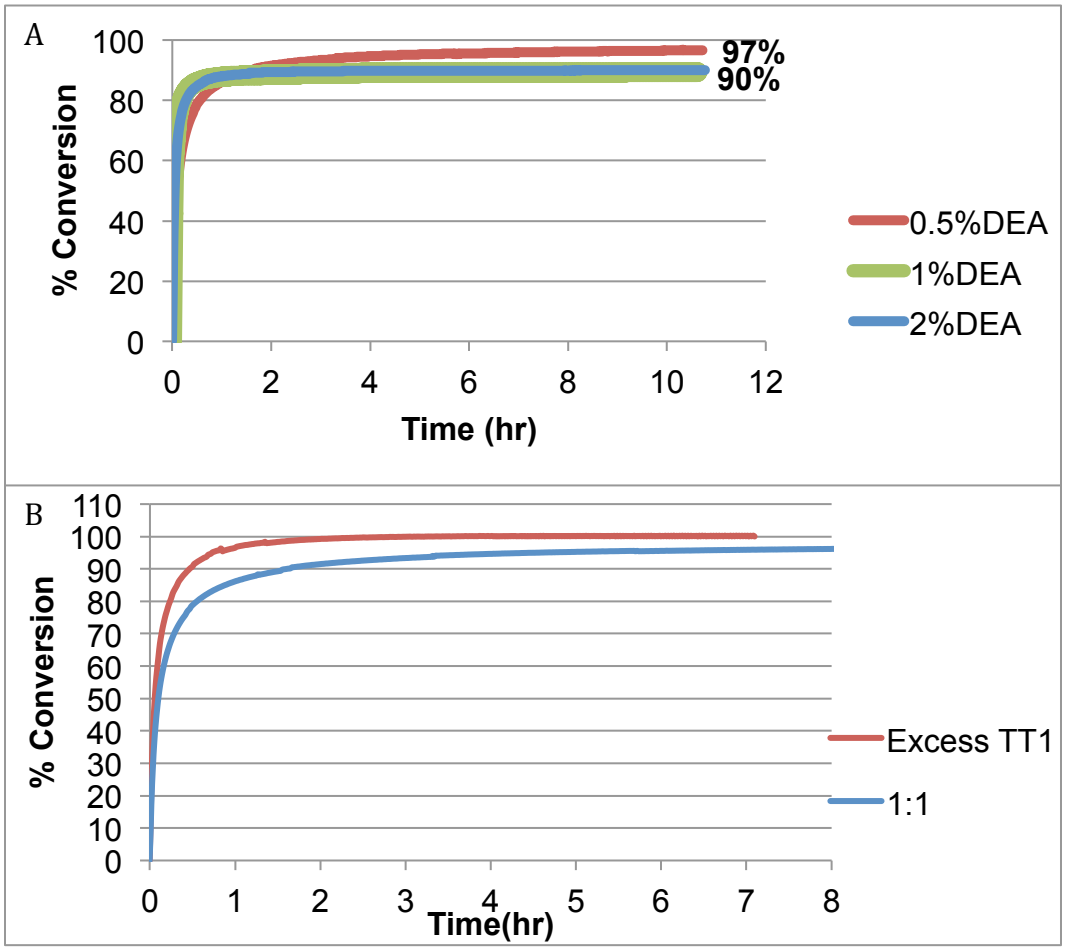

Figure 4-2. The acrylate (%) conversion as a function of time studied using FTIR. A. 0.5%, 1%, 2% DEA PEGDA(700) polymers B. 0.5% DEA PEGDA(700) 20% excess thiol and 1:1.

consumed immediately. Having more thiol present caused the acrylates to increase in conversion because any unreacted acrylate would be consumed by the excess thiol present.

4.6.2 Swelling Ratio

The swelling ratio (%) reached 60% for the 0.5% DEA PEGDA(700) polymer over 10 hours (Figure 4-3), which is relatively low compared to other biomedical materials used for tissue engineering that usually swell to an average % swelling ratio between 200-300%.[133] On the contrary, the PETA did not swell over the 10-hour time study, which coincides with it not having the hydrophilic ethoxylated backbone found in PEGDA molecules that is responsible for PEG based materials swelling.

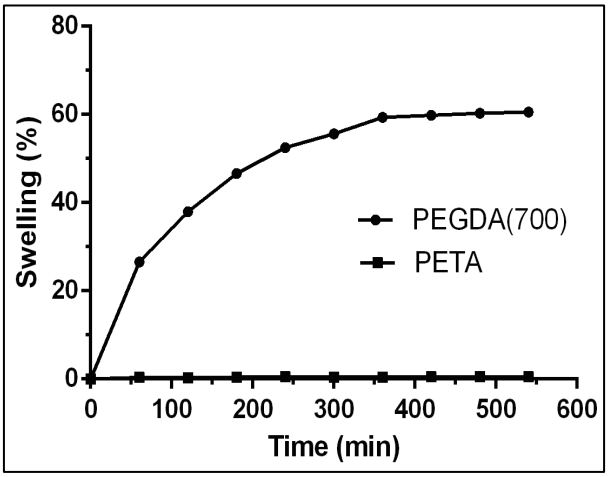

Figure 4-3. Swelling ratio of PEGDA(700) and PETA polymer over a 10-hour time period

4.6.3 SEM (Cytotoxicity)

SEM dehydration methods of fixing cells prior to electron microscopy imaging is important in order to preserve the cellular structure in its living state. The fixation process is time-consuming and expensive, therefore choosing the right fixation method is important. The theory behind cell fixation is an ongoing study, but it is generally understood that it involves the crosslinking of proteins with other molecules found within the cells and ECM being secreted.[134] Glutaraldehyde (GA) and FAA (formaldehyde, acetic acid, and alcohol) were the main fixatives used in the SEM cell preparation work

with each having its own advantages. GA is considered a better crosslinker than formaldehyde because it rapidly forms intra and inter molecular bonds with proteins and surrounding tissue. GA yields a higher crosslinking density because it has two aldehyde groups versus the one aldehyde group in formaldehyde. FAA fixes cells by crosslinking too but also penetrates the cells faster since formaldehyde is smaller in size. The alcohol and acetic acid component contained within FAA gives it an added feature by helping keep a balance between the swelling (acetic acid) and shrinkage (alcohol) of the cells.

The fixation step is followed by the dehydration step to remove any water left in the sample using ethanol or acetone, and thus can be placed under the vacuum in the SEM. Another common drying method, critical point drying, works by replacing water with CO_2 gas.[135] The chemicals used in microscopy fixation protocols are known for their harsh effects on materials and surface topology. Different cell image preparation techniques were used to determine which method would not alter the polymer surface; therefore GA, FAA, and CO_2 drying techniques were used.

Excess thiol concentrations (10, 20, 30, and 40%) and 1:1 (thiol:acrylate) were synthesized, seeded with cells, and imaged to analyze cell attachment on the different PEGDA(700) formulated polymers all catalyzed with 0.5% DEA. According to SEM imaging (Figure 4-4, B&C), the stem cells were inconsistently attaching to the 1:1 thiol-acrylate formulation, but no attachment was observed on the 20% excess thiol polymer despite the different fixation protocols used. This is contradictory to research that reports thiol would promote cell attachment by forming disulfide bonds with thiol containing proteins secreted by the ECM when cells begin to attach.[136] The FTIR results

(Figure 4-2, B) also showed the complete conversion of the acrylate monomer (known toxicity) quickly when excess thiol is present which could perhaps help the overall toxicity of the polymer. The 20% excess thiol sample displayed lower cell viability likely due to the acidic nature of the excess monomer, TMPTMP. Similar monofunctional thiols, ethyl 2-mercaptopropionate and methyl 3-mercaptopropionate, were studied by Chan et.al., and shown to have a pK_a of 9.66 suggesting the pK_a of TMPTMP should be similar.[8]

Polymers without stem cells were also analyzed for comparison of the different methods. The polymers treated with GA showed a rippling effect on the surface, which is usually indicative of dehydration while the FAA treated polymers presented darker and lighter stripes on the surface resembling an inhomogeneous sample. (Figure 4-4, A) The CO_2 drying appeared to keep the polymer surface the smoothest. For the 1:1 PEGDA(700) samples, cell fragments were observed among the different protocols except one random trial using FAA shown in the boxed column in Figure 4-4, B. However, these results were unable to be replicated; cells on the excess thiol did not exhibit the proliferated spindle shaped cell morphology but rather disconnected cell pieces. Analyzing cell attachment by SEM proved to not only be time consuming but also affected the surface topology of the polymer. Therefore, cell morphology was analyzed by live/dead staining for the next set of experiments.

4.6.4 AlamarBlue® Results: PEGDA(700) Nucleophile-Initiated

AlamarBlue® is a cytotoxicity test that uses live cells to reduce its active ingredient (resazurin) to a fluorescent compound. The higher the fluorescence, the higher the number of live cells found on the samples. AlamarBlue® testing was

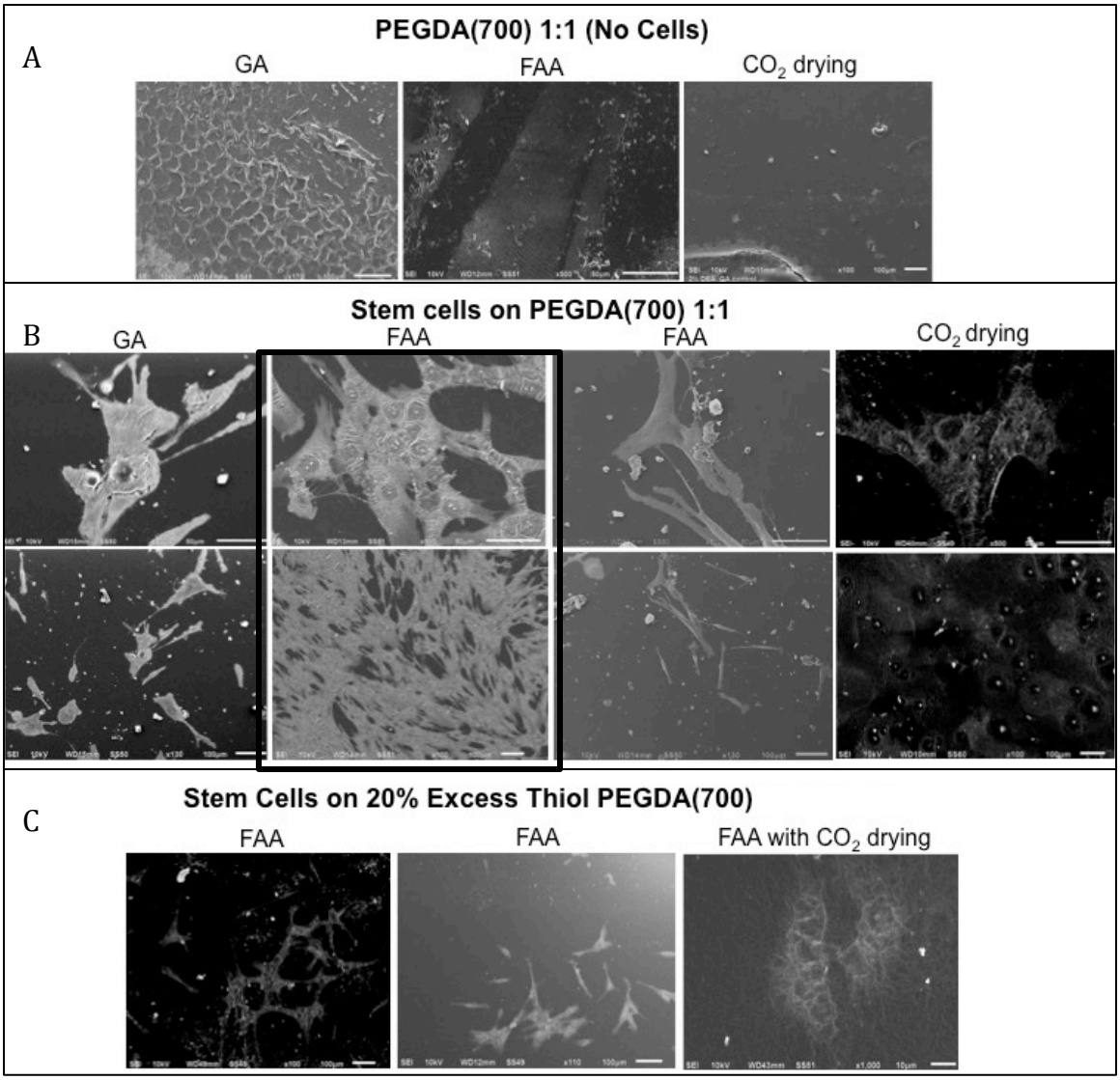

Figure 4-4. SEM imaging using different cell fixatives and drying (GA, FAA, and CO_2 drying) on (A) 1:1 PEGDA(700) 1:1 without stem cells (B) 1:1 PEGDA(700) with hASCs 1:1 (C) 20% excess thiol

performed on hASC seeded samples including PCL, PEGDA polymer, and a positive control after 3 days of incubation time. The 1:1 PEGDA polymer showed a 50% metabolic activity compared to the 70% that PCL displayed. Seeded studies using hASCs were also done for a samples set containing a 1:1 ratio (acrylate:thiol), 10%, 20%, and 40% excess thiol after 7 days to determine if increasing or decreasing the excess thiol concentration would alter the cytotoxicity results. The 20% excess thiol

concentration polymer agreed with the SEM results with only a 25% metabolic activity revealed. The 10 and 40% did not display any higher metabolic relative activity as shown in Figure 4-5. It should be noted that the 1:1 polymer sample dropped in metabolic activity from day 3 to day 7 suggesting that the seeded cells on the polymer were dying.

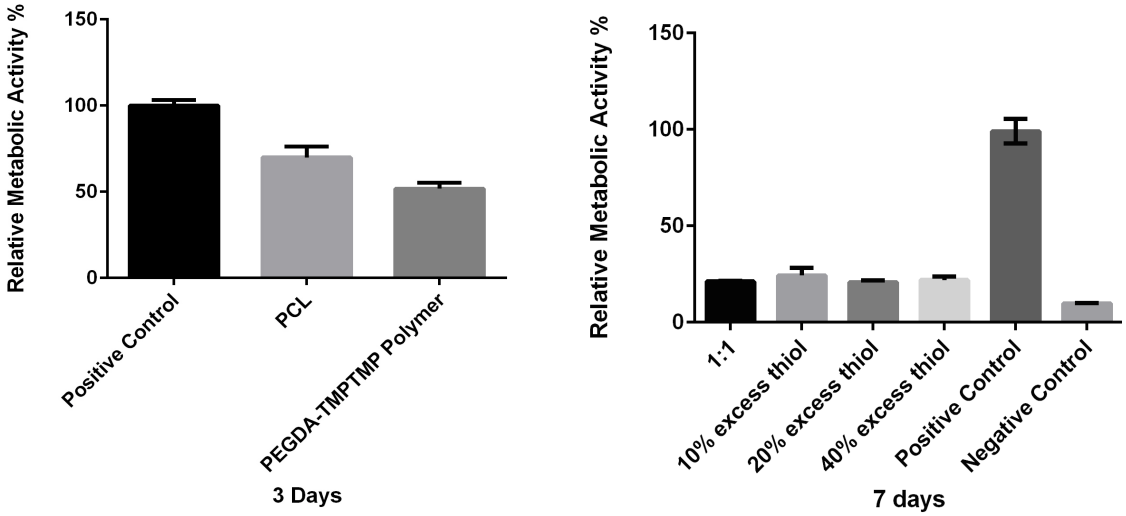

Figure 4-5. Relative Metabolic Activity of 1:1 PEGDA(700)-co-TMPTMP and differing excess thiol concentrations at hASCs at day 3 and 7.

4.7 Results: PEGDA (Base-Catalyzed)

The poor results from cell studies involving the PEGDA(700) nucleophile-initiated (1:1 and excess thiol) polymer caused a change in direction for the project. Since PETA-co-TMPTMP was effective at promoting cell-growth, the development of the stock solution (tertiary amine catalyst) formed from a Michael addition between an acrylate and nucleophilic amine was re-evaluated. The structure of the PETA monomer contains an hydroxyl group which may be responsible for donating the proton during the formation of the tertiary amine catalyst (Scheme 1-3).[8] Minimal PBS content (0.5% relative to PEGDA weight) was added and tested via FTIR to ensure addition occurred. The sample was prepared by adding PEGDA(700) to % PBS, mixing for 30 seconds

then adding 20% DEA. Figure 4-6 shows the % acrylate conversion reached ~18% conversion in under 5 hours, which correlates with the 20% DEA that was added to synthesize the stock solution with a 2% likely attributed to evaporation. By adding a proton source to the PEGDA(700)/DEA system, the amine adds on similar to the PETA system.

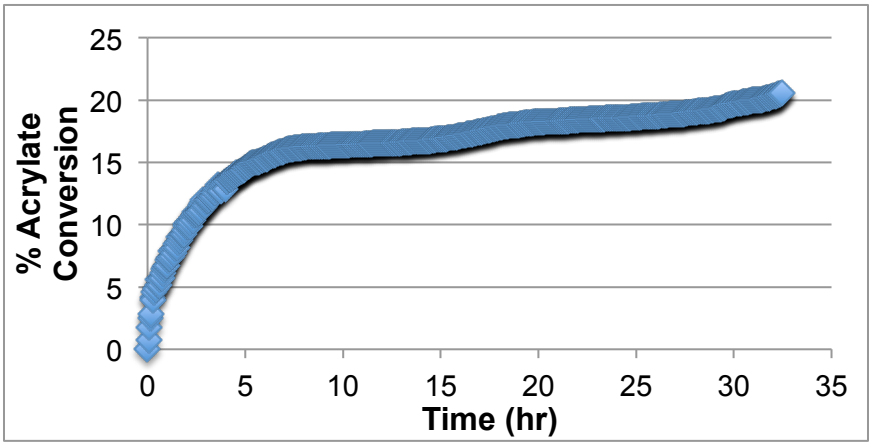

Figure 4-6. The percentage acrylate conversion determined via FTIR of PEGDA(700)/ PBS/20% DEA as a function of time.

For the remaining experiments, 7.5% and 10% of water relative to the amount of PEGDA was added to make a stock solution. Prior to adding a proton source, the samples synthesized for cytotoxicity were a mixture of base-catalyzed and nucleophile initiated synthesized polymers since the amine could only add on to the acrylate when the thiol (acidic hydrogen source) was available.

4.7.1 Gel Time

The samples synthesized via a base-catalyzed mechanism with 10% PBS relative to PEGDA(700) have gel times ranging from 5-35 minutes decreasing as the DEA concentration increased (Figure 4-7).

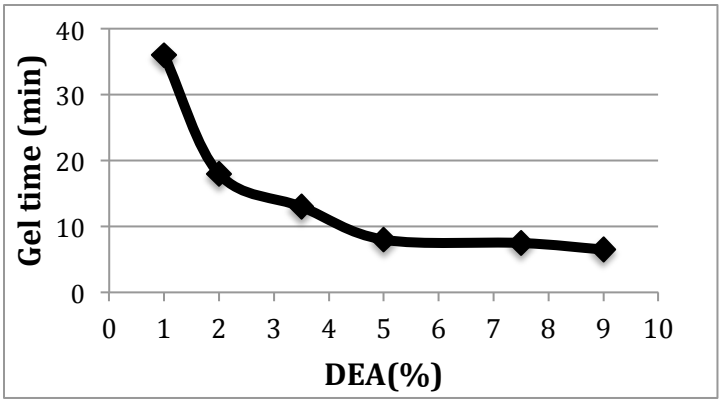

Figure 4-7. Gel time as a function of amine concentration for PEGDA(700) base-catalyzed system

4.7.2 Swelling/Mechanical Strength of Base-Catalyzed PEGDA Polymer

The % swelling ratio increased for PEGDA(700)-co-TMPTMP polymers with increasing DEA concentration (Figure 4-8B). This is related to crosslinking density decreasing with increasing amine content since the amine performs a Michael addition with the double bond thus decreasing acrylate functionality. In contrast, the compressive strength decreased with an increase in DEA concentration (Figure 4-8, A). This coincides with the crosslinking density and is in agreement with the swelling data. A polymer will absorb more water and drop in mechanical strength as the functionality decreases, which can occur as you increase DEA. Only the compressive strength was reported for the PEGDA polymers since each exhibited low moduli of less than 1MPa due to their elastic nature. Similar elastic materials display the same trend.

4.7.3 Extract Cytotoxicity of Base-Catalyzed PEGDA polymer

To determine if the PBS concentration in the stock solution would cause a difference in the cytotoxicity results, the extract cytotoxicity was measured for samples consisting of 1, 2, and 3.5% DEA with 7.5% and 10% PBS. There was no significant difference in the metabolic activity between the two different PBS concentrations, which

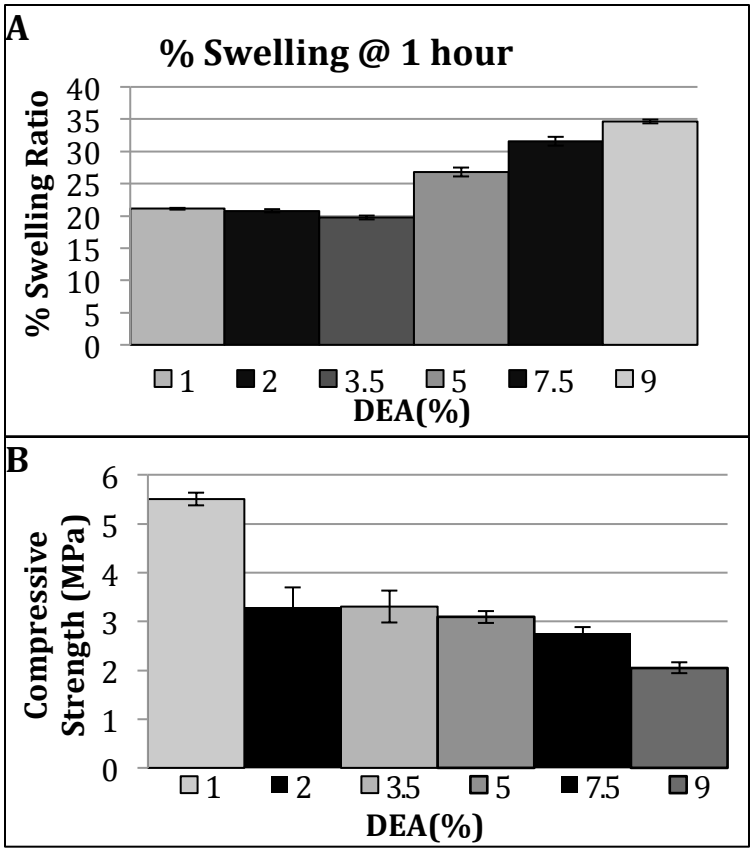

Figure 4-8. A. Swelling % ratio at 1 hour B. Compressive Strength of PEGDA polymers of varying DEA (%)

is expected since PBS is a well-known buffer used in biological systems for many

different applications (Figure 4-9).

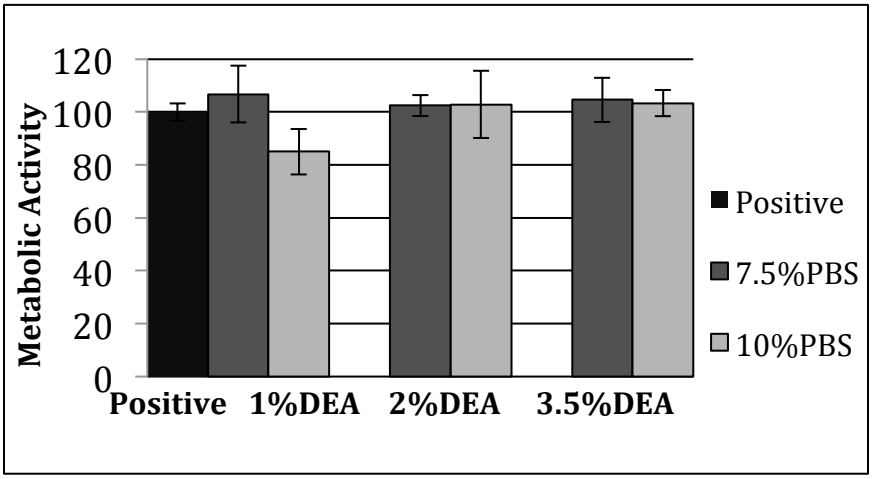

Figure 4-9. The cytotoxicity of the extracts from the PEGDA polymer to study the difference between the PBS content.

4.7.4 Live Dead Staining

PEGDA(700) 2%, 5%, and 9% DEA was seeded with hASCs and stained/imaged at 24 hours post seeding to allow for attachment. These three DEA concentrations were chosen to get an overview of amine composition in regards to cell attachment. The change in morphology from sphere to spindle shaped is indicative of cell adhesion on surfaces. Cells on PEGDA(700) and TMPTA did not show a change in morphology while cells on PETA did change in morphology. The cells seeded onto the PEGDA-co-TMPTMP polymer described earlier, maintained sphere morphology after 24 hours (Figure 4-10). The cells on the TMPTA did not change morphology, but cells on PETA changed morphology to spindle shape, demonstrating that cell adhesion may not be

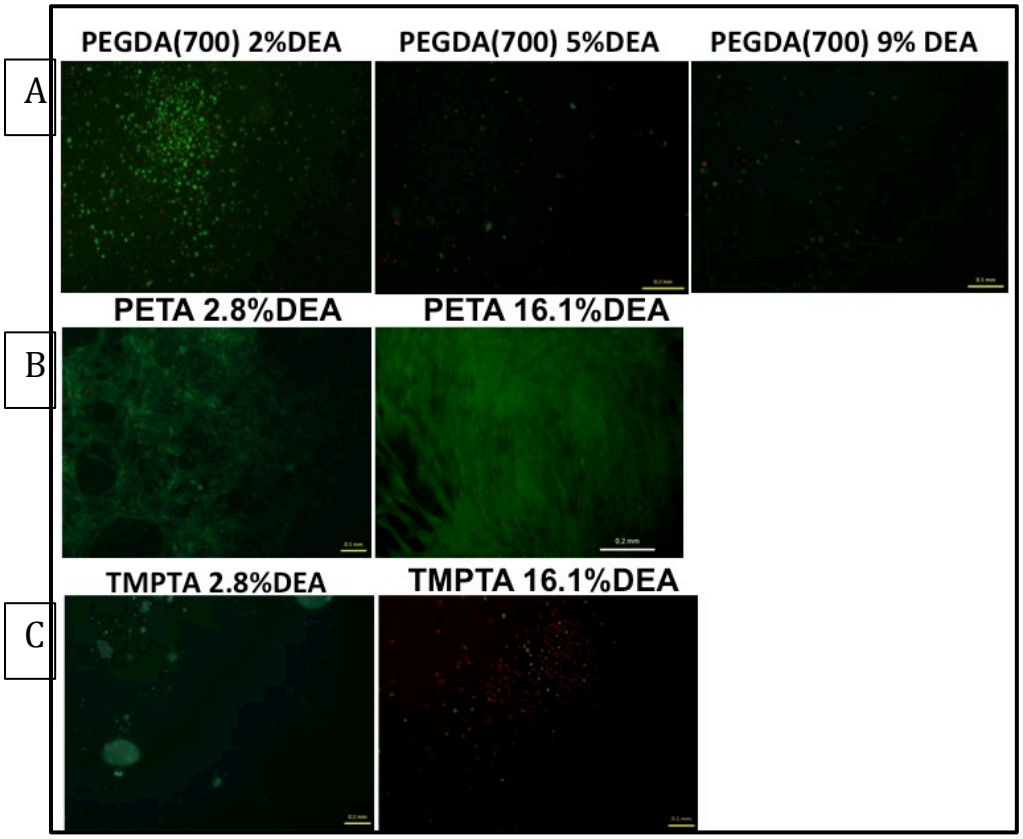

Figure 4-10. Live/Dead staining of hASCs on different polymers. A. PEGDA(700) 2%, 5%, 9% DEA B. 2.8% and 16.1% DEA PETA C. 2.8% and 16.1% DEA TMPTA

dependent on crosslinking density alone. TMPTA and PETA have similar MW's and are both trifunctional differing only by a methyl group and a hydroxyl group suggesting another property, wettability may be a factor in cell adhesion. Wettability in relation to cell adhesion is discussed in more detail in the results and discussion (Section 4.8) for the TMPeTA(692) and TMPeTA(912).

4.8 Results Material Characterization (TMPeTA 692 & 912)

Thiol-acrylate polymers synthesized via Michael addition were studied further to understand why the adhesion of stem cells occurs to their surface without modification or functionalization with cell adhesive peptides. As shown in the mechanism (Scheme 4-1), the scheme begins with the formation of a tertiary amine catalyst by the Michael addition of an amine to the alkene group found within an acrylate. This tertiary amine acts as a semi-strong base deprotonating the thiol and starting the polymerization reaction. The thiolate anion adds onto the acrylate's double bond forming a crosslinked polymer network. As the concentration of the tertiary amine catalyst increases, so does the rate of the reaction, which allows for tunable cure times and other properties depending on the application.[14] These anionic step-growth polymerization reactions lack a termination step, which reduces the concentration of unreacted monomers left in the cured material. This property is important to the cytocompatibility of a substrate, but characteristics including hydrophilicity, crosslinking density, and chemical composition have greater influence on the adhesion and differentiation of cells.

The extent of crosslinking of a substrate plays a significant role in the anchoring of stem cells to biocompatible materials by providing mechanical feedback to the cells.[125] The cells exert tractional forces and gauge the feedback during substrate

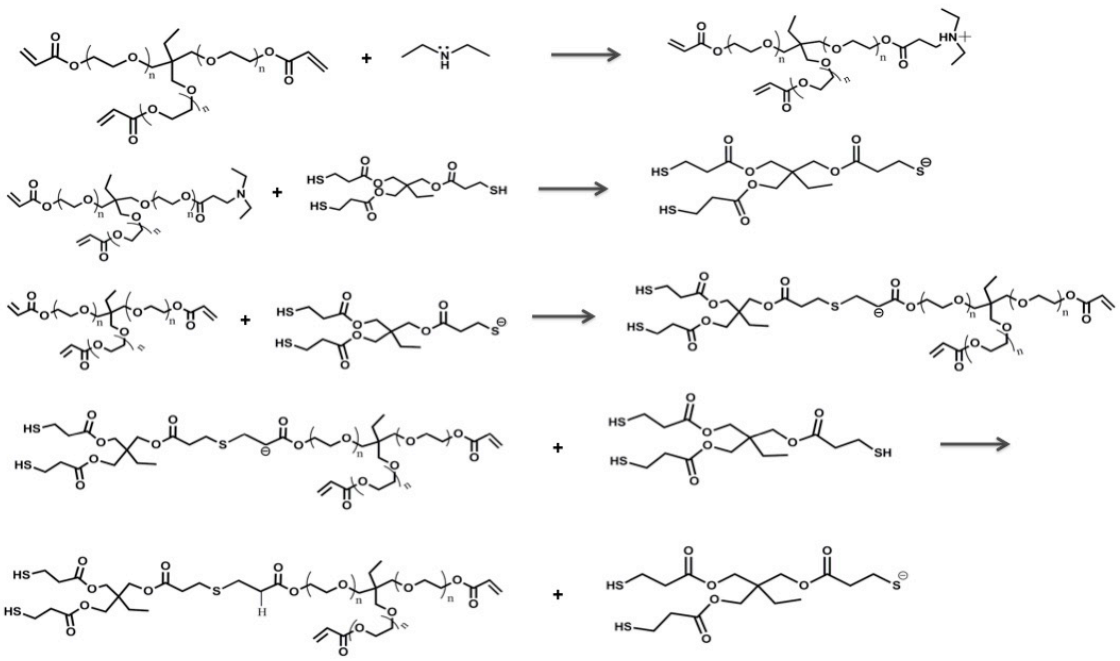

Scheme 4-1. The base-catalyzed Michael addition step growth polymerization reaction scheme. The first step denotes the synthesis of the tertiary amine catalyst.

adhesion and locomotion, thus the substrate needs to be able to withstand these forces for further spreading and proliferation of cells.[126] Therefore, lightly crosslinked substrates cause a delicate cytoskeleton to be formed from the weaker forces that are exerted by the cells.

Cell adhesion on highly crosslinked substrates allows the generation of greater numbers of focal adhesion sites resulting in cell adhesion and spreading[137] (Figure 4-11). Cell morphology is rounded on soft substrates (Figure 4-11), indicating poor cell adhesion, whereas the cells are more spindle shape on day 1 on the TMPeTA(912) correlating to its inability to form an organized cytoskeleton. These weak cytoskeletons cannot support the extent of tissue regeneration needed for bone tissue.[138]

Since Young's modulus and crosslinking density are related[139], the compression modulus was determined for each of the polymers to verify the correlation between the

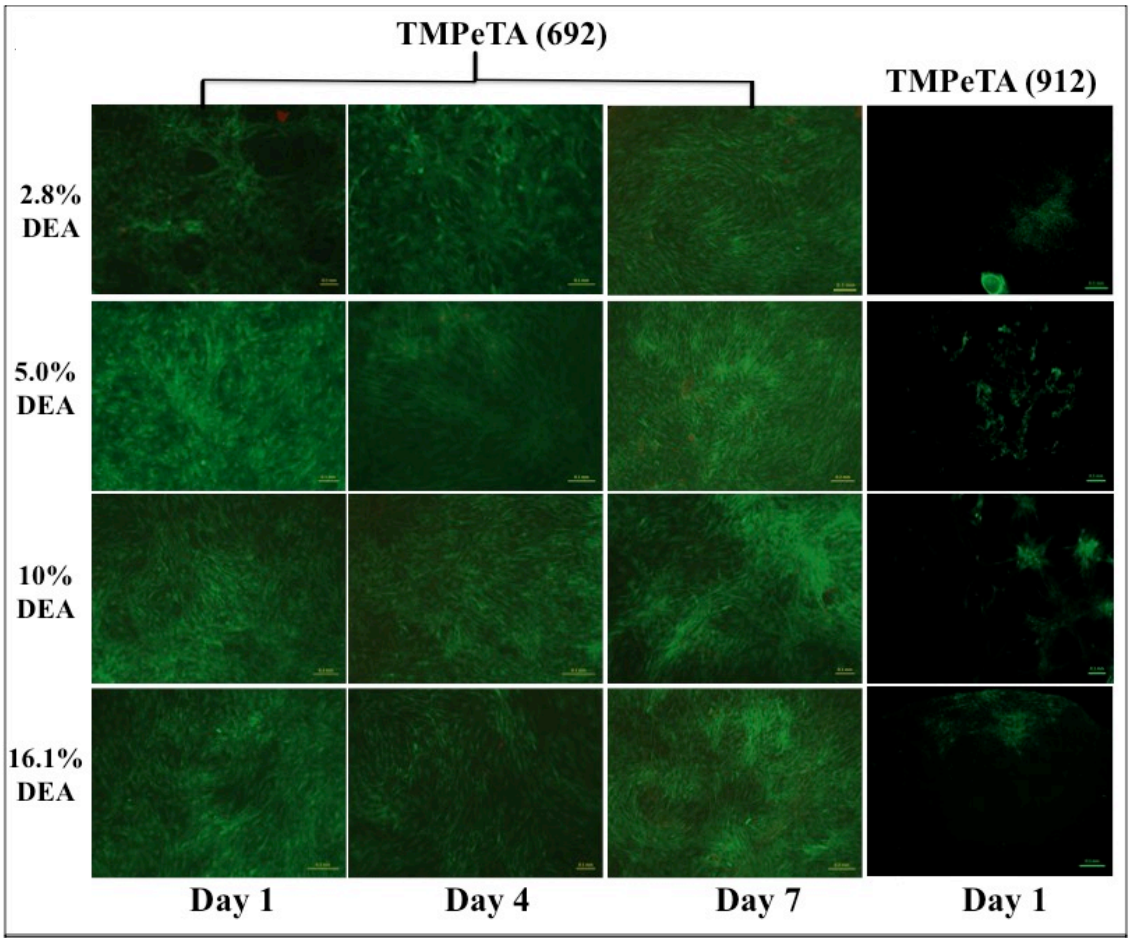

Figure 4-11. Live/dead fluorescence imaging of hASCs on A. TMPeTA(692) at day 1, 4, 7 and TMPeTA(912) at day 1. B. PEGDA(700)-co-TMPTMP with 2.8% DEA after 1 day.

cross-linking of the polymer network and cell attachment. Figure 4-12 shows a decrease in modulus with increasing amine for both TMPeTA(692) and TMPeTA(912). The varying amine content did not have an effect on cell proliferation for the TMPeTA(692) and (912) samples over the 7 day study. Figure 4-12 also illustrates that the TMPeTA(692) possessed an overall higher modulus compared to TMPeTA(912) due to TMPeTA(692) having a shorter backbone compared to TMPeTA(912). The shorter backbone yields a more tightly crosslinked network which may be responsible for the increase in cell adhesion on TMPeTA(692) compared to TMPeTA(912) (Figure 4-

12).[140,141] This correlates with crosslinking density as PEGDA(700)-co-TMPTMP synthesized in Section 4.4.1 is a less crosslinked polymer compared to the tri-functional TMPeTA containing system. The PEGDA polymers, also according to Section 4.7.2 displayed a modulus of less than 1 MPa, which may contribute to its low cell attachment. This data is consistent with previous studies wherein the higher the average functionality of a polymer, the higher the overall crosslinking density of the network.[142]

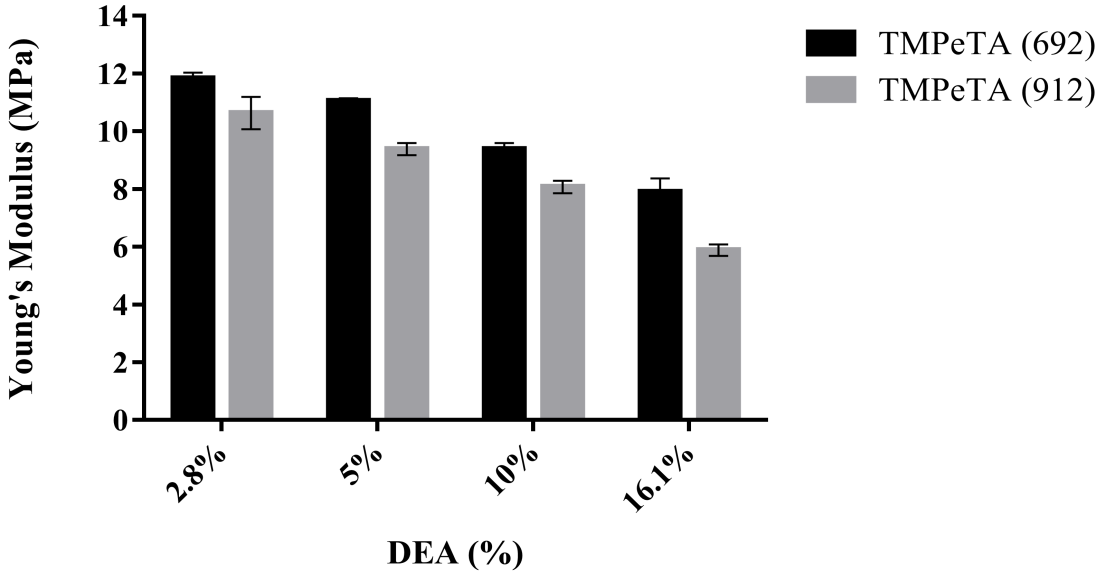

Figure 4-12. Young's Modulus as a function of DEA concentration for TMPeTA(692) and TMPeTA(912).

A previously studied thiol-acrylate system, PETA-co-TMPTMP, was shown to support cell adhesion by SEM and proliferation over a 7-day study. The PETA monomer has an average functionality of 3 and does not have a repeating group as in the monomer, PEGDA(700). This yielded an even tighter crosslinked polymer compared to both TMPeTA and PEGDA containing polymers. As described in a previous section, cells on TMPTA did not exhibit a change to spindle morphology despite it having the

same structure as PETA minus the hydroxyl group suggesting more than one property must be analyzed to predict its adhesion to stem cells.

Wettability is another factor that affects cell adhesion on polymeric substrates. It was reported that a moderate wettability that had contact angles ranging from 20-40 degrees is desired to promote the adhesion of cells, where more hydrophobic/hydrophilic substrates do not support cell adhesion well.[143,121] Hydrophilic surfaces such as tissue culture polystyrene adsorb more proteins, such as fibronectin, than hydrophobic materials. Watchem et al. studied the effect of wettability on polymeric substrates used in tissue engineering, such as PMMA (poly(methyl methacrylate)), PLLA (poly-L-lactic acid) and TCPS (tissue-culture polystyrene), and observed increasing cell adhesion with increasing contact angles.[144]

Figure 4-13 shows the initial contact angles for TMPeTA(692) and TMPeTA(912) polymers ranging between 28-45 degrees with an increase in hydrophilicity with increasing amine content. This is likely a result of the amine catalyst formed in the first step of this polymerization increasing the polarity of the overall polymer. Another factor contributing to its hydrophilicity is the ethoxylated repeating groups contained within the monomer, TMPeTA.[145] However, decreased cell adhesion was noted on polymer substrates that exhibit contact angles below 30 degrees, which supports the hypothesis that the TMPeTA (912) may be too hydrophilic for sustained cell attachment.[146] As previously discussed, TMPTA did not display a change in morphology while PETA did. This may be attributed to PETA containing a hydroxyl group for its fourth arm while TMPTA contains a methyl group making TMPTA less hydrophilic.

Surface charge also contributes to cell adhesion as a result of the interaction of charged proteins, such as extracellular matrix, and the substrate. Many commercially available culture flasks and dishes used for cell proliferation experiments are coated with poly-L-lysine, which also contains a charged amine functional group.[147] The

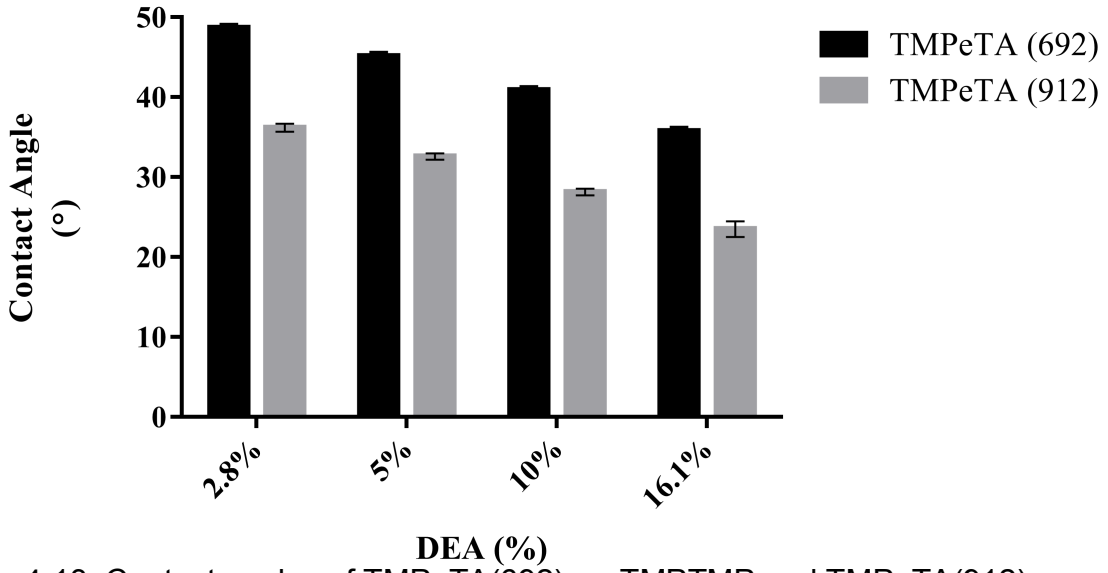

Figure 4-13. Contact angles of TMPeTA(692)-co-TMPTMP and TMPeTA(912)-co-TMPTMP with varying %DEA

chemical composition of the TMPeTA polymers includes the incorporation of the amine catalyst, shown in the first step of Scheme 4-1**,** which is integrated into the polymer network. The tertiary amine catalyst formed is positively charged at physiological pH causing an overall positive charge to the polymer. This increase in overall charge with respect to amine content may explain in part why the 16.1% DEA TMPeTA(692) polymer promotes cell attachment/proliferation while the 2.8% DEA TMPeTA(912) does not promote attachment despite both polymers yielding similar contact angles and modulus.

The degradation of well-studied polymers such as PCL and poly-lactic-co-glycolic acid copolymers (PLGA) have been shown to affect the cell adhesion/proliferation of

stem cells.[148] The disruption of the crosslinked network in ester containing monomers (TMPeTA, PLGA, and PCL) has been shown due to the hydrolysis of the ester bonds in acidic or basic environments.[149] The change in mass over 7 days was measured for each DEA concentration in TMPeTA(692)-co-TMPTMP and TMPeTA(912)-co-TMPTMP to study how mass loss may affect their ability to adsorb proteins needed for cell adhesion (Figure 4-14). Despite the 16.1% DEA 692 polymer having a mass loss of ~10%, it was able to sustain attachment/proliferation. This is likely due to the overall increase in charge per surface area from the *in situ* catalyst found on the smaller monomer (692) compared to the 912 monomer.

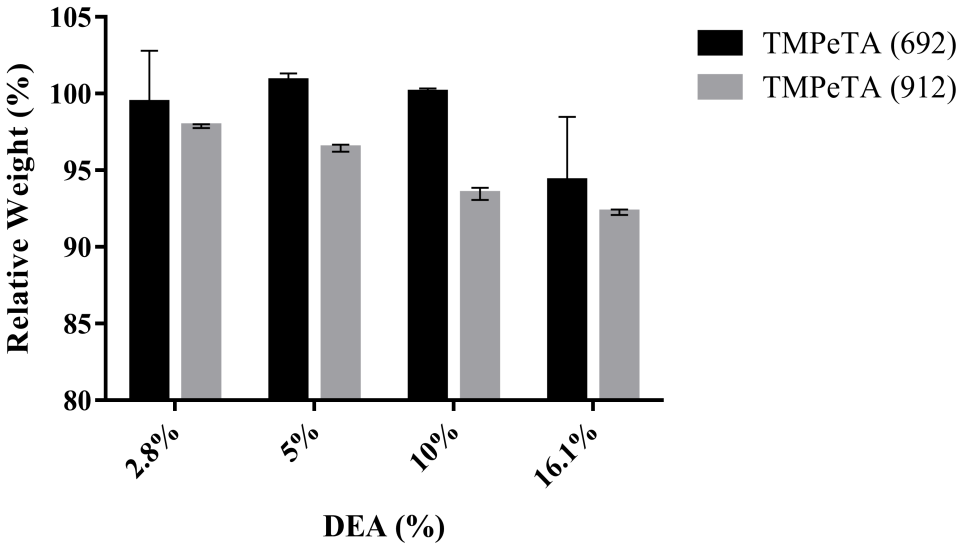

Figure 4-14. The degradation profile of TMPeTA(692) and TMPeTA(912) as a function of DEA mol(%) and TMPeTA(Mn) over 7 days.

Attachment of hASCs to TMPeTA-co-TMPTMP substrates was verified using fluorescent microscopy imaging at 1, 4, and 7 days. Live/dead staining showed the viability of the live cells by fluorescing green and dead cells by fluorescing red. The adhesion of the hASCs on the polymer surface was analyzed by observing the spindle shape cell morphology at day 1. Controls containing no cells were included as a means of comparison. As shown in Figure 4-11, cells successfully attached to the surface of

the TMPeTA(692) 2.8%-16.1% DEA polymer at day 1 post cell-seeding and remained attached throughout the 7 day study. The live/dead stain images showed that cells initially attached on TMPeTA(912)-co-TMPTMP samples (2.8-16.1% DEA) but at day 4 and 7 non-viable cells remained attached (Figure 4-11).

Cell proliferation studies were performed at different time points (day 1, 4, 7) for a total of 7 days. The PicoGreen® results for all 8 groups have been shown in Figure 4-15. For the 4 TMPeTA(692) samples, an increase in cell number was indicated from day 1 to 7 after seeding, similar to the positive control samples. In contrast, TMPeTA(912) samples revealed a low number of cells initially adhered followed by a steady decrease in attached cells from day 1 and 7. Analysis of DNA values showed that TMPeTA polymers synthesized with the lower average molecular weight, 692, are more suitable substrates for cellular proliferation. Live/dead staining results are in agreement with the PicoGreen® results (Figure 4-14), which showed a significant drop in the number of cells for TMPeTA(912) while showing a proliferation of cells for the TMPeTA(692) samples.

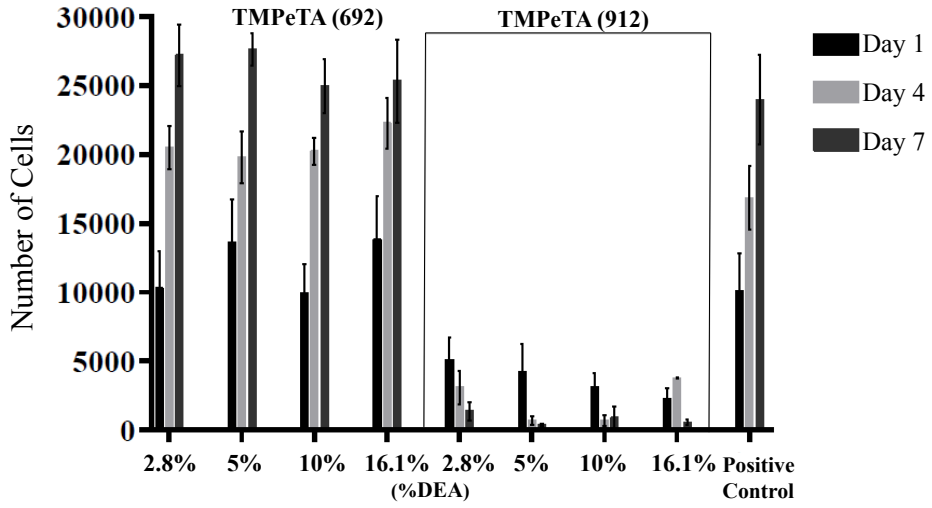

Figure 4-15. DNA content TMPeTA(692)-TMPTMP samples (2.8%, 5%, 10% and 16.1% DEA), and TMPeTA(912)-TMPTMP (2.8%, 5%, 10% and 16.1% DEA).

4.9 Stem Cell Encapsulation Methods

4.9.1 Fabrication of Cell Encapsulation Within Polymers

The agarose gel was prepared by mixing 2.0 g agarose with 100 ml stromal media followed by heating in the microwave for 30 seconds. HASC were cultured according to Section 4.3.5 and dispersed in agarose/stromal medium immediately before the agarose reached its gelation temperature of ~37 °C. The agarose gel was sieved through a piece of metal mesh to create smaller gel pieces and to allow for better distribution when mixed with the monomer precursor solution. The PEGDA(700), TMPTMP and DEA were filtered with a 0.45 μm nylon filter to ensure complete sterilization. The nucleophile-initiated PEGDA(700) polymer was prepared similar to Section 4.3.1 except the foaming apparatus was used alike to PETA. The DEA was added to the PEGDA(700) monomer first, mixed for 30 seconds, TMPTMP was added, and the foam was expelled from the canister and mixed with cell laden agarose gel bits before gelation of the polymer at ~8 minutes. The *in-situ* live cell polymerization reaction was repeated 3 times to ensure reproducibility.

The agarose was replaced with alginate for the remaining encapsulation experiments due to its homogenous uniform size compared to agarose. The alginate solution was synthesized by dissolving sodium alginate powder into stromal media at a 2% concentration by stirring for 4 hours. The hASCs were mixed gently with the filtered alginate solution. The alginate/cell mixture was added dropwise using a syringe into a 1% calcium chloride solution instantaneously forming a bead upon contact. A syringe pump set at a rate of 1 mL/min was used to assist in the bead formation to ensure the

encapsulation is finished in less than one hour. The alginate beads were washed 3x with PBS.

For the alginate bead encapsulation experiments, the base-catalyzed PEGDA polymer was prepared as mentioned in Section 4.3.1 and foamed like PETA in chapter 2 and 3. Once the precursor monomer/DEA stock solution and TMPTMP was mixed, it was foamed and allowed to sit for 5 minutes to allow for the maximum reaction temperature to be reached and for cooling to occur. The beads were then added and gently stirred using a sterile spatula. For the positive control of each, the alginate beads and agarose pieces weren't encapsulated into the polymer but rather placed in a 6 well plate with 500 µl of stromal media.

4.9.2 Temperature Measurement, Live/Dead Staining, and AlamarBlue®

The maximum temperature of the reaction before gelation was measured for each of the PEGDA(700) samples(1, 2, 3.5, 5, 7.5, 9% DEA) for 7.5 and 10% PBS. A thermocouple wire was placed in the PEGDA(700)/DEA/TMPTMP solution as soon as the thiol was added and Logger Pro software from Vernier was used to measure the temperature.

Live/Dead Staining was carried out on both the agarose and alginate experiments according to Section 4.4.5. One hour prior to imaging, the agarose gel pieces were removed from the PEGDA(700) nucleophile-initiated polymer, the stain was added to the pieces, and the pieces were imaged. For the alginate bead experiments, the beads were removed from the polymer (base-catalyzed PEGDA or TMPeTA) 1 hour prior to imaging, the stain was added, and the beads were imaged.

AlamarBlue® experiments were executed on the alginate beads that were contained within the TMPeTA(692) 5 and 10% polymer. The beads were removed from the polymer matrix after 3 days of incubation at 37 °C, and the fluorescence were read on the plate reader.

4.10 Encapsulation Results

The PEGDA polymer synthesized by nucleophilic and base-catalyzed mechanisms did not support cell attachment to the surface of the polymer as shown by the cell morphology in both live/dead staining and SEM imaging. Therefore, the PEGDA polymer was used as a transfer matrix to bind the cell encapsulated agarose or alginate beads together. Although stem cell encapsulation for tissue engineering has been a challenge, some research groups in recent years have been successful by using nature-derived polysaccharides that form a hydrogel once dissolved in water.

To prevent heat shock and death to the encapsulated cells, the temperature of the exothermic thiol-acrylate polymerization was measured. The temperature of the PEGDA polymer nucleophile reaction with 0.5% DEA was measured and decreased from 47 °C to 39 °C in ~5 minutes, leaving time for the addition of the agarose encapsulated cells pieces before gelation. The 0.5% DEA is attractive for cell encapsulation as it gives off less heat than the 2% DEA, and its gel time is slower at 8 min. The 0.5% DEA should give off more heat because there is higher conversion **(**Figure 4-2) while the 2% DEA's temperature may increase higher because the reaction is faster. For the base-catalyzed PEGDA reaction using alginate beads, the temperature was also tested for the different PEGDA polymers catalyzed by varying DEA (%). The

reaction temperature increased with increasing catalyst concentration due to the rate increasing which decreases the time needed for heat to dissipate.

The live/dead staining image (Figure 4-16) shows the viability of cells trapped in agarose within the 0.5% DEA nucleophile-initiated PEGDA(700) polymer. Green dots represent live cells, while the red dots represent dead cells. Existing green dots show cells are alive after the process of encapsulating in the agarose gel and furthermore mixing it into the pre-cursor solution. The cells survived the polymerization reaction as shown in the live/dead assay.

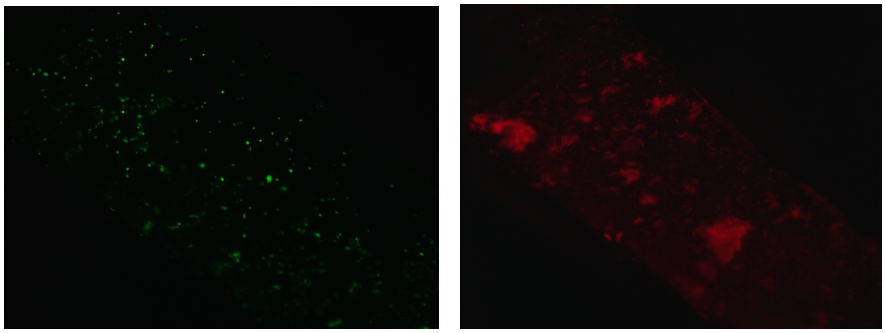

Figure 4-16. Agarose live/dead image. The left shows live cells while the right image shows dead cells

Due to the ability of alginate, another polysaccharide hydrogel, to form uniform beads with calcium chloride, the agarose was no longer used in remaining encapsulation experiments. Since the solution that the cells are in is not pure stromal media but rather contains alginate dissolved in stromal media, the cells will begin to die after one hour. The formation of the cell alginate capsules was done in less than one hour to prevent unnecessary cell death. The 1 ml/minute produced alginate particles that ranged in size from 2.4-3.0 mm.

Live/dead staining in conjunction with confocal microscopy at the 7 and 14-day time mark was used to determine if cell survival would be observed and shown in Figure

4-17. The difference between the 7 and 14-day results is the cell viability where more red cells were observed at day 14 compared to day 7 images.

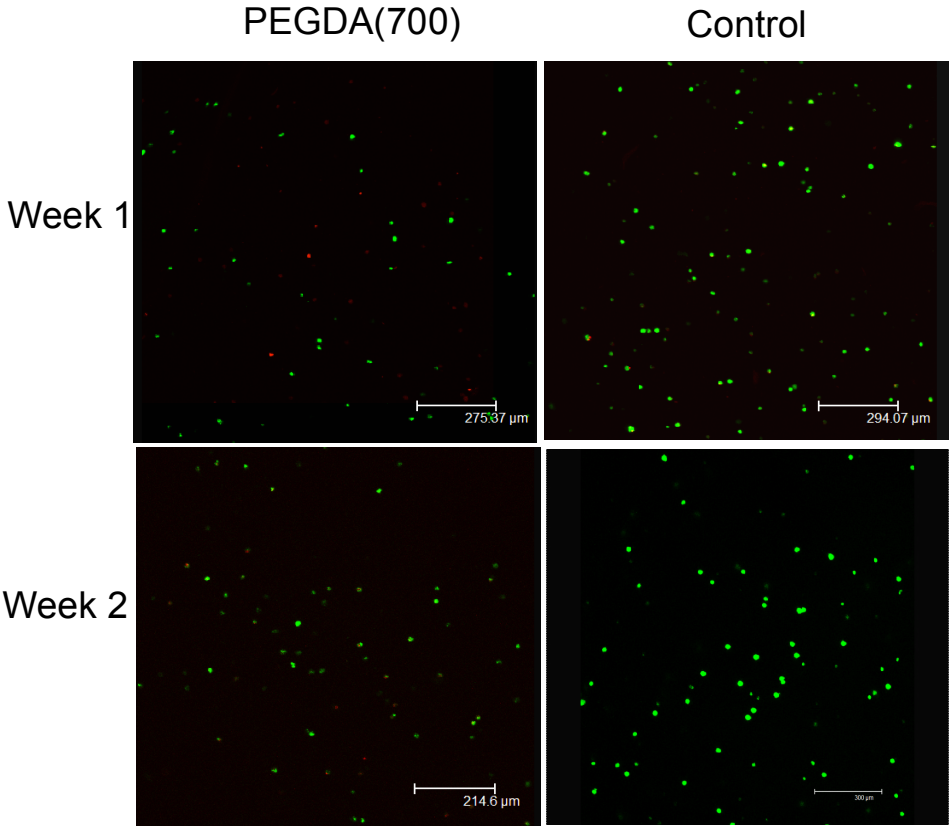

Figure 4-17. Live/dead staining of the PEGDA(700) base-catalyzed polymer compared to the control

TMPeTA(692) 5 and 10% DEA was also tested as cell-laden alginate bead carriers. The live/dead imaging (Figure 4-18) for both were relatively similar, therefore AlamarBlue® was tested for the cell viability within the beads (Figure 4-19). The 5% DEA had 80% relative metabolic activity while the 10% had almost 100%, which is comparable to the positive control beads. The positive control was the alginate beads that were not added to the precursor monomer solution before gelation.

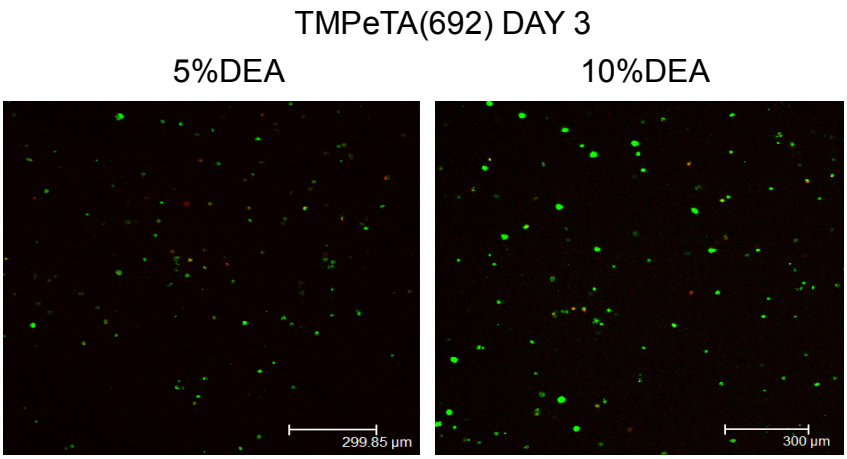

Figure 4-18. Live/dead staining of hASC/alginate within 5 and 10% DEA TMPeTA(692)

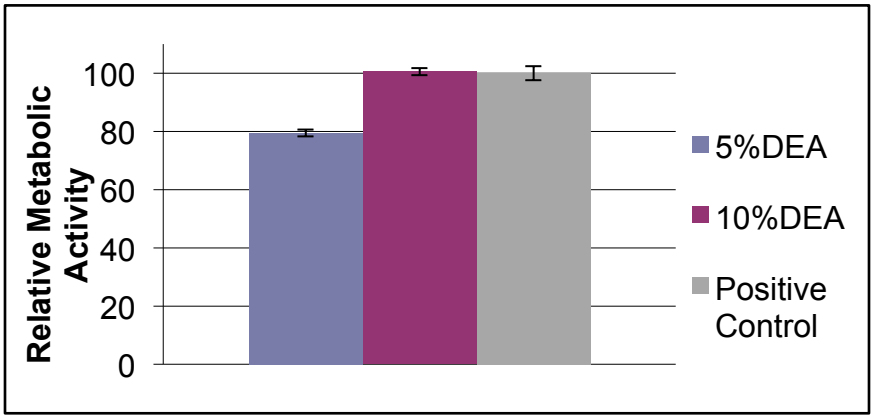

Figure 4-19. Relative Metabolic Activity of hASC alginate beads encapsulated in 5 and 10% DEA TMPeTA(692) polymer at day 3

4.11 Conclusion

The mechanism by which hASCs attach to polymeric substrates is a complicated process involving many factors such as wettability, crosslinking density, and degradability. The TMPTA and PEGDA(700) did not display any cell attachment which may be due to a combination of wettability and crosslinking density. When comparing TMPeTA(692) to TMPeTA(912), the TMPeTA(692) polymer displayed better cell attachment/proliferation versus the TMPeTA(912) samples due to its higher crosslinking density, moderate hydrophilicity, and greater stability in physiological solution. The *in*

situ amine catalyst was also a contributing factor, as seen in the 16.1% DEA TMPeTA(692) sample which exhibited mass loss comparable to 912 samples, but it is hypothesized that the higher charge density of the 692 sample promotes cell attachment/proliferation. The 10% DEA TMPeTA(692) is the best candidate overall for tissue regeneration due to its lack of degradation and sustained cell attachment/proliferation over 7 days. An alternative for materials such as PEGDA that do not support cell attachment is encapsulation. The PEGDA(700) displayed more live cells than dead cells even after 14 days.

Chapter 5. Overall Conclusion

The PETA-co-TMPTMP polymer was characterized extensively, not only in reference to material properties but also its biocompatibility properties. The 16.1% PETA-co-TMPTMP gelled in ~20 minutes which allowed for preparation and foaming time. FTIR analysis displayed that the acrylate conversion reaches close to 100% in less than 24 hours. The compressive strength of the solid was comparable to the strength of cancellous bone. Adding hydroxyapatite presented an inorganic phase to the polymer material and increased mechanical properties. It did however reduce pore size of the foamed composite due its increased viscosity. Gas foaming using nitrous oxide as the porogen produced the porosity of the scaffolds. The extractive cytotoxicity of PCL (foam) displayed a drop in relative cell viability while all the PETA (solid/foam) displayed comparable cell viability to the live control. Cell seeding on the PCL and PETA + HA displayed reduced metabolic activity that is often associated with HA, which suggests that the cells were differentiating and taking on a different metabolic activity. The PETA foams prepared in stromal media versus *in situ* did not show a difference in porosity or mechanical strength. Moreover, hASCs cultured on foamed PETA:HA (80:20) scaffolds resulted in the greatest mineralization, increased alkaline phosphatase (*ALP*) expression, and the highest osteocalcin (*OCN*) expression after 21 days.

Adding an antimicrobial portion to the polymer by soaking the PETA-co-TMPTMP (20%excess thiol) in a SNP containing solvent, known as the coating method, aided in the transport and release of SNPs. This antimicrobial element led to the PETA scaffold having a defense mechanism against common hospital acquired infections, *E. coli* and *Staph. Aureus.*

For the cell adhesion study, PEGDA(700) synthesized via nucleophile-initiated and base-catalyzed mechanisms did not yield promising results for cell attachment. Despite studies showing thiols promoting cell attachment, excess thiol formulations exhibited negative results the cytotoxicity studies at 7 days. The TMPeTA(692) 10% DEA was the most favorable material for future projects due it's lack of degradation and support of cell proliferation/adhesion.

Future applications for base-catalyzed Michael addition reactions are vast due to their robust nature and ease of synthesis at room temperature. Future work for these thiol-acrylate polymers could involve the incorporation of RGD, a cell adhesive tripeptide, by performing a Michael addition between the acrylate and the amine group found on the RGD molecule. This would directly incorporate the peptide into the polymerization reaction resulting in an even greater increase in cell attachment/proliferation on these thiol-acrylate materials.

Additionally, to further the understanding between cell and surface interactions, focal adhesion of the samples could be performed to prove the relationship between the surface modulus and cell attachment. Other variables besides the ones studied in the 4^{th} chapter of the polymer could be altered such as using a tertiary amine, which would not impart a positive charge or add onto the acrylate. This would give more insight to the overall surface charge of the polymer and how it affects the cell adhesion.

References

1. Hoyle, C. E.; Lee, T. Y.; Roper, T., Thiol-enes: Chemistry of the past with promise for the future. *Journal of Polymer Science Part A: Polymer Chemistry* **2004,** *42* (21), 5301-5338.

2. Kade, M. J.; Burke, D. J.; Hawker, C. J., The power of thiol-ene chemistry. *Journal of Polymer Science Part A: Polymer Chemistry* **2010,** *48* (4), 743-750.

3. Li, G.-Z.; Randev, R. K.; Soeriyadi, A. H.; Rees, G.; Boyer, C.; Tong, Z.; Davis, T. P.; Becer, C. R.; Haddleton, D. M., Investigation into thiol-(meth)acrylate Michael addition reactions using amine and phosphine catalysts. *Polymer Chemistry* **2010,** *1* (8), 1196-1204.

4. Wei, H.; Senyurt, A. F.; Jönsson, S.; Hoyle, C. E., Photopolymerization of ternary thiol–ene/acrylate systems: Film and network properties. *Journal of Polymer Science Part A: Polymer Chemistry* **2007,** *45* (5), 822-829.

5. Lowe, A. B., Thiol-ene “click” reactions and recent applications in polymer and materials synthesis. *Polymer Chemistry* **2010,** *1* (1), 17-36.

6. O'Brien, A. K.; Cramer, N. B.; Bowman, C. N., Oxygen inhibition in thiol–acrylate photopolymerizations. *Journal of Polymer Science Part A: Polymer Chemistry* **2006,** *44* (6), 2007-2014.

7. Bounds, C. O. G., R.; Pojman, J. A.; Vandersall, M., Preparation and application of microparticles prepared via the primary amine-catalyzed michael addition of a trithiol to a triacrylate. *Journal of Polymer Science Part A: Polymer Chemistry* **2011,** *50*, 409-422.

8. Chan, J. W.; Hoyle, C. E.; Lowe, A. B.; Bowman, M., Nucleophile-Initiated Thiol-Michael Reactions: Effect of Organocatalyst, Thiol, and Ene. *Macromolecules* **2010,** *43* (15), 6381-6388.

9. Garber, L.; Chen, C.; Kilchrist, K. V.; Bounds, C.; Pojman, J. A.; Hayes, D., Thiol-acrylate nanocomposite foams for critical size bone defect repair: A novel biomaterial. *Journal of Biomedical Materials Research Part A* **2013**, 3531-3541.

10. Chan, J. W.; Hoyle, C. E.; Lowe, A. B., Sequential Phosphine-Catalyzed, Nucleophilic Thiol−Ene/Radical-Mediated Thiol−Yne Reactions and the Facile Orthogonal Synthesis of Polyfunctional Materials. *Journal of the American Chemical Society* **2009,** *131* (16), 5751-5753.

11. Masuki, K.; Nomura, Y.; Bhawal, U. K.; Sawajiri, M.; Hirata, I.; Nahara, Y.; Okazaki, M., Apoptotic and Necrotic Influence of Dental Resin Polymerization Initiators in Human Gingival Fibroblast Cultures. *Dental Materials Journal* **2007,** *26* (6), 861-869.

12. Bjugstad, K. B.; Redmond, J., D. E.; Lampe, K. J.; Kern, D. S.; Sladek, J., J. R.; Mahoney, M. J., Biocompatibility of PEG-Based Hydrogels in Primate Brain. *Cell Transplantation* **2008,** *17* (4), 409-415.

13. Papavasiliou, G.; Sokic, S.; Turturro, M., *Synthetic PEG Hydrogels as Extracellular Matrix Mimics for Tissue Engineering Applications*. 2012.

14. Bounds, C. O.; Upadhyay, J.; Totaro, N.; Thakuri, S.; Garber, L.; Vincent, M.; Huang, Z.; Hupert, M.; Pojman, J. A., Fabrication and Characterization of Stable Hydrophilic Microfluidic Devices Prepared via the in Situ Tertiary-Amine Catalyzed Michael Addition of Multifunctional Thiols to Multifunctional Acrylates. *ACS Applied Materials & Interfaces* **2013,** *5* (5), 1643-1655.

15. Shoufeng Yang, K.-F. L., Zhaohui Du, and Chee-Kai Chua, The Design of Scaffolds for Use in Tissue Engineering. Part I. Traditional Factors

. *Tissue Engineering 7* (6), 679-689.

16. O'Brien, F. J., Biomaterials & scaffolds for tissue engineering. *Materials Today* **2011,** *14* (3), 88-95.

17. Wei, G.; Ma, P. X., Structure and properties of nano-hydroxyapatite/polymer composite scaffolds for bone tissue engineering. *Biomaterials* **2004,** *25* (19), 4749-4757.

18. Ahn, H. H.; Kim, K. S.; Lee, J. H.; Lee, J. Y.; Kim, B. S.; Lee, I. W.; Chun, H. J.; Kim, J. H.; Lee, H. B.; Kim, M. S., In vivo osteogenic differentiation of human adipose-derived stem cells in an injectable in situ-forming gel scaffold. *Tissue engineering. Part A* **2009,** *15* (7), 1821-32.

19. Degano, I. R.; Vilalta, M.; Bago, J. R.; Matthies, A. M.; Hubbell, J. A.; Dimitriou, H.; Bianco, P.; Rubio, N.; Blanco, J., Bioluminescence imaging of calvarial bone repair using bone marrow and adipose tissue-derived mesenchymal stem cells. *Biomaterials* **2008,** *29* (4), 427-37.

20. Liu, Q.; Cen, L.; Yin, S.; Chen, L.; Liu, G.; Chang, J.; Cui, L., A comparative study of proliferation and osteogenic differentiation of adipose-derived stem cells on akermanite and β-TCP ceramics. *Biomaterials* **2008,** *29* (36), 4792-4799.

21. Bergsma, J. E.; Bos, R. R. M.; Rozema, F. R.; Jong, W.; Boering, G., Biocompatibility of intraosseously implanted predegraded poly(lactide): an animal study. *Journal of Materials Science: Materials in Medicine* **1996,** *7* (1), 1-7.

22. van Gaalen, S.; Kruyt, M.; Meijer, G.; Mistry, A.; Mikos, A.; van den Beucken, J.; Jansen, J.; de Groot, K.; Cancedda, R.; Olivo, C.; Yaszemski, M.; Dhert, W., Chapter 19 - Tissue engineering of none. In *Tissue Engineering*, van Blitterswijk, C.; Thomsen, P.; Lindahl, A.; Hubbell, J.; Williams, D. F.; Cancedda, R.; de Bruijn, J. D.; Sohier, J., Eds. Academic Press: Burlington, 2008; pp 559-610.

23. Papadimitropoulos, A.; Scherberich, A.; Guven, S.; Theilgaard, N.; Crooijmans, H. J.; Santini, F.; Scheffler, K.; Zallone, A.; Martin, I., A 3D in vitro bone organ model using human progenitor cells. *European cells & materials* **2011,** *21*, 445-58; discussion 458.

24. Wang, C. Z.; Chen, S. M.; Chen, C. H.; Wang, C. K.; Wang, G. J.; Chang, J. K.; Ho, M. L., The effect of the local delivery of alendronate on human adipose-derived stem cell-based bone regeneration. *Biomaterials* **2010,** *31* (33), 8674-83.

25. Choi, H. J.; Kim, J. M.; Kwon, E.; Che, J. H.; Lee, J. I.; Cho, S. R.; Kang, S. K.; Ra, J. C.; Kang, B. C., Establishment of efficacy and safety assessment of human adipose tissue-derived mesenchymal stem cells (hATMSCs) in a nude rat femoral segmental defect model. *Journal of Korean medical science* **2011,** *26* (4), 482-91.

26. Gastaldi, G.; Asti, A.; Scaffino, M. F.; Visai, L.; Saino, E.; Cometa, A. M.; Benazzo, F., Human adipose-derived stem cells (hASCs) proliferate and differentiate in osteoblast-like cells on trabecular titanium scaffolds. *Journal of biomedical materials research. Part A* **2010,** *94* (3), 790-9.

27. Pallua, N.; Suscheck, C. V., *Tissue engineering: from lab to clinic*. Springer Verlag: 2010.

28. Karageogiou, V.; Kaplan, D., Porosity of 3D biomaterial scaffolds and osteogenisis. *Biomaterials* **2005,** *26* (27), 5474-5491.

29. Sanzana, E. S.; Navarro, M.; Ginebra, M.-P.; Planell, J. A.; Ojeda, A. C.; Montecinos, H. A., Role of porosity and pore architecture in the in vivo bone regeneration capacity of biodegradable glass scaffolds. *Journal of Biomedical Materials Research Part A* **2013**, n/a-n/a.

30. Ma, P. X., Scaffolds for tissue fabrication. *Materials Today* **2004,** *7* (5), 30-40.

31. Saravanan, S.; Nethala, S.; Pattnaik, S.; Tripathi, A.; Moorthi, A.; Selvamurugan, N., Preparation, characterization and antimicrobial activity of a bio-composite scaffold containing chitosan/nano-hydroxyapatite/nano-silver for bone tissue engineering. *International Journal of Biological Macromolecules* **2011,** *49* (2), 188-193.

32. Siddhartha, S.; Tanmay, B.; Arnab, R.; Gajendra, S.; Ramachandrarao, P.; Debabrata, D., Characterization of enhanced antibacterial effects of novel silver nanoparticles. *Nanotechnology* **2007,** *18* (22), 225103.

33. Hersel, U.; Dahmen, C.; Kessler, H., RGD modified polymers: biomaterials for stimulated cell adhesion and beyond. *Biomaterials* **2003,** *24* (24), 4385-4415.

34. Rydholm, A. E.; Held, N. L.; Benoit, D. S. W.; Bowman, C. N.; Anseth, K. S., Modifying network chemistry in thiol-acrylate photopolymers through postpolymerization functionalization to control cell-material interactions. *Journal of Biomedical Materials Research Part A* **2008,** *86A* (1), 23-30.

35. Khire, V. S.; Benoit, D. S. W.; Anseth, K. S.; Bowman, C. N., Ultrathin gradient films using thiol-ene polymerizations. *Journal of Polymer Science Part A: Polymer Chemistry* **2006,** *44* (24), 7027-7039.

36. Chang Mo, H.; Shilpa, S.; Mahdokht, M.; Nezamoddin, N. K.; Behnam, Z.; Sang-Hoon, L.; Ali, K., Fabrication of three-dimensional porous cell-laden hydrogel for tissue engineering. *Biofabrication* **2010,** *2* (3), 035003.

37. Li, R. H.; Altreuter, D. H.; Gentile, F. T., Transport characterization of hydrogel matrices for cell encapsulation. *Biotechnology and Bioengineering* **1996,** *50* (4), 365-373.

38. Siti-Ismail, N.; Bishop, A. E.; Polak, J. M.; Mantalaris, A., The benefit of human embryonic stem cell encapsulation for prolonged feeder-free maintenance. *Biomaterials* **2008,** *29* (29), 3946-3952.

39. Sakai, S.; Yamaguchi, S.; Takei, T.; Kawakami, K., Oxidized Alginate-Cross-Linked Alginate/Gelatin Hydrogel Fibers for Fabricating Tubular Constructs with Layered Smooth Muscle Cells and Endothelial Cells in Collagen Gels. *Biomacromolecules* **2008,** *9* (7), 2036-2041.

40. Rui, Y.; Renji, Z.; Jie, L.; Feng, L., Alginate and alginate/gelatin microspheres for human adipose-derived stem cell encapsulation and differentiation. *Biofabrication* **2012,** *4* (2), 025007.

41. Baniasadi, M.; Minary-Jolandan, M., Alginate-Collagen Fibril Composite Hydrogel. *Materials* **2015,** *8* (2), 799.

42. Gasperini, L.; Mano, J. F.; Reis, R. L., Natural polymers for the microencapsulation of cells. *Journal of The Royal Society Interface* **2014,** *11* (100),

43. Wang, L.; Lu, S.; Lam, J.; Kasper, F. K.; Mikos, A. G., Fabrication of Cell-Laden Macroporous Biodegradable Hydrogels with Tunable Porosities and Pore Sizes. *Tissue Engineering Part C: Methods* **2014,** *21* (3), 263-273.

44. Hoffman, M. D.; Van Hove, A. H.; Benoit, D. S., Degradable hydrogels for spatiotemporal control of mesenchymal stem cells localized at decellularized bone allografts. *Acta biomaterialia* **2014**,

45. Kloxin, A. M.; Kasko, A. M.; Salinas, C. N.; Anseth, K. S., Photodegradable Hydrogels for Dynamic Tuning of Physical and Chemical Properties. *Science* **2009,** *324* (5923), 59-63.

46. Benoit, D. S. W.; Schwartz, M. P.; Durney, A. R.; Anseth, K. S., Small molecule functional groups for the controlled differentiation of human mesenchymal stem cells encapsulated in poly(ethylene glycol) hydrogels. *Nature materials* **2008,** *7* (10), 816-823.

47. Gaalen, S. v.; Kruyt, M.; Meijer, G.; Mistry, A.; Mikos, A.; Beucken, J. v. d.; Jansen, J.; Groot, K. d.; Cancedda, R.; Olivo, C.; Yaszemski, M.; Dhert, W., Chapter 19 - Tissue engineering of bone. In *Tissue Engineering*, Clemens van, B.; Peter, T.; Anders, L.; Jeffrey, H.; David, F. W.; Ranieri, C.; Joost, D. d. B.; Jérôme SohierA2 -

Clemens van Blitterswijk, P. T. A. L. J. H. D. F. W. R. C. J. D. d. B.; Jérôme, S., Eds. Academic Press: Burlington, 2008; pp 559-610.

48. Pallua N, S. C., *Tissue Engineering: from lab to clinic*. Springer Verlag: 2010.

49. Wu, F.; Wei, J.; Liu, C.; O'Neill, B.; Ngothai, Y., Fabrication and properties of porous scaffold of zein/PCL biocomposite for bone tissue engineering. *Composites Part B: Engineering* **2012,** *43* (5), 2192-2197.

50. Ravichandran, R.; Venugopal, J. R.; Sundarrajan, S.; Mukherjee, S.; Sridhar, R.; Ramakrishna, S., Composite poly-l-lactic acid/poly-(α , β)-dl-aspartic acid/collagen nanofibrous scaffolds for dermal tissue regeneration. *Materials Science and Engineering: C* **2012,** *32* (6), 1443-1451.

51. Liu, L.; Wang, Y.; Guo, S.; Wang, Z.; Wang, W., Porous polycaprolactone/nanohydroxyapatite tissue engineering scaffolds fabricated by combining NaCl and PEG as co-porogens: Structure, property, and chondrocyte–scaffold interaction in vitro. *Journal of Biomedical Materials Research Part B: Applied Biomaterials* **2012,** *100B* (4), 956-966.

52. Hwang, S.; Todo, M., Characterization of compressive deformation behavior of multi-layer porous composite materials for articular tissue engineering. *Journal of Mechanical Science and Technology* **2012,** *26* (7), 1999-2004.

53. Ohba, S.; Wang, W.; Itoh, S.; Takagi, Y.; Nagai, A.; Yamashita, K., Acceleration of new bone formation by an electrically polarized hydroxyapatite microgranule/platelet-rich plasma composite. *Acta Biomaterialia* **2012,** *8* (7), 2778-2787.

54. Jeon, B. J.; Jeong, S. Y.; Koo, A. N.; Kim, B.-C.; Hwang, Y.-S.; Lee, S. C., Fabrication of porous PLGA microspheres with BMP-2 releasing polyphosphate-functionalized nano-hydroxyapatite for enhanced bone regeneration. *Macromolecular Research* **2012,** *20* (7), 715-724.

55. Rydholm, A. E.; Bowman, C. N.; Anseth, K. S., Degradable thiol-acrylate photopolymers: polymerization and degradation behavior of an in situ forming biomaterial. *Biomaterials* **2005,** *26* (22), 4495-4506.

56. Rydholm, A. E.; Reddy, S. K.; Anseth, K. S.; Bowman, C. N., Controlling Network Structure in Degradable Thiol−Acrylate Biomaterials to Tune Mass Loss Behavior. *Biomacromolecules* **2006,** *7* (10), 2827-2836.

57. Bounds, C. O.; Goetter, R.; Pojman, J. A.; Vandersall, M., Preparation and Application of Microparticles Prepared Via the Primary Amine-catalyzed Michael Addition of a Trithiol to a Triacrylate. *Journal of Polymer Science Part A: Polymer Chemistry* **2012,** *50*, 409–422.

58. Bounds, C. Fabrication, Analysis, Application, and Characterization of Core-Containing Microparticles and Hydrophilic microfluidic Devices Produced via the Primary and In Situ Tertiary Amine Catalyzed Michael Addition of Multifunctional Thiols to Multifunctional Acrylates. Louisiana State University, Baton Rouge, LA, 2012.

59. Zanetti, A. S.; McCandless, G. T.; Chan, J. Y.; Gimble, J. M.; Hayes, D. J., Characterization of novel akermanite:poly- ε -caprolactone scaffolds for human adipose-derived stem cells bone tissue engineering. *Journal of Tissue Engineering and Regenerative Medicine* **2012**, n/a-n/a.

60. Gimble, J. M.; Guilak, F.; Bunnell, B. A., Clinical and preclinical translation of cell-based therapies using adipose tissue-derived cells. *Stem Cell Research & Therapy* **2010,** *1* (2), 1-8.

61. Burdick, J. A.; Anseth, K. S., Photoencapsulation of osteoblasts in injectable RGD-modified PEG hydrogels for bone tissue engineering. *Biomaterials* **2002,** *23* (22), 4315-4323.

62. Nuttelman, C. R.; Benoit, D. S. W.; Tripodi, M. C.; Anseth, K. S., The effect of ethylene glycol methacrylate phosphate in PEG hydrogels on mineralization and viability of encapsulated hMSCs. *Biomaterials* **2006,** *27* (8), 1377-1386.

63. Salinas, C. N.; Anseth, K. S., Mixed Mode Thiol−Acrylate Photopolymerizations for the Synthesis of PEG−Peptide Hydrogels. *Macromolecules* **2008,** *41* (16), 6019-6026.

64. Freed, L. E.; Engelmayr, G. C.; Borenstein, J. T.; Moutos, F. T.; Guilak, F., Advanced Material Strategies for Tissue Engineering Scaffolds. *Advanced Materials* **2009,** *21* (32-33), 3410-3418.

65. Rezwan, K.; Chen, Q. Z.; Blaker, J. J.; Boccaccini, A. R., Biodegradable and bioactive porous polymer/inorganic composite scaffolds for bone tissue engineering. *Biomaterials* **2006,** *27* (18), 3413-3431.

66. Hong, Z.; Reis, R. L.; Mano, J. F., Preparation and in vitro characterization of scaffolds of poly(l-lactic acid) containing bioactive glass ceramic nanoparticles. *Acta Biomaterialia* **2008,** *4* (5), 1297-1306.

67. Reynaud, E.; Jouen, T.; Gauthier, C.; Vigier, G.; Varlet, J., Nanofillers in polymeric matrix: a study on silica reinforced PA6. *Polymer* **2001,** *42* (21), 8759-8768.

68. Pitt, G. G.; Gratzl, M. M.; Kimmel, G. L.; Surles, J.; Sohindler, A., Aliphatic polyesters II. The degradation of poly (DL-lactide), poly (ε -caprolactone), and their copolymers in vivo. *Biomaterials* **1981,** *2* (4), 215-220.

69. Ahn, H. H.; Kim, K. S.; Lee, J. H.; Lee, J. Y.; Kim, B. S.; Lee, I. W.; Chun, H. J.; Kim, J. H.; Lee, H. B.; Kim, M. S., In Vivo Osteogenic Differentiation of Human Adipose-Derived Stem Cells in an Injectable In Situ–Forming Gel Scaffold. *Tissue Engineering Part A* **2009,** *15* (7), 1821-1832.

70. Liu, Q.; Cen, L.; Yin, S.; Chen, L.; Liu, G.; Chang, J.; Cui, L., A comparative study of proliferation and osteogenic differentiation of adipose-derived stem cells on akermanite and β-TCP ceramics. *Biomaterials* **2008,** *29* (36), 4792-4799.

71. Hulbert, S. F.; Young, F. A.; Mathews, R. S.; Klawitter, J. J.; Talbert, C. D.; Stelling, F. H., Potential of ceramic materials as permanently implantable skeletal prostheses. *Journal of biomedical materials research* **1970,** *4* (3), 433-456.

72. Cartmell, S. H.; Thurstan, S.; Gittings, J. P.; Griffiths, S.; Bowen, C. R.; Turner, I. G., Polarization of porous hydroxyapatite scaffolds: Influence on osteoblast cell proliferation and extracellular matrix production. *Journal of Biomedical Materials Research Part A* **2014,** *102* (4), 1047-1052.

73. Schneider, G. B.; English, A.; Abraham, M.; Zaharias, R.; Stanford, C.; Keller, J., The effect of hydrogel charge density on cell attachment. *Biomaterials* **2004,** *25* (15), 3023-3028.

74. Di Maggio, N.; Piccinini, E.; Jaworski, M.; Trumpp, A.; Wendt, D. J.; Martin, I., Toward modeling the bone marrow niche using scaffold-based 3D culture systems. *Biomaterials* **2011,** *32* (2), 321-329.

75. Lawrence, B. J.; Madihally, S. V., Cell colonization in degradable 3D porous matrices. *Cell Adhesion & Migration* **2008,** *2* (1), 9-16.

76. Mehrkens A, M. A., Schafer D, Jakob M, Martin I, Scherberich A. . Swiss Medical Weekly 2009;139(23-24):23S-23S., Towards an intraoperative engineering of osteogenic grafts from the stromal vascular fraction of human adipose tissue. *European Cells and Materials* **2010,** *19*, 127-135.

77. Scherberich, A.; Galli, R.; Jaquiery, C.; Farhadi, J.; Martin, I., Three-Dimensional Perfusion Culture of Human Adipose Tissue-Derived Endothelial and Osteoblastic Progenitors Generates Osteogenic Constructs with Intrinsic Vascularization Capacity. *Stem Cells* **2007,** *25* (7), 1823-1829.

78. Papadimitropoulos A, S. A., Guven S, Theilgaard N, Crooijmans HJ, Santini F, Scheffler K, Zallone A, Martin I. , A 3D in vitro bone organ model using human progenitor cells. *Eur Cell Mater* **2011,** *21*, 445-458.

79. Lendeckel, S.; Jödicke, A.; Christophis, P.; Heidinger, K.; Wolff, J.; Fraser, J. K.; Hedrick, M. H.; Berthold, L.; Howaldt, H.-P., Autologous stem cells (adipose) and fibrin glue used to treat widespread traumatic calvarial defects: case report. *Journal of Cranio-Maxillofacial Surgery* **2004,** *32* (6), 370-373.

80. Pallua, N.; Suscheck, C. V., *Tissue Enginnering: from lab to clinic*. Springer Verlag: 2010.

81. Ahlmann, E.; Patzakis, M.; Roidis, N.; Shepherd, L.; Holtom, P., Comparison of Anterior and Posterior Iliac Crest Bone Grafts in Terms of Harvest-Site Morbidity and Functional Outcomes. *The Journal of Bone & Joint Surgery* **2002,** *84* (5), 716-720.

82. Alex A. Aimetti, A. J. M., Kristi S. Anseth, Poly(ethylene glycol) hydrogels formed by thiol-ene photopolymerization for enzyme-responsive protein delivery. *Biomaterials* **2009,** *30* (30), 6048-6054.

83. Jennifer Z. Paxton, K. D., Robert P. Keatch, and Keith Baar., Engineering the Bone–Ligament Interface Using Polyethylene Glycol Diacrylate Incorporated with Hydroxyapatite. *Tissue Engineering Part A* **2009,** *15* (6), 1201-1209.

84. Sun, J.-Y.; Zhao, X.; Illeperuma, W. R. K.; Chaudhuri, O.; Oh, K. H.; Mooney, D. J.; Vlassak, J. J.; Suo, Z., Highly Stretchable and touch hydrogels. *Nature* **2012,** *489* (7414), 133-136.

85. Zanetti, A. S.; Sabliov, C.; Gimble, J. M.; Hayes, D. J., Human adipose‐derived stem cells and three‐dimensional scaffold constructs: A review of the biomaterials and

models currently used for bone regeneration. *Journal of Biomedical Materials Research Part B: Applied Biomaterials* **2013,** *101* (1), 187-199.

86. Hutmacher, D. W., Scaffolds in tissue engineering bone and cartilage. *Biomaterials* **2000,** *21* (24), 2529-2543.

87. Bohner, M., Resorbable biomaterials as bone graft substitutes. *Materials Today* **2010,** *13* (1–2), 24-30.

88. Sundelacruz, S.; Kaplan, D. L. In *Stem cell-and scaffold-based tissue engineering approaches to osteochondral regenerative medicine*, Seminars in cell & developmental biology, Elsevier: 2009; pp 646-655.

89. Prabhu, S.; Poulose, E. K., Silver nanoparticles: mechanism of antimicrobial action, synthesis, medical applications, and toxicity effects. *International Nano Letters* **2012,** *2* (1), 1-10.

90. Wang, L.; Luo, J.; Shan, S.; Crew, E.; Yin, J.; Zhong, C.-J.; Wallek, B.; Wong, S. S. S., Bacterial Inactivation Using Silver-Coated Magnetic Nanoparticles as Functional Antimicrobial Agents. *Analytical Chemistry* **2011,** *83* (22), 8688-8695.

91. Henglein, A.; Meisel, D., Spectrophotometric observations of the adsorption of organosulfur compounds on colloidal silver nanoparticles. *The Journal of Physical Chemistry B* **1998,** *102* (43), 8364-8366.

92. Liau, S. Y. R., D. C.; Pugh, W. J.; Furr, J. R.; Russell, A. D., Interaction of silver nitrate with readily identifiable groups: relationship to the antibacterial action of silver ions. *Letters in Applied Microbiology* **1997,** *25* (4), 279-283.

93. Singh, R.; Lee, P. D.; Lindley, T. C.; Dashwood, R. J.; Ferrie, E.; Imwinkelried, T., Characterization of the structure and permeability of titanium foams for spinal fusion devices. *Acta Biomater* **2009,** *5* (1), 477-87.

94. Degasne, I.; Basle, M. F.; Demais, V.; Hure, G.; Lesourd, M.; Grolleau, B.; Mercier, L.; Chappard, D., Effects of roughness, fibronectin and vitronectin on attachment, spreading, and proliferation of human osteoblast-like cells (Saos-2) on titanium surfaces. *Calcif Tissue Int* **1999,** *64* (6), 499-507.

95. Levine, B., A New Era in Porous Metals: Applications in Orthopaedics. *Advanced Engineering Materials* **2008,** *10* (9), 788-792.

96. Karageorgiou, V.; Kaplan, D., Porosity of 3D biomaterial scaffolds and osteogenesis. *Biomaterials* **2005,** *26* (27), 5474-5491.

97. Yeh, J. C.; Tucker, N., The Use of Tisseel in Oculoplastics. *Invest. Ophthalmol. Vis. Sci.* **2005,** *46* (5), 4252.

98. Topart, P.; Vandenbroucke, F.; Lozac'h, P., Tisseel versus tack staples as mesh fixation in totally extraperitoneal laparoscopic repair of groin hernias. *Surgical Endoscopy And Other Interventional Techniques* **2005,** *19* (5), 724-727.

99. Gertzman, A. A.; Sunwoo, M. H., Malleable paste for filling bone defects. Google Patents: 2000.

100. Aust, L.; Devlin, B.; Foster, S.; Halvorsen, Y.; Hicok, K.; Du Laney, T.; Sen, A.; Willingmyre, G.; Gimble, J., Yield of human adipose-derived adult stem cells from liposuction aspirates. *Cytotherapy* **2004,** *6* (1), 7-14.

101. Lopez, M. J.; McIntosh, K. R.; Spencer, N. D.; Borneman, J. N.; Horswell, R.; Anderson, P.; Yu, G.; Gaschen, L.; Gimble, J. M., Acceleration of spinal fusion using syngeneic and allogeneic adult adipose derived stem cells in a rat model. *Journal of Orthopaedic Research* **2009,** *27* (3), 366-373.

102. Ahn, S. H.; Kim, S. H.; Lee, S. G., Surface-modified silica nanoparticle–reinforced poly(ethylene 2,6-naphthalate). *Journal of Applied Polymer Science* **2004,** *94* (2), 812-818.

103. Zhang, R.; Ma, P. X., Poly(alpha-hydroxyl acids)/hydroxyapatite porous composites for bone-tissue engineering. I. Preparation and morphology. *Journal of biomedical materials research* **1999,** *44* (4), 446-55.

104. Caruso, M. M.; Davis, D. A.; Shen, Q.; Odom, S. A.; Sottos, N. R.; White, S. R.; Moore, J. S., Mechanically-Induced Chemical Changes in Polymeric Materials. *Chemical Reviews* **2009,** *109* (11), 5755-5798.

105. Ho, S. T.; Hutmacher, D. W., A comparison of micro CT with other techniques used in the characterization of scaffolds. *Biomaterials* **2006,** *27* (8), 1362-1376.

106. Qureshi, A. T.; Monroe, W. T.; Dasa, V.; Gimble, J. M.; Hayes, D. J., miR-148b–Nanoparticle conjugates for light mediated osteogenesis of human adipose stromal/stem cells. *Biomaterials* **2013,** *34* (31), 7799-7810.

107. Schaer, T. P.; Stewart, S.; Hsu, B. B.; Klibanov, A. M., Hydrophobic polycationic coatings that inhibit biofilms and support bone healing during infection. *Biomaterials* **2012,** *33* (5), 1245-1254.

108. Qureshi, A. T.; Terrell, L.; Monroe, W. T.; Dasa, V.; Janes, M. E.; Gimble, J. M.; Hayes, D. J., Antimicrobial biocompatible bioscaffolds for orthopaedic implants. *Journal of Tissue Engineering and Regenerative Medicine* **2014,** *8* (5), 386-395.

109. Barby, D.; Haq, Z., Low density porous cross-linked polymeric materials and their preparation and use as carriers for included liquids. Google Patents: 1985.

110. Bernhardt, A.; Despang, F.; Lode, A.; Demmler, A.; Hanke, T.; Gelinsky, M., Proliferation and osteogenic differentiation of human bone marrow stromal cells on alginate-gelatine-hydroxyapatite scaffolds with anisotropic pore structure. *Journal of Tissue Engineering and Regenerative Medicine* **2009,** *3* (1), 54-62.

111. He, J.; Genetos, D. C.; Leach, J. K., Osteogenesis and trophic factor secretion are influenced by the composition of hydroxyapatite/poly(lactide-co-glycolide) composite scaffolds. *Tissue Eng Part A* **2010,** *16* (1), 127-37.

112. Chen, C., Garber, L., Smoak, M., Fargason, C., Scherr, T., Blackburn, C., Bacchus, S., Lopez, M. J., Pojman J. A., Del Piero, F., and Hayes, D. J., In Vitro and In Vivo Characterization of Pentaerythritol Triacrylate-co-Trimethylolpropane Nanocomposite Scaffolds as Potential Bone Augments and Grafts. *Tissue Engineering Part A* **2015,** *21* (1-2), 320-331.

113. Polymeric Scaffolds in Tissue Engineering Application: A Review. *International Journal of Polymer Science* **2011,** *2011*,

114. Schulte, V. A.; Díez, M.; Möller, M.; Lensen, M. C., Surface Topography Induces Fibroblast Adhesion on Intrinsically Nonadhesive Poly(ethylene glycol) Substrates. *Biomacromolecules* **2009,** *10* (10), 2795-2801.

115. Lensen, M. C.; Diez, M.; Schulte, V. A., *Cell Adhesion and Spreading on an Intrinsically Anti-Adhesive PEG Biomaterial*. INTECH Open Access Publisher: 2011.

116. Koh, W.-G.; Revzin, A.; Pishko, M. V., Poly(ethylene glycol) Hydrogel Microstructures Encapsulating Living Cells. *Langmuir* **2002,** *18* (7), 2459-2462.

117. Zhu, J., Bioactive modification of poly(ethylene glycol) hydrogels for tissue engineering. *Biomaterials* **2010,** *31* (17), 4639-4656.

118. Lutolf, M. P.; Hubbell, J. A., Synthetic biomaterials as instructive extracellular microenvironments for morphogenesis in tissue engineering. *Nat Biotech* **2005,** *23* (1), 47-55.

119. Barrera, D. A.; Zylstra, E.; Lansbury, P. T.; Langer, R., Synthesis and RGD peptide modification of a new biodegradable copolymer: poly(lactic acid-co-lysine). *Journal of the American Chemical Society* **1993,** *115* (23), 11010-11011.

120. Shin, H.; Jo, S.; Mikos, A. G., Biomimetic materials for tissue engineering. *Biomaterials* **2003,** *24* (24), 4353-4364.

121. Webb, K.; Hlady, V.; Tresco, P. A., Relative importance of surface wettability and charged functional groups on NIH 3T3 fibroblast attachment, spreading, and cytoskeletal organization. *Journal of biomedical materials research* **1998,** *41* (3), 422-430.

122. Webb, K.; Hlady, V.; Tresco, P. A., Relationships among cell attachment, spreading, cytoskeletal organization, and migration rate for anchorage-dependent cells on model surfaces. *Journal of biomedical materials research* **2000,** *49* (3), 362-368.

123. Vyner, M. C.; Liu, L.; Sheardown, H. D.; Amsden, B. G., The effect of elastomer chain flexibility on protein adsorption. *Biomaterials* **2013,** *34* (37), 9287-9294.

124. Li, H.-L.; Zhang, H.; Huang, H.; Liu, Z.-Q.; Li, Y.-B.; Yu, H.; An, Y.-H., The effect of amino density on the attachment, migration, and differentiation of rat neural stem cells In Vitro. *Molecules and Cells* **2013,** *35* (5), 436-443.

125. Breuls, R. G. M.; Jiya, T. U.; Smit, T. H., Scaffold Stiffness Influences Cell Behavior: Opportunities for Skeletal Tissue Engineering. *The Open Orthopaedics Journal* **2008,** *2*, 103-109.

126. Discher, D. E.; Janmey, P.; Wang, Y.-l., Tissue Cells Feel and Respond to the Stiffness of Their Substrate. *Science* **2005,** *310* (5751), 1139-1143.

127. Mason, B.; Califano, J.; Reinhart-King, C., Matrix Stiffness: A Regulator of Cellular Behavior and Tissue Formation. In *Engineering Biomaterials for Regenerative Medicine*, Bhatia, S. K., Ed. Springer New York: 2012; pp 19-37.

128. Winer, J. P.; Janmey, P. A.; McCormick, M. E.; Funaki, M., Bone Marrow-Derived Human Mesenchymal Stem Cells Become Quiescent on Soft Substrates but Remain Responsive to Chemical or Mechanical Stimuli. *Tissue Engineering Part A* **2008,** *15* (1), 147-154.

129. Smoak, M.; Chen, C.; Qureshi, A.; Garber, L.; Pojman, J. A.; Janes, M. E.; Hayes, D. J., Antimicrobial cytocompatible pentaerythritol triacrylate‐co‐trimethylolpropane composite scaffolds for orthopaedic implants. *Journal of Applied Polymer Science* **2014,** *131* (22),

130. Roberts, J. J.; Bryant, S. J., Comparison of photopolymerizable thiol-ene PEG and acrylate-based PEG hydrogels for cartilage development. *Biomaterials* **2013,** *34* (38), 9969-9979.

131. Han, L. H.; Tong, X.; Yang, F., Photo‐crosslinkable PEG‐Based Microribbons for Forming 3D Macroporous Scaffolds with Decoupled Niche Properties. *Advanced Materials* **2014,** *26* (11), 1757-1762.

132. Chiou, B.-S.; Khan, S. A., Real-Time FTIR and in Situ Rheological Studies on the UV Curing Kinetics of Thiol-ene Polymers. *Macromolecules* **1997,** *30* (23), 7322-7328.

133. Sarvestani, A. S.; Xu, W.; He, X.; Jabbari, E., Gelation and degradation characteristics of in situ photo-crosslinked poly(l-lactide-co-ethylene oxide-co-fumarate) hydrogels. *Polymer* **2007,** *48* (24), 7113-7120.

134. Maupin, P.; Pollard, T. D., Improved preservation and staining of HeLa cell actin filaments, clathrin-coated membranes, and other cytoplasmic structures by tannic acid-glutaraldehyde-saponin fixation. *The Journal of Cell Biology* **1983,** *96* (1), 51-62.

135. Small, J. V.; Rottner, K.; Hahne, P.; Anderson, K. I., Visualising the actin cytoskeleton. *Microscopy Research and Technique* **1999,** *47* (1), 3-17.

136. Zhu, J.; Marchant, R. E., Design properties of hydrogel tissue-engineering scaffolds. *Expert review of medical devices* **2011,** *8* (5), 607-626.

137. Trappmann, B.; Gautrot, J. E.; Connelly, J. T.; Strange, D. G. T.; Li, Y.; Oyen, M. L.; Cohen Stuart, M. A.; Boehm, H.; Li, B.; Vogel, V.; Spatz, J. P.; Watt, F. M.; Huck, W. T. S., Extracellular-matrix tethering regulates stem-cell fate. *Nat Mater* **2012,** *11* (7), 642-649.

138. Gong, T.; Xie, J.; Liao, J.; Zhang, T.; Lin, S.; Lin, Y., Nanomaterials and bone regeneration. *Bone Research* **2015,** *3*, 15029.

139. Head, D. A.; Levine, A. J.; MacKintosh, F. C., Deformation of Cross-Linked Semiflexible Polymer Networks. *Physical Review Letters* **2003,** *91* (10), 108102.

140. Saxena, S.; Spears Jr, M. W.; Yoshida, H.; Gaulding, J. C.; Garcia, A. J.; Lyon, L. A., Microgel film dynamics modulate cell adhesion behavior. *Soft Matter* **2014,** *10* (9), 1356-1364.

141. Rowland, C. R.; Lennon, D. P.; Caplan, A. I.; Guilak, F., The effects of crosslinking of scaffolds engineered from cartilage ECM on the chondrogenic differentiation of MSCs. *Biomaterials* **2013,** *34* (23), 5802-5812.

142. Rydholm, A. E.; Reddy, S. K.; Anseth, K. S.; Bowman, C. N., Development and characterization of degradable thiol-allyl ether photopolymers. *Polymer* **2007,** *48* (15), 4589-4600.

143. Schakenraad, J. M.; Busscher, H. J.; Wildevuur, C. R. H.; Arends, J., The influence of substratum surface free energy on growth and spreading of human fibroblasts in the presence and absence of serum proteins. *Journal of biomedical materials research* **1986,** *20* (6), 773-784.

144. Van Wachem, P.; Beugeling, T.; Feijen, J.; Bantjes, A.; Detmers, J.; Van Aken, W., Interaction of cultured human endothelial cells with polymeric surfaces of different wettabilities. *Biomaterials* **1985,** *6* (6), 403-408.

145. Paul, R., *Denim: Manufacture, Finishing and Applications*. Elsevier Science: 2015.

146. Dowling, D. P.; Miller, I. S.; Ardhaoui, M.; Gallagher, W. M., Effect of Surface Wettability and Topography on the Adhesion of Osteosarcoma Cells on Plasma-modified Polystyrene. *Journal of Biomaterials Applications* **2011,** *26* (3), 327-347.

147. Mazia, D.; Schatten, G.; Sale, W., Adhesion of cells to surfaces coated with polylysine. Applications to electron microscopy. *The Journal of Cell Biology* **1975,** *66* (1), 198-200.

148. Vance, R. J.; Miller, D. C.; Thapa, A.; Haberstroh, K. M.; Webster, T. J., Decreased fibroblast cell density on chemically degraded poly-lactic-co-glycolic acid, polyurethane, and polycaprolactone. *Biomaterials* **2004,** *25* (11), 2095-2103.

149. Freidig, A. P.; Verhaar, H. J. M.; Hermens, J. L. M., Quantitative structure-property relationships for the chemical reactivity of acrylates and methacrylates. *Environmental Toxicology and Chemistry* **1999,** *18* (6), 1133-1139.

Appendix A. Permission for Chapter 2

JOHN WILEY AND SONS LICENSE
TERMS AND CONDITIONS
May 23, 2016

This Agreement between Leah Garber ("You") and John Wiley and Sons ("John Wiley and Sons") consists of your license details and the terms and conditions provided by John Wiley and Sons and Copyright Clearance Center.

License Number
3856090711909
License date
Apr 25, 2016
Licensed Content Publisher
John Wiley and Sons
Licensed Content Publication
Journal of Biomedical Materials Research
Licensed Content Title
Thiol-acrylate nanocomposite foams for critical size bone defect repair: A novel biomaterial
Licensed Content Author
Leah Garber,Cong Chen,Kameron V. Kilchrist,Christopher Bounds,John A. Pojman,Daniel Hayes
Licensed Content Date
Apr 29, 2013
Pages
11
Type of use
Dissertation/Thesis
Requestor type
Author of this Wiley article
Format
Print and electronic
Portion
Full article
Will you be translating?
No
Title of your thesis / dissertation
Biomedical Applications of Thiol-Acrylate Polymers
Expected completion date
Aug 2016
Expected size (number of pages)
130
Requestor Location
Leah Garber

Terms and Conditions

TERMS AND CONDITIONS

This copyrighted material is owned by or exclusively licensed to John Wiley & Sons, Inc. or one of its group companies (each a"Wiley Company") or handled on behalf of a society with which a Wiley Company has exclusive publishing rights in relation to a particular work (collectively "WILEY"). By clicking "accept" in connection with completing this licensing transaction, you agree that the following terms and conditions apply to this transaction (along with the billing and payment terms and conditions established by the Copyright Clearance Center Inc., ("CCC's Billing and Payment terms and conditions"), at the time that you opened your RightsLink account (these are available at any time at http://myaccount.copyright.com).

Terms and Conditions

- The materials you have requested permission to reproduce or reuse (the "Wiley Materials") are protected by copyright.

- You are hereby granted a personal, non-exclusive, non-sub licensable (on a stand-alone basis), non-transferable, worldwide, limited license to reproduce the Wiley Materials for the purpose specified in the licensing process. This license, **and any CONTENT (PDF or image file) purchased as part of your order,** is for a one-time use only and limited to any maximum distribution number specified in the license. The first instance of republication or reuse granted by this license must be completed within two years of the date of the grant of this license (although copies prepared before the end date may be distributed thereafter). The Wiley Materials shall not be used in any other manner or for any other purpose, beyond what is granted in the license. Permission is granted subject to an appropriate acknowledgement given to the author, title of the material/book/journal and the publisher. You shall also duplicate the copyright notice that appears in the Wiley publication in your use of the Wiley Material. Permission is also granted on the understanding that nowhere in the text is a previously published source acknowledged for all or part of this Wiley Material. Any third party content is expressly excluded from this permission.

- With respect to the Wiley Materials, all rights are reserved. Except as expressly granted by the terms of the license, no part of the Wiley Materials may be copied, modified, adapted (except for minor reformatting required by the new Publication), translated, reproduced, transferred or distributed, in any form or by any means, and no derivative works may be made based on the Wiley Materials without the prior permission of the respective copyright owner. **For STM Signatory Publishers clearing permission under the terms of the STM Permissions Guidelines only, the terms of the license are extended to include subsequent editions and for editions in other languages, provided such editions are for the work as a whole in situ and does not involve the separate exploitation of the permitted figures or extracts,**You may not alter, remove or suppress in any manner any copyright, trademark or other notices displayed by the Wiley Materials. You may not license, rent, sell, loan, lease, pledge, offer as security, transfer or assign the Wiley Materials on a stand-alone basis, or any of the rights granted to you hereunder to any other person.

- The Wiley Materials and all of the intellectual property rights therein shall at all times remain the exclusive property of John Wiley & Sons Inc, the Wiley Companies, or their respective licensors, and your interest therein is only that of having possession of and the right to reproduce the Wiley Materials pursuant to Section 2 herein during the continuance of this Agreement. You agree that you own no right, title or interest in or to the Wiley Materials or any of the intellectual property rights therein. You shall have no rights hereunder other than the license as provided for

above in Section 2. No right, license or interest to any trademark, trade name, service mark or other branding ("Marks") of WILEY or its licensors is granted hereunder, and you agree that you shall not assert any such right, license or interest with respect thereto

- NEITHER WILEY NOR ITS LICENSORS MAKES ANY WARRANTY OR REPRESENTATION OF ANY KIND TO YOU OR ANY THIRD PARTY, EXPRESS, IMPLIED OR STATUTORY, WITH RESPECT TO THE MATERIALS OR THE ACCURACY OF ANY INFORMATION CONTAINED IN THE MATERIALS, INCLUDING, WITHOUT LIMITATION, ANY IMPLIED WARRANTY OF MERCHANTABILITY, ACCURACY, SATISFACTORY QUALITY, FITNESS FOR A PARTICULAR PURPOSE, USABILITY, INTEGRATION OR NON-INFRINGEMENT AND ALL SUCH WARRANTIES ARE HEREBY EXCLUDED BY WILEY AND ITS LICENSORS AND WAIVED BY YOU.

- WILEY shall have the right to terminate this Agreement immediately upon breach of this Agreement by you.

- You shall indemnify, defend and hold harmless WILEY, its Licensors and their respective directors, officers, agents and employees, from and against any actual or threatened claims, demands, causes of action or proceedings arising from any breach of this Agreement by you.

- IN NO EVENT SHALL WILEY OR ITS LICENSORS BE LIABLE TO YOU OR ANY OTHER PARTY OR ANY OTHER PERSON OR ENTITY FOR ANY SPECIAL, CONSEQUENTIAL, INCIDENTAL, INDIRECT, EXEMPLARY OR PUNITIVE DAMAGES, HOWEVER CAUSED, ARISING OUT OF OR IN CONNECTION WITH THE DOWNLOADING, PROVISIONING, VIEWING OR USE OF THE MATERIALS REGARDLESS OF THE FORM OF ACTION, WHETHER FOR BREACH OF CONTRACT, BREACH OF WARRANTY, TORT, NEGLIGENCE, INFRINGEMENT OR OTHERWISE (INCLUDING, WITHOUT LIMITATION, DAMAGES BASED ON LOSS OF PROFITS, DATA, FILES, USE, BUSINESS OPPORTUNITY OR CLAIMS OF THIRD PARTIES), AND WHETHER OR NOT THE PARTY HAS BEEN ADVISED OF THE POSSIBILITY OF SUCH DAMAGES. THIS LIMITATION SHALL APPLY NOTWITHSTANDING ANY FAILURE OF ESSENTIAL PURPOSE OF ANY LIMITED REMEDY PROVIDED HEREIN.

- Should any provision of this Agreement be held by a court of competent jurisdiction to be illegal, invalid, or unenforceable, that provision shall be deemed amended to achieve as nearly as possible the same economic effect as the original provision, and the legality, validity and enforceability of the remaining provisions of this Agreement shall not be affected or impaired thereby.

- The failure of either party to enforce any term or condition of this Agreement shall not constitute a waiver of either party's right to enforce each and every term and condition of this Agreement. No breach under this agreement shall be deemed waived or excused by either party unless such waiver or consent is in writing signed by the party granting such waiver or consent. The waiver by or consent of a party to

a breach of any provision of this Agreement shall not operate or be construed as a waiver of or consent to any other or subsequent breach by such other party.

- This Agreement may not be assigned (including by operation of law or otherwise) by you without WILEY's prior written consent.
- Any fee required for this permission shall be non-refundable after thirty (30) days from receipt by the CCC.
- These terms and conditions together with CCC's Billing and Payment terms and conditions (which are incorporated herein) form the entire agreement between you and WILEY concerning this licensing transaction and (in the absence of fraud) supersedes all prior agreements and representations of the parties, oral or written. This Agreement may not be amended except in writing signed by both parties. This Agreement shall be binding upon and inure to the benefit of the parties' successors, legal representatives, and authorized assigns.
- In the event of any conflict between your obligations established by these terms and conditions and those established by CCC's Billing and Payment terms and conditions, these terms and conditions shall prevail.
- WILEY expressly reserves all rights not specifically granted in the combination of (i) the license details provided by you and accepted in the course of this licensing transaction, (ii) these terms and conditions and (iii) CCC's Billing and Payment terms and conditions.
- This Agreement will be void if the Type of Use, Format, Circulation, or Requestor Type was misrepresented during the licensing process.
- This Agreement shall be governed by and construed in accordance with the laws of the State of New York, USA, without regards to such state's conflict of law rules. Any legal action, suit or proceeding arising out of or relating to these Terms and Conditions or the breach thereof shall be instituted in a court of competent jurisdiction in New York County in the State of New York in the United States of America and each party hereby consents and submits to the personal jurisdiction of such court, waives any objection to venue in such court and consents to service of process by registered or certified mail, return receipt requested, at the last known address of such party.

WILEY OPEN ACCESS TERMS AND CONDITIONS

Wiley Publishes Open Access Articles in fully Open Access Journals and in Subscription journals offering Online Open. Although most of the fully Open Access journals publish open access articles under the terms of the Creative Commons Attribution (CC BY) License only, the subscription journals and a few of the Open Access Journals offer a choice of Creative Commons Licenses. The license type is clearly identified on the article.

The Creative Commons Attribution License

Appendix B. Permision for Chapter 3 from Tissue Engineering

Leah Garber <garbl203@gmail.com> Apr 25

to reprints

Hello,

I would like to use the paper below that I published(Tissue Engineering Part A) in my dissertation. I did not see resuse in dissertation as an option listed. Is there another option that is comparable to that?

In Vitro and *In Vivo* Characterization of Pentaerythritol Triacrylate-co-Trimethylolpropane Nanocomposite Scaffolds as Potential Bone Augments and Grafts

Thanks!

Ballen, Karen <KBallen@liebertpub.com> Apr 25

to me

Dear Leah:

Copyright permission is granted for inclusion of your article from TISSUE ENGINEERING Part A in your dissertation.

Kind regards,

Karen Ballen
Manager

Vita

Leah Alyce Garber was born in Temple, Texas on March 9th, 1988. At the age of 3, Leah and her family moved to Thibodaux, Louisiana. Leah attended St. Genevieve Catholic Elementary School from the ages of 5 to 13. In May of 2001, Leah and her family moved to Houma, Louisiana, where Leah attended high school at Vandebilt Catholic. In May of 2006, Leah's parents moved to Crowley, Louisiana and Leah moved back to her hometown of Thibodaux, Louisiana to attend college at Nicholls State University. She majored in Chemistry and received her bachelor degree in December of 2011. In the Fall of 2011, Leah began working toward her Doctorate of Philosophy in the chemistry department at Louisiana State University and anticipates graduating with her Ph.D. degree in August of 2016.